

DISSERTATION

DROUGHT TOLERANCE AND IMPLICATIONS FOR
VEGETATION-CLIMATE INTERACTIONS IN THE AMAZON FOREST

Submitted by

Anna Biagi Harper

Department of Atmospheric Science

In partial fulfillment of the requirements

For the Degree of Doctor of Philosophy

Colorado State University

Fort Collins, Colorado

Spring 2012

Doctoral Committee:

Advisor: Alan Scott Denning

David Randall

Christian Kummerow

Francesca Cotrufo

ABSTRACT

DROUGHT TOLERANCE AND IMPLICATIONS FOR VEGETATION-CLIMATE INTERACTIONS IN THE AMAZON FOREST

On seasonal and annual timescales, the Amazon forest is resistant to drought, but more severe droughts can have profound effects on ecosystem productivity and tree mortality. The majority of climate models predict decreased rainfall in tropical South America over this century. Until recently, land surface models have not included mechanisms of forest resistance to seasonal drought. In some coupled climate models, the inability of tropical forest to withstand warming and drying leads to replacement of forest by savanna by 2050. The main questions of this research are: What factors affect forest drought tolerance, and what are the implications of drought tolerance mechanisms for climate?

Forest adaptations to drought, such as development of deep roots, enable Amazon forests to withstand seasonal droughts, and the maintenance of transpiration during dry periods can affect regional climate. At high levels of water stress, such as those imposed during a multiyear rainfall exclusion experiment or during interannual drought, trees prevent water loss by closing their stomata.

We examine forest response to drought in an ecosystem model (SiB3 - the Simple Biosphere model) compared to two rainfall exclusion experiments in the Amazon. SiB3 best reproduces the observed drought response using realistic soil parameters and annual LAI, and by adjusting soil depth. SiB3's optimal soil depth at each site serves as a proxy

for forest drought resistance. Based on the results at the exclusion sites, we form the hypothesis that forests with periodic dry conditions are more adapted to drought.

We parameterize stress resistance as a function of precipitation climatology, soil texture, and percent forest cover. The parameterization impacts carbon and moisture fluxes during extreme drought events. The loss of productivity is of similar magnitude as plot-based measurements of biomass loss during the 2005 drought.

Changing stress resistance in SiB3 also affects surface evapotranspiration during dry periods, which has the potential to affect climate through changing sensible and latent heat fluxes. We examine the effects of forest stress resistance on climate through coupled experiments of SiB3 in a GCM. In a single column model, we find evidence for a more active hydrologic cycle due to increased stress resistance. The boundary layer responds through changes in its depth, relative humidity, and turbulent kinetic energy, and the changes feed back to influence wet season onset and intensity. In a full global GCM, increased stress resistance often decreases drought intensity through enhanced ET and changes to circulation. The circulation responds to changes in atmospheric latent heating and can affect precipitation in the South Atlantic Convergence Zone.

ACKNOWLEDGEMENTS

This work would not be possible without the contributions of numerous people. My advisor, Dr. Scott Denning, has shared his enthusiasm for climate research with me, and I am proud to work under his leadership. He has always encouraged my development as a student and a scientist. My committee members have been very helpful in providing feedback throughout the PhD process - Drs. David Randall, Chris Kummerow and Francesca Cotrufo. I am indebted to several research scientists: Ian Baker and I have spent many hours discussing the Amazon ecosystem and climate. Mark Branson and Don Dazlich have been instrumental in enabling me to use the BUGS5 climate model. I'm grateful for all the computer support I've received from Matt Bishop, Kelley Wittmeyer, and Ammon Redman. Others in my group who have provided useful insight include Erica McGrath-Spangler and Andrew Schuh. I'm thankful to my office-mate, Nick Parazoo, for being available to bounce ideas off of and providing laughter to our sometimes somber working environment.

Equally important to all the professional support I've received is the personal support. My husband should be an honorary doctor for all of his help, especially during the last six months of dissertation writing, which also coincided with having a newborn. Life as a graduate student can be stressful and frustrating, and I am grateful for the outlet provided by the Thursday morning coffee group, particularly fellow founders Rachel McCrary and Levi Silvers. I strive to be cognizant of God's presence and gracious love in my daily life, and I find this verse fitting for this section:

Trust in the Lord with all your heart and lean not on your own understanding. In all your ways acknowledge Him, and He will make your paths straight." (Proverbs 3: 5-6)

Lastly my work has been funded through the National Science Foundation's Science and Technology Center for Multi-Scale Modeling of Atmospheric Processes, managed by Colorado State University under cooperative agreement ATM-0425247. I would like to thank the scientists involved in the LBA-ECO exclusion experiments at Caxiuanã and Tapajós, and in particular the director of the Museu Paraense Emilio Goeldi in Belem, Dr N. Gabas, who has supported the dry down experiment at Caxiuanã and made possible its continuation and the related international collaboration. I also thank those who have contributed data and helped edit my manuscripts - Rosie Fisher, Patrick Meir, David Galbraith, Paulo Brando, and Daniel Markewitz.

TABLE OF CONTENTS

1. INTRODUCTION AND BACKGROUND

1. Introduction.....	2
1.1 Theories of forest drought response.....	4
1.2 Observed forest drought response.....	6
1.3 Importance of deep roots and soil moisture.....	8
1.4 Modeling Amazon forest seasonality and climate response.....	10
2. Background.....	14
2.1 Amazon hydroclimate.....	14
2.2 Drought response during the throughfall exclusion experiments.....	17
3. Figures.....	20

2. MODELING DROUGHT TOLERANCE IN THE EQUATORIAL AMAZON FOREST

1. Introduction.....	24
2. Methods.....	25
2.1 The exclusion experiments.....	25
a) Site descriptions.....	25
b) Observations used in analysis.....	26
2.2 SiB3.....	27
a) Model simulation of exclusion.....	27
b) SiB3 soil moisture & stress factors.....	28
c) Roots and soil depth in SiB3.....	31
d) Other changes to SiB3.....	33
2.3 Water deficit.....	35
3. Results.....	36
3.1 Tapajós exclusion.....	36
3.2 Caxiuanã exclusion.....	38
3.3 Optimal soil depth at Tapajós and Caxiuanã.....	41
3.4 Environmental controls on ET and NPP.....	41
3.5 Thresholds in ecosystem resistance.....	43
4. Discussion.....	46
4.1 Exploring differential responses at Tapajós and Caxiuanã.....	46
4.2 Implications for modeling forest drought tolerance.....	47
4.3 Limitations in SiB3.....	49
5. Figures.....	50

3. REPRESENTING SEASONAL AND INTERANNUAL DROUGHT RESISTANCE IN AN ECOSYSTEM MODEL

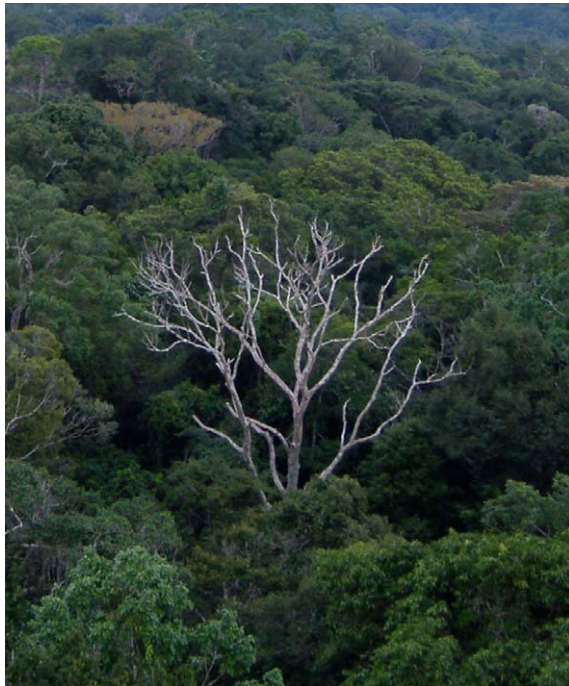
1. Introduction.....	65
2. Data and Methods.....	66

2.1 Formulation of Stress Resistance Index.....	66
2.2 Model simulations.....	71
3. Results.....	72
3.1 New parameterization: Effects on seasonal fluxes.....	72
3.2 Effect on ecosystem response to interannual climate variations.....	75
3.3 Case study of two interannual droughts.....	78
4. Discussion.....	81
5. Figures.....	83
4. ROLE OF DEEP SOIL MOISTURE IN MODULATING CLIMATE IN THE AMAZON RAINFOREST	
1. Introduction.....	94
2. Methods.....	95
2.1 SiB.....	95
2.2 SCM.....	96
2.3 Site description.....	98
3. Results.....	99
3.1 Seasonal hydrologic cycle.....	99
3.2 Seasonal heat and moisture fluxes.....	99
3.3 Dynamical implications.....	100
3.4 Wet season characteristics.....	101
4. Discussion.....	103
5. Figures.....	104
5. LAND-ATMOSPHERE INTERACTIONS DURING AMAZONIAN DROUGHTS	
1. Introduction.....	109
2. Methods.....	111
2.1 SiB3.....	111
2.2 BUGS5.....	113
3. Results.....	115
3.1 Overall model performance.....	115
3.2 Modeled seasonal climate in tropical South America.....	117
3.3 Impacts of stress resistance on seasonal fluxes.....	120
3.4 Dry periods in the southern Amazon region.....	122
3.5 Dry periods in the northwestern region.....	124
4. Discussion.....	127
4.1 Does stress resistance decrease drought intensity?.....	127
4.2 Does forest drought response affect remote precipitation and circulation patterns?.....	128
5. Figures.....	129
6. CONCLUSIONS.....	146

1. How well do we understand Amazon forest stress response during extremely dry conditions?.....	146
2. Can modeled plant available water and ecosystem stress indicate thresholds in ecosystem drought tolerance?.....	148
3. Do climatology, soil texture, and forest cover affect forest stress resistance?.....	148
4. How does forest stress resistance affect the climate?.....	149
5. Can forest stress resistance affect drought intensity and circulation in regions outside of Amazonia?.....	150
7. BIBLIOGRAPHY.....	152

CHAPTER ONE:

Introduction and Background



1. Introduction

The Amazon rainforest covers 4 million km² in Brazil alone, contains the equivalent of roughly 10 years of current human emissions of carbon (Fearnside, 1997), and accounts for approximately 10% of the world's annual net primary productivity (NPP). The combined threats of climate change and deforestation could result in marked degradation of this huge ecosystem. A potential consequence of climate change is decreased precipitation, particularly during the dry season. The aim of this work is to investigate the response of the forest to drought and the effects of the forest's drought tolerance mechanisms on climate.

Over the past decade, a better understanding of Amazon forest responses to drought has emerged. Studies of drought ranging from seasonal to interannual to multiyear depict resistance to short-term drought (e.g.: Saleska et al., 2003; Nepstad et al., 2002; Huete et al., 2006; Meir et al., 2009) but susceptibility to severe or multiyear drought (e.g.: Phillips et al., 2010; Nepstad et al., 2007; da Costa et al., 2010). An impetus for these studies is the uncertainty of the future climate and forest coverage in Amazonia. Recent droughts are linked to El Niño (e.g. 1997-1998) and warming in the northern tropical Atlantic Ocean (e.g. 2005) (Aragão et al., 2007; Marengo et al., 2008; Zeng et al., 2008). Both patterns are predicted to continue or potentially increase in the future (Li et al., 2006; van Oldenborgh et al., 2005; Cox et al., 2008). The models used in the IPCC Fourth Assessment Report predict a slight decrease in annual precipitation in tropical

South America, with moderate precipitation increases during DJF and strong decreases in precipitation during JJA (IPCC, 2007) (Figure 1.1). The range in predictions vary greatly from model to model (e.g. Li et al., 2006), and a large source of uncertainty is the response of the land surface to both climate change and increased atmospheric CO₂ (Friedlingstein et al., 2006).

The main questions and hypotheses addressed in this study are:

1. How well do we understand Amazon forest stress response during extremely dry conditions? (Chapter 2)
2. Modeled plant available water (PAW) and ecosystem stress can indicate thresholds in ecosystem drought tolerance. (Chapter 2)
3. Climatology, soil texture, and forest cover affect forest stress resistance, and including an index of stress resistance based on these factors improves modeled drought response in terms of carbon fluxes. (Chapter 3)
4. Forest stress resistance can affect the climate through changes in surface heat and moisture fluxes. (Chapter 4)
5. Forest stress resistance can reduce intensity of droughts, and impact precipitation and circulation in regions outside of Amazonia. (Chapter 5)

Following is an introduction and background information pertinent to the rest of the study. Each chapter consists of a brief introduction, distinct methods, results, and discussions. A summary and final conclusions are in Chapter 6. Figures are located at the end of each chapter.

1.1 Theories of forest drought response

Severe drought in tropical forests can lead to soil water deficits, decreased productivity, CO₂ emissions, and increased mortality rates (Allen et al., 2010). Droughts accompanied by warmer temperatures can increase forest respiration, thereby releasing further CO₂ into the atmosphere (Adams et al., 2010). Increases in dry season water stress in the eastern Amazon could trigger a transition from evergreen to seasonal forests (Malhi et al., 2009b), though any transition is likely to be strongly dependent on other factors, especially soil fertility and fire incidence (Furley et al. 1992, Hirota et al. 2010). An extreme possible outcome of climate change is conversion of forest to savanna, with enormous transfer of CO₂ from the biosphere into the atmosphere (Cox et al., 2004; Galbraith et al., 2010).

Ecosystems exposed to periodic drought can develop either drought resistance/tolerance or resilience (Chapin et al., 2002; Jones 1994). Drought-resistant species are able to survive and reproduce even in relatively dry conditions. Ecosystems that are drought resistant show little change in structure, productivity, or rate of nutrient cycling in response to a drought. Resilient ecosystems might undergo a change in one of these factors, but are able to return to their original state following a disturbance. Determination of whether an ecosystem is resilient to drought requires long term monitoring, since recovery can take years (Phillips et al., 2010). In this study we focus on drought resistance.

Three mechanisms can explain drought-induced tree mortality - carbon starvation in isohydric plants, hydraulic failure in anisohydric plants, and heightened vulnerability to

biotic attack (McDowell 2008). Isohydric plants regulate transpiration through stomatal closure, which inhibits water loss and prevents xylem cavitation. However, they are susceptible to carbon starvation since assimilation is limited while respiration costs may remain high. Warmer temperatures can make the situation worse by increasing evaporative demand (in the case of anisohydric plants) or by increasing respiration (in isohydric plants) (Allen et al., 2010; McDowell, 2008).

Plants can resist drought through stress avoidance, stress tolerance, or efficiency mechanisms (Jones 1992). Isohydric plants typically rely on deep roots to access ample soil moisture. They often avoid stress by investing more carbohydrates into root growth (relative to shoot growth) (McDowell, 2008; Jones 1992). In seasonally dry forests, plants often grow roots during the wet season in preparation for uptake during water deficits (Metcalf et al., 2008). Deficiencies in soil water and nutrients can lead to allocation of photosynthate to root growth (Kozłowski, 2002). The development of deep roots comes at a cost, reducing carbon available for above-ground growth and competition (Kleidon and Heimann, 1999). In tropical forests, observations show reduced fine root growth associated with low moisture availability, although at least one study found increased growth during the dry season. Another mechanism of stress avoidance is flowering early in the dry season when water is still available.

Stress tolerance mechanisms include increasing cell solute concentration to maintain turgor, rapid recovery following desiccation, and antioxidant mechanisms to protect against free radicals created during water deficits (Jones 1992). Lastly, plants can increase water use efficiency (WUE), defined as the ratio of net assimilation to water

loss. However, high WUE is best suited for plants in water-limited environments, since increased efficiency also slows water use and makes plants less competitive. Stomatal closure during midday and the afternoon enables rapid photosynthesis during times when evaporative demand is low, and improves a plant's WUE. The tendency for midday closure increases with decreasing soil water content (Jones 1992). In regions where drought occurs relatively often, it is likely that plants efficient in one or more of the above stress avoidance/tolerance techniques will survive. As successive droughts occur, the more drought-hardy species will dominate.

1.2 Observed forest drought response

In Central and South America, there have been five reported cases of increased mortality in tropical forests since 1970 (Allen et al., 2010). During these events, mortality increased by 39 to 94%, except one case in southeastern Brazil when mortality increased by 221%. The latter occurred in an Atlantic moist forest with relatively low annual rainfall (1200 mm) (Allen et al., 2010). Most severe droughts in Amazonia are associated with the El Niño Southern Oscillation (ENSO). El Niño events result in subsidence and reduced precipitation in the northern/northeastern Amazon (e.g. Malhi and Wright, 2004). The subsidence in the Amazon results from a shift in the Walker Circulation and is linked to a low-level anticyclone in eastern Brazil (Grimm 2003). In general, during El Niños there are suppressed growth rates and negative NDVI anomalies during the dry season (Asner et al., 2000). The sensitivity of the forest is higher in the southeastern Amazon basin.

In 2005, a drought occurred in the western Amazon, a region usually associated with heavy precipitation. The trees in this region have likely evolved with different drought response mechanisms than those in the more seasonally dry Amazon. The drought was linked to anomalously warm sea surface temperatures in the northern tropical Atlantic Ocean, and was most intense during the dry season (Marengo et al., 2008). The response of the forest to the 2005 drought is unclear, with some studies finding a loss in biomass (Phillips et al., 2009), and others finding an increase in forest productivity (Saleska et al., 2007). Biomass measurements across the Amazon basin show an estimated 1.2 to 1.6 Pg C was lost from the biosphere during the 2005 drought (Phillips et al., 2009), which represents ~1% of the annual global vegetation uptake, or 15-20% of annual anthropogenic emissions (IPCC, 2007). Mortality response to the 2005 Amazon drought showed a strongly linear relationship with soil moisture deficits (Phillips et al., 2010). Very severe water deficits produced much stronger mortality response, suggesting the existence of a threshold in drought resistance. Water deficits had greater impacts on mortality in drier climates (Phillips et al., 2010). This event was a 100-year drought, and yet an even larger drought occurred during the dry season of 2010 (Lewis et al., 2011).

An important set of experiments reproduced the effects of reduced rainfall on the forest, and can be used to increase our understanding of forest drought response. The experiments were conducted as part of the Large-Scale Biosphere-Atmosphere Experiment in Amazonia (LBA) campaign, an international research initiative led by Brazil, and took place in the Tapajós and Caxiuanã National Forest Reserves (Nepstad et

al., 2007; da Costa et al., 2010). Generally, each experiment involved monitoring two plots of forest - one control plot and a throughfall exclusion (TFE) plot where a system of panels prevented ~50% of the rainfall from reaching the forest floor. Trenches were dug around each plot to prevent the lateral flow of soil moisture into or out of the plots (1.0 m deep at Caxiuanã and 1.0-1.7 m deep at Tapajós; Fisher et al., 2007, Nepstad et al., 2007, respectively). At both exclusion sites, the forests were resistant to the early stages of drought, although some drought effects were observed during the first two years of exclusion. Interestingly, mortality rates were not significantly different in either TFE plot until three to four years in the experiments.

During the Caxiuanã exclusion, evidence was found for isohydric control on leaf water potential (Fisher et al., 2006). Dry season water use by the trees was restricted due to increases in soil-to-leaf hydraulic resistance. Minimum values of leaf water potential coincided with reduced stomatal conductance during the dry season. The implication is that during times of water stress, hydraulic limitation has more control on stomatal openings than atmospheric demand or light availability (Fisher et al., 2006).

1.3 Importance of deep roots and soil moisture

Deep roots are important for plant access to soil moisture during the dry season (e.g. Poulter et al., 2009; Nepstad et al., 1994). Observed root depths vary from 1 to 20 m in tropical South America (Poulter et al., 2009; Nepstad et al., 1994). Root depth at a given location likely depends on a variety of often poorly observed parameters, such as soil type, local climate, and the presence of an impermeable layers (Kleidon and

Heimann, 1999).

Regardless of root depth, a forest's ability to maintain transpiration and photosynthesis during dry periods is constrained by the amount of moisture available. Sap flow measurements at the Tapajós TFE plot indicated nighttime replenishment of surface soil water by upward movement in the tap roots and outward movement in lateral roots (Oliveira et al., 2005). The return of heavy rainfall led to movement of water from shallow to deep soils. This mechanism (hydraulic redistribution) has been proposed as important for reducing plant water stress and for quickly moving rainwater from the surface to deep storage (Oliveira et al., 2005).

It is now widely accepted that equatorial forests maintain transpiration (Hasler and Avissar, 2007; Lee et al., 2005) and, to a lesser degree, photosynthesis (Huete et al., 2006; Saleska et al., 2003) during the dry season, due in part to deep roots and hydraulic redistribution (e.g. Nepstad et al., 1994; Oliveira et al., 2005). Based on measurements at eddy covariance sites in the Amazon, ET is mostly controlled by net radiation during both wet and dry seasons (Hasler and Avissar, 2007; Fisher et al., 2009). Particularly in the moist equatorial Amazon, the forest is more productive and has higher ET rates during the dry season (Saleska et al., 2003; da Rocha et al., 2009; Fisher et al., 2009). According to offline runs with the Simple Biosphere model, version 3 (SiB3), incoming solar radiation is highly correlated with photosynthesis in the central Amazon basin (Figure 1.2). Ecosystem functioning can become moisture-limited under unusually dry conditions or during the dry season in regions with less rainfall (Hasler and Avissar, 2007). Both ET and photosynthesis are affected by vapor pressure deficit (VPD), leaf area, and plant

available water in dry sites and forests with low canopy cover (Fisher et al., 2009; Brando et al., 2010). On the southern edge of the forest, temperature, humidity, soil moisture, and precipitation are highly correlated with photosynthesis (Baker et al., 2011a).

Results from the two throughfall exclusion experiments agree with the picture of the Amazon as resilient to short-term drought, but susceptible to longer periods of dryness (Nepstad et al., 2007; da Costa et al., 2010). There is a limit to forest drought tolerance, which is closely related to soil moisture availability (Phillips et al., 2010), and during long-term droughts the forest eventually switches from light-limited to water-limited.

1.4 Modeling Amazon forest seasonality & climate response

Observations of how the forest responds to seasonal and longer term drought must be synthesized into ecosystem models to help improve predictions of climate and land cover change. Until recently, many ecosystem models predicted severe water supply constraints on transpiration during seasonal drought in the Amazon (e.g.: Saleska et al., 2003; Baker et al., 2008; Lee et al., 2005; Ichii et al., 2007; Poulter et al., 2009). Root depth is an essential component of forest adaptation to climatic variability. The contribution of deep roots to overall plant water use was important for modeling soil water levels during the Tapajós exclusion (Markewitz et al., 2010), and for capturing seasonal cycles of carbon and moisture fluxes (Ichii et al., 2007; Baker et al., 2008; Poulter et al., 2009; Verbeeck et al., 2011).

In the study of Markewitz et al. (2010), modeled water contents closely matched observations when wet layers were allowed to compensate root uptake in dry layers. The latest version of SiB3 implements a similar procedure. Deep roots can access soil moisture in amounts disproportionate to their density, which avoids unrealistic soil moisture stress caused by drying of surface layers where the majority of roots are located. This formulation represents the effects of hydraulic redistribution without explicitly modeling it. The addition of deeper soils and revised root water uptake in SiB3 enabled a more realistic representation of seasonal fluxes throughout the Amazon (Baker et al., 2008; Baker et al., 2011a).

Previous versions of SiB simulated decreased dry season latent heat flux and carbon uptake in the Amazon (Baker et al., 2008; Randall et al., 1996; Liu, 2004). In coupled runs of SiB2 and CSU's GCM (BUGS5), strong soil moisture stress led to increased Bowen ratio during the dry season (Liu, 2004). The overly strong sensible heat flux resulted in a hot, dry, and deep planetary boundary layer (PBL), which diluted the advected moisture during the subsequent wet season. Convection was inhibited and rainfall sharply decreased over the three-year simulation. The hydrologic cycle shutdown and associated ecosystem stress is analogous to the Amazon dieback found by Cox et al. (2004), where the forest transitioned to savannah due to decreased rainfall over western Amazonia in the 21st century. Similar results, albeit less dramatic, were found by Friedlingstein et al. (2001). Given the potentially extreme consequences of ecosystem stress, it is important to better understand how the forest copes with seasonal drought and the effect of these adaptations on the Amazonian climate.

Given the high spatial variability in root depth and its importance for forest drought tolerance, improved representations of root depth in models are desirable. Modeling studies of root depth have focused on optimizing model results to match the MODIS enhanced vegetation index (EVI - Ichii et al., 2007), MODIS GPP (Poulter et al., 2009), and flux measurements (Verbeeck et al., 2011). Another approach was to find the root depth that maximizes GPP, based on the hypothesis that plants will grow roots to a depth that optimizes carbon assimilation while minimizing carbon loss (Kleidon and Heimann, 1998). There appears to be a relationship between dry season length and root depth. For a dry season of 0 to 2 months, precipitation is high enough to sustain GPP with no water deficit. 1-3 m roots may be sufficient in such wet regions (Ichii et al., 2007; Poulter et al., 2009). Dry seasons lasting 3-4 months increase the soil moisture limitations, and root depths of 3-5 m (Ichii et al., 2007) to 8 m (Poulter et al., 2009) are necessary. Where the dry season lasts 5-6 months, the former study found that 5-10 m deep roots were sufficient, while the latter found dry season GPP suppression regardless of root depth.

Based on observed soil profiles regressed against global data sets of annual precipitation and potential ET, one study characterized probability of encountering deep roots (Schenk and Jackson, 2004). Deep roots were defined as soil profiles with at least 5% of all roots below 2 m. They found a high probability of deep roots in seasonal, tropical climates surrounding moist tropical forests, and fine and coarse textured soils were more likely to contain deep roots (Schenk and Jackson, 2004). Deep roots are less likely to occur in tropical forests, except in strongly seasonal forests like those in eastern Brazil (Sternberg et al., 1998; Schenk and Jackson, 2004).

Adaptations such as deep roots increase drought tolerance, enable the plants to maintain evapotranspiration (ET) and carbon sequestration during seasonal droughts (Saleska et al. 2003; Huete et al., 2006), and improve the seasonal cycles of ET and carbon fluxes in land models (Lee et al., 2005; Baker et al., 2008, respectively). However, few studies have looked at the effects of deep roots on climate in a coupled sense (e.g. Lee et al., 2005; Kleidon and Heimann, 1999; Lawrence and Chase, 2009).

2. Background

2.1 Amazon hydroclimate

The wet season in Amazonia occurs during austral summer (December - February), and heavy precipitation extends to the southeast in the South Atlantic Convergence Zone (SACZ). Large-scale circulation is characterized by anticyclonic rotation above Bolivia (the Bolivian high) and a downstream trough (the Nordeste low) in the upper troposphere. The location and intensity of the Bolivian high are controlled by precipitation over the Amazon basin, central Andes, and the SACZ. A heat source above the Amazon is essential for maintaining the high and also affects the cyclonic rotation to the east (Gandu and Silva Dias 1998; Lenters and Cook, 1997; Silva Dias et al., 1983). The Andes affect the Bolivian high mostly through precipitation enhancement.

Wet season precipitation in tropical South America is modulated by intraseasonal oscillations, especially near the SACZ (e.g. Jones and Carvalho, 2002; Carvalho et al., 2011). Large-scale shifts in circulation and convection have been characterized based on wind anomalies in Rondonia, Brazil (western Amazon). For example, during the easterlies regime, there is reversal of the low-level jet along the Andes, low-level anticyclonic rotation above southern South America, reduced precipitation in southern Brazil, and enhanced precipitation in the western Amazon (Jones and Carvalho, 2002). Amazon precipitation can affect convection in other regions through the low level jets,

atmospheric heating, and large-scale circulation features, although there is a lack of knowledge about how forest drought response can impact these links.

The dry season lasts anywhere from zero to five months in the Amazon forest (Figure 1.3, where months with less than 100 mm are defined as the dry season). The western equatorial Amazon receives the most rainfall (more than 3 m per year) and even during the driest three months of the year, the average rainfall is greater than 7 mm/day. Annual rainfall decreases and dry season severity increases to the south and east of the maximum rainfall. In regions with a dry season lasting more than 5 to 6 months, the forest begins to transition to savanna.

We can look at previous droughts and their effects on the ecosystem to help us understand what the effect of a drier climate could be on the tropical forest. In 1997 and 1998, a strong El Niño and warming in the tropical north Atlantic Ocean lead to a drought in northern and eastern Amazonia. In 2004 and 2005, an unusually warm tropical north Atlantic Ocean resulted in drought in western Amazonia. The anomalously low rainfall during these years is apparent in several datasets, but the timing and spatial extent can vary (Marengo et al., 2008; Aragao et al., 2007). We utilize the Global Precipitation Climatology Project (GPCP) data set to analyze the droughts in this study.

2.1a The 1997-1998 El Niño

1998 was a strong El Niño year, but the tropical north Atlantic was also anomalously warm. The warming was centered from 10°N to 10°S. Aragao et al. (2007) suggest that the warm Atlantic influenced rainfall in southern Amazonia, while the warm

tropical eastern Pacific influenced rainfall in northern Amazonia.

The 97-98 drought first showed widespread negative anomalies during March/April/May (MAM) of 1997 and continued for nearly a year (Figure 1.4). The most widespread negative anomalies occurred from September 1997 through February 1998. The negative rainfall anomalies lasted the longest in the northern Amazon and coincided with the wet and dry seasons of 1997-1998. Below-average rainfall in the western and southern Amazon was most severe during the 97/98 wet season. By MAM of 1998, positive rainfall anomalies occurred north of the equator and slowly marched southward. The southern Amazon had returned to above-average precipitation by July 1998. According to GPCP, the entire basin received positive rainfall anomalies by September-December (SON) 1998, perhaps related to the incipient La Niña.

2.1b 2005 drought

The 2005 drought was shorter, less widespread, but in many ways more interesting. First, it was not associated with an El Niño, but instead with strong meridional SST gradients in the tropical Atlantic. In 2005 the tropical north Atlantic was warmer than it had been since 1920. This resulted in a northward displacement of the intertropical convergence zone (ITCZ) (Marengo et al., 2008). Second, the drought was focused in the western Amazon, a region usually associated with the heaviest precipitation. The trees in this region may not have the same adaptive mechanisms for dealing with drought as some of the more seasonally dry Amazon, and therefore the 2005 drought effects were different than during El Niño droughts.

As discussed in Marengo et al. (2008), during SON 2004, there was below-average moisture flux from the tropical north Atlantic. Continuing into December-February (DJF), the northeasterly trade winds weakened further, as the subtropical north Atlantic high was weakened and displaced to the north. During the austral summer, there was a southerly anomaly along the Andes, where the low level jet (LLJ) typically transports moisture southward. Therefore, the moisture flow from the northern Amazon to the southwest was reduced. Upward motion was weakened over the central-western equatorial Amazon during DJF, and over the southern Amazon from December through May (Marengo et al., 2008). Parts of southern and western Amazonia experienced decreased rainfall during the wet season of 2004-2005 (Marengo et al., 2008; and Figure 1.5), although there were isolated areas of excess rainfall.

Negative rainfall anomalies were most intense during the dry season of 2005 (MJJAS) in the western Amazon according to both GPCP and CPTEC (Centro de Previsão de Tempo e Estudos Climáticos/ Prediction Center for Weather and Climate Studies) (Marengo et al., 2008). Meanwhile, there was above average rainfall in central and eastern Amazonia, related to above average convergence in these regions during MAM (Marengo et al., 2008).

2.2 Drought response during the throughfall exclusion experiments

At the rainfall exclusion experiments at Tapajós and Caxiuanã, the forests were resistant to the early stages of drought, although some drought effects were observed during the first two years of exclusion. At Caxiuanã, dry season sap flow in the control

plot was 44% higher than during the wet season, but it was 15% lower in the treatment plot. These observations were made in the second year of exclusion, indicating a 1-2 year response time for hydraulic impacts on canopy functioning. In contrast, there was no reduction in predawn leaf water potential (Ψ_L) in the first two years of exclusion at Tapajós (Nepstad et al., 2002), although above-ground net primary production (ANPP) declined by one-quarter in the TFE plot. Soil-to-root resistance was implicated in limiting water uptake by deep roots – related to low density of fine-root biomass and high matric potentials as the soil dried (Markewitz et al., 2010). Drought effects on mortality, leaf area index (LAI), and soil respiration were more severe at Caxiuanã, but effects on wood production were greater at Tapajós. Mortality rates were not significantly different in either TFE plot until three to four years in the experiments.

Differences in experimental set-up, site meteorology, longer-term climate, soil and water table characteristics, and root profiles could explain the higher sensitivity at Caxiuanã. First, at Tapajós, panels diverted rainfall during the wet seasons only, while panels were in place year-round at Caxiuanã. Second, the two sites have very different soils (clay-rich at Tapajós, and sandy at Caxiuanã), although their water-holding capacities might be very similar. Measured soil texture at Tapajós is 60% clay and 38% sand (Nepstad et al., 2002; Silver et al., 2000). At Caxiuanã the soil is 12-19% clay and 75-83% sand (Fisher et al., 2006). Typically, clay soils are able to hold more water, although this is not always the case in Amazonian soils. Estimated values of the van Genuchten parameters at the two sites indicate a higher capacity in the Caxiuanã soils (Belk et al., 2007; Fisher et al., 2008). Also the saturated hydraulic conductivity is higher

at Caxiuanã, which would be expected for a sandy soil, so although the soil may hold more water than at Tapajós, drainage occurs more rapidly. Root biomass profiles were similar down to 8 m (Belk et al., 2007; Fisher et al., 2008). A stony laterite layer at 3-4 m depth could hamper the development of deep roots at Caxiuanã, although some roots were observed below this layer (Fisher et al., 2007).

A likely third difference is the rooting strategies and climatic conditions to which the forests have adapted. The water table can rise to 10 m during the wet season at Caxiuanã (Fisher et al., 2007), compared to year-round depth of 100 m at Tapajós (Nepstad et al., 2002). Tapajós has a more seasonally dry climate according to GPCP. Over the 31-year record (1979-2009), Caxiuanã has slightly more annual precipitation (2736 mm vs. 2042 mm), a shorter dry season (3 months vs. 4-5 months), and a lower likelihood to experience extreme dry seasons (in terms of both length and precipitation amounts). Site-level observations vary slightly but support the same conclusion. Average annual precipitation was 2032 mm at the Tapajós exclusion site from 2000-2004, and 2231 mm from 2001-2008 at Caxiuanã (da Costa et al., 2010). The average dry season at Tapajós was 4.6 months with 470 mm rain, and at Caxiuanã it was 4.4 months with 532 mm rain. These factors suggest that the forest at Tapajós has evolved to tolerate slightly drier conditions than at Caxiuanã, possibly through the development of very deep roots. Other adaptive mechanisms, mediated by species differences, might include variations in plant hydraulic strategy (Fisher et al. 2006), hydraulic architecture (Meinzer et al. 2001), and carbohydrate storage (Poorter et al. 2008), but site-level observations are not available to support this.

Change in annual precipitation predicted during the 21st century

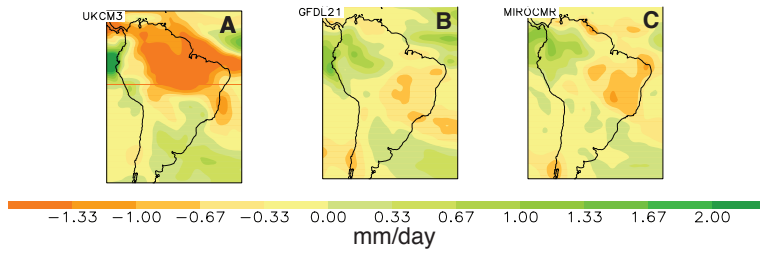


Figure 1.1 Three models used in the IPCC Fourth Assessment that show decreased precipitation throughout the 21st century in South America: A) UK Met. Office's HadCM3, B) GFDL version 2.1, C) MIROC medium resolution

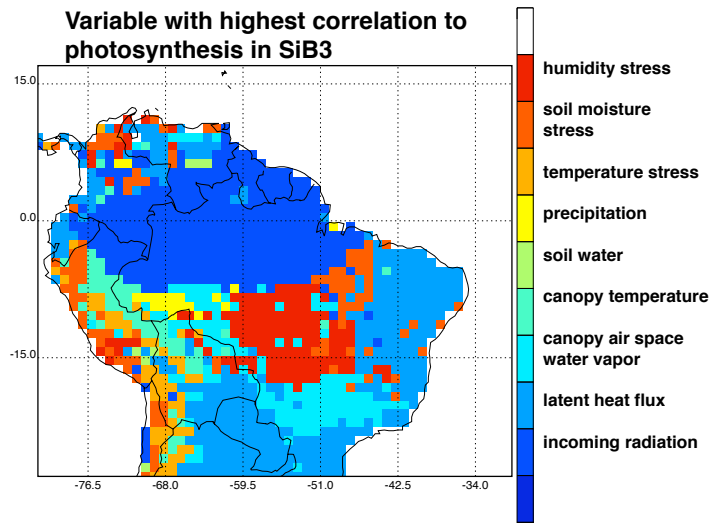


Figure 1.2

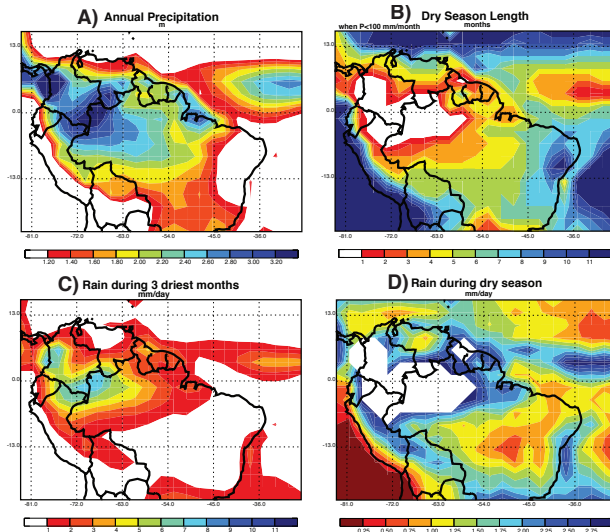


Figure 1.3 A) Annual precipitation (m); B) length of dry season (months); C) Average daily rain rate during the driest three months of the year (mm/day); D) Average daily rain rate during the dry season (mm/day)

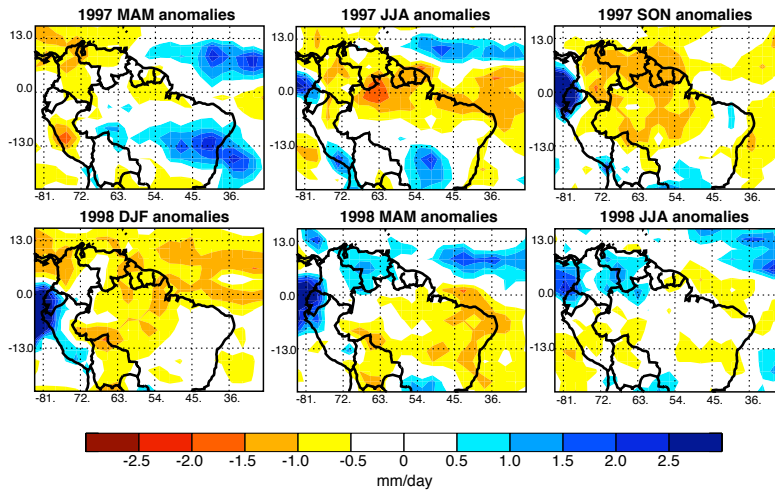


Figure 1.4 Precipitation anomalies during the 97/98 El Niño. Anomalies are based off the 1979-2009 mean in GPCP, and at each point are divided by the standard deviation for the season.

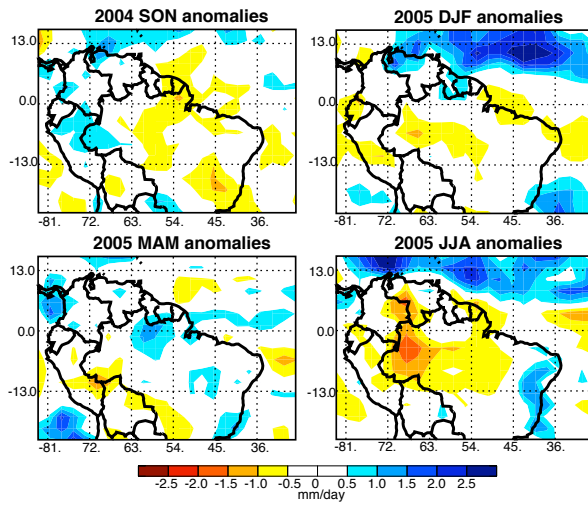


Figure 1.5 As in Fig. 1.4 but for the drought of 2005.

CHAPTER TWO:

Modeling drought tolerance in the equatorial Amazon forest

1. Introduction

Studies of drought ranging from seasonal to interannual to multiyear depict resistance to short-term drought (e.g.: Saleska et al., 2003; Nepstad et al., 2002; Huete et al., 2006; Meir et al., 2009) but susceptibility to severe or multiyear drought (e.g.: Phillips et al., 2010; Nepstad et al., 2007; da Costa et al., 2010, Meir and Woodward, 2010). The addition of deeper soils and revised root water uptake in SiB3 enabled a more realistic representation of seasonal fluxes throughout the Amazon (Baker et al., 2008; Baker et al., 2011). A logical next step in our research is to test the mechanisms employed in SiB3 against observations from long-term drought.

The rainfall exclusion experiments provide insight into how two forests with similar above-ground structure in the Eastern Amazon respond to decreases in soil moisture availability. In this paper, we evaluate the response of SiB3 to the observed meteorology at the exclusion sites. This is the first time the two experiments have been directly compared at the level of plant physiology. The two goals of this chapter are to: 1. Evaluate the stress responses of the model; and 2. Determine some thresholds in ecosystem drought tolerance common to the model and observations. In doing this we will also assess the viability of accurately representing drought response on a large scale.

2. METHODS

2.1 The exclusion experiments

2.1a Site Descriptions

The Tapajós experiment took place from 1999-2005 at the Seca Floresta site (2.90S, 54.96W), near Santarém, in the state of Pará, Brazil. The site is west of BR 163, near kilometer 67. Two flux towers are located nearby: the K67 primary forest site (2.86S, 54.96W) and the K83 selectively logged forest site (3.02S, 54.97W). The exclusion took place from 2000-2004, with panels in place during the wet season only (Jan.-June). The observed soil texture is clay, with some sand and sandy loam (Nepstad et al., 2002; Silver et al., 2000). Roots have been observed below 12 m (Nepstad et al., 2002). During the experiment, the average precipitation was 2034 mm, with 470 mm of rain during the dry season (July-Dec.) (Figure 2.1).

The Caxiuanã experiment took place from 2001-2008 in Caxiuanã National Forest (1.72S, 51.46W), also in the state of Pará, and remains ongoing. The panels were left in place throughout the entire experiment because of variability in dry season rainfall, with the exception of one week in November 2002 and 2004. The soil is a sandy loam, with 12-19% clay and 75-83% sand (yellow oxisol) (Fisher et al., 2007, Malhi et al., 2009a). Roots have been observed to 9 m, the maximum depth of excavation (Fisher et al., 2007). Average precipitation was 2149 mm, with 532 mm of dry season precipitation. More

detail of the Tapajós and Caxiuanã exclusion experiments is provided by Nepstad et al. (2002) and da Costa et al. (2010), respectively, and there is a synthesis of early results by Meir et al. (2009).

2.1b Observations used in analysis

Annual aboveground net primary productivity (ANPP) was collected for the control and exclusion plots at Tapajós and Caxiuanã (Brando et al., 2008; da Costa et al. 2010). In addition, Malhi et al. (2009a) compiled observed plot level carbon flux data at Caxiuanã and Tapajós, including components of NPP and ecosystem respiration. At Caxiuanã, total NPP was estimated for 2005 (Metcalf et al., 2010, with much source data taken from da Costa et al., 2010).

SiB3 assumes annual carbon balance, meaning that gross primary productivity (GPP) and respiration are approximately equal each year (Denning et al., 1996). However, we adjust this restriction by lagging the respiration response by one year, so that the previous years productivity determines biomass available for respiration. This results in slight imbalance year-to-year. SiB3 also assumes that respiration is evenly divided between autotrophic and heterotrophic components. Because of these assumptions, the NPP is one-half of GPP, a value based on measurements in temperate broadleaf forests (DeLucia et al., 2007) but potentially not applicable in tropical forests (Malhi et al. 2009a). SiB3 does not separate above- and below-ground carbon pools. ANPP is 70-80% of total NPP at three lowland forest sites in the Amazon (Malhi et al., 2009a), therefore we estimate ANPP as 75% of total NPP in the SiB3 results.

Latent heat observations were taken at the K67 and K83 towers, but the fluxes are only applicable to the control plot. For evapotranspiration (ET) from the Tapajós exclusion plot, we use estimates from the one-dimensional hydrologic model of Markewitz et al. (2010). At Caxiuanã, daily measurements of sap flow were made in 2002 and 2003 and scaled to the plot level using observed regressions between tree diameter and sap flux velocity applied over the whole plot (Fisher et al., 2007). These estimates can be compared qualitatively to SiB3's ET.

Volumetric water content (VWC) was observed at 13 levels extending to 11 m at Tapajós (Markewitz et al., 2010). At Caxiuanã, VWC was observed at 7 levels to 5 m (Fisher et al., 2007). SiB3 has 10 soil depths of variable thickness that extend to 10 m (Baker et al., 2008). We interpolate VWC in the observations and the model to seven levels at Tapajós, and to six levels at Caxiuanã. In both experiments, SiB3 is initialized with a soil volumetric water content similar to the observations from Belk et al. (2007) at Tapajós and from Fisher et al. (2008) at Caxiuanã.

2.2 SiB3

2.2a Model Simulation of Exclusion

The simple biosphere model (SiB3) was originally developed to simulate biophysical processes in climate models but also includes ecosystem metabolism (Sellers et al., 1986; Denning et al., 1996; Sellers et al., 1996a; Baker et al., 2008). SiB3 is run at Tapajós from 1999-2005, with rainfall excluded during the wet seasons of 2000-2004; and at Caxiuanã from 2001-2005, with year-round exclusion from 2002-2005. We

simulate the exclusion by multiplying the hourly precipitation by 0.5. The SiB3-Tapajós experiment uses observations from the K83 tower from 2001-2003 (similar results were found using meteorology from the nearby K67 tower), with the annual precipitation scaled to match what was observed in the control plot. Since we only have three full years of tower observations, the model is driven using observations from 2002 and 2003 during the first two years (1999-2000) and using observations from 2001 and 2002 during the last two years (2004-2005).

The SiB3-Caxiuanã experiment uses observations from a tower located 1 km away from the experimental plot from 2001-2003 (Fisher et al., 2007). Most meteorological variables were observed over the entire exclusion, with the exception of longwave radiation. For this we use a filled data set provided by Natalia Restrepo-Coupe (Restrepo-Coupe et al., in preparation). The years 2004 and 2005 are driven by meteorology from 2001 and 2002, respectively.

In the next section, we describe some relevant terms in SiB3's soil hydraulics and soil moisture stress calculations. For the experiment, we run three versions of SiB3 at each site: the default SiB3 of Baker et al. (2008), a version with a site-specific optimal rooting depth (Section 2.2c), and a version with more realistic soil physical parameters and leaf area index (Section 2.2d).

2.2b SiB3 soil moisture and stress factors

SiB3's potential photosynthesis is linearly weighted by three stress factors, which relate to temperature, humidity, and soil moisture. The product of the three stress factors

is the total ecosystem stress. Soil moisture stress depends on the fraction of maximum plant available water in the root zone (PAW_{frac}):

$$SM_{stress} = \frac{(1 + wssp) * pawfrac}{(wssp + pawfrac)} \quad \text{Equation 2.1}$$

where a value of one means no stress from soil moisture limitations, and a value of zero means complete stress. $Wssp$ is the water stress shape parameter and ranges from 0.1 to 1.0. In SiB3, $wssp=0.2$. Stress increases with decreasing soil moisture in a near-linear manner when $wssp=1.0$. For low values of $wssp$, stress is fairly insensitive to variations of soil moisture at high volumetric water content (VWC), but increases rapidly as soil moisture approaches the wilt point.

PAW is the water available to plants for root uptake, and is defined as the difference between the soil's VWC and wilt point. Since the maximum VWC is controlled by soil porosity,

$$PAW_{max} = P - \theta_{wp} \quad \text{Equation 2.2}$$

where P is the porosity, and θ_{wp} is the VWC at wilt point.

SiB3's field capacity and wilt point are calculated using a relationship between soil water potential and volumetric water content (Clapp and Hornberger, 1978):

$$\psi = \psi_{sat} (\theta / \theta_{sat})^{-b} \quad \text{Equation 2.3}$$

where ψ is the matric potential, ψ_{sat} is the matric potential at saturation (MPa), θ is the volumetric water content (VWC, unitless), and b is an empirical parameter. In SiB, $\psi = -0.015$ MPa (or -1.53 m) is used to calculate VWC at field capacity (θ_{fc}), and $\psi = -1.5$

MPa (or -153 m) is used to calculate VWC at wilt point (θ_{wp}):

$$\theta_{fc} = P \left[\frac{\psi_{fc} / g}{\psi_{sat}} \right]^{-\frac{1}{b}}$$

$$\theta_{wp} = P \left[\frac{\psi_{wp} / g}{\psi_{sat}} \right]^{-\frac{1}{b}}$$

Equations 2.4 & 2.5

The parameters b and ψ_{sat} are determined based on the percent sand and clay, following pedo-transfer regression equations provided by Cosby et al. (1984, their Table 5). In equations 2.2 and 2.3, P is the porosity of the soil and g is 9.8 m/s^2 . Water retention above the field capacity is not uncommon in SiB3, particularly during the wet season.

SiB3 accounts for gravitational drainage using Darcy's Law, and the change in soil moisture with time in each layer is solved for using the Richard's equation:

$$\frac{\partial \theta}{\partial t} = \frac{\partial}{\partial z} \left[k \left(\frac{\partial \theta}{\partial z} \frac{\partial \psi}{\partial \theta} \right) + 1 \right]$$

Equation 2.6

where the hydraulic conductivity (k) depends non-linearly on soil water and linearly on the hydraulic conductivity at saturation (k_{sat}):

$$k = k_{sat} \left(\frac{\theta}{\theta_{sat}} \right)^{2b+3}$$

Equation 2.7

Table 2.1 shows the porosity, field capacity, wilt point, and maximum plant available water for SiB3 at the Tapajós and Caxiuanã sites, based on sand/clay fractions specified by IGBP (Global Soil Data Task Group, 2000). The IGBP soil texture map is used in global simulations of SiB3, and therefore we use these values as a starting point. See Section 2.2d for experiments with changing the soil texture.

2.2c Roots and Soil Depth in SiB3

SiB3 assumes exponential decrease in root biomass with depth, based on a biome-dependent calculation of total root biomass.

$$\begin{aligned} totalroot &= \frac{1 - \exp(kroot_b * z_{10})}{kroot_b} \\ rootf_j &= \frac{\exp(-kroot_b * z_{top}) - \exp(-kroot_b * z_{bot})}{kroot_b * totalroot} \end{aligned} \quad \text{Equation 2.8}$$

where z_{10} is the depth of the lowest model layer (10 m in the default SiB3) and $kroot$ is a root density extinction coefficient (3.9 for the tropical evergreen forest biome). The root fraction ($rootf$) is calculated in each soil level (j). z_{bot} and z_{top} are the depths at the bottom and top of the soil level j . For the soil depth adjustments made in this study, roots are present at all levels.

SiB does not rely solely upon root fraction to determine water uptake in each layer. Several studies have shown the importance of deep roots for accessing water during the dry season in Amazonia (Nepstad et al., 1994; Jipp et al., 1998; Markewitz et al., 2010). Therefore, SiB3 uses an “apparent” root fraction ($rootr$) in each layer for water removal by transpiration, where actual root fraction ($rootf$) is weighted by the amount of water in each layer (θ_j) through the equation:

$$rootr_i = \left(\frac{1 - \frac{\theta_{wp}}{\theta_i}}{1 - \frac{\theta_{wp}}{\theta_{fc}}} \right) (rootf_i) \quad \text{Equation 2.9}$$

The apparent root fraction can be higher or lower than the actual root fraction depending on the amount of moisture in each individual layer (Baker et al., 2008). In practice, this enables the deep layers to access soil moisture in amounts disproportionate to their root density and helps avoid unrealistic soil moisture stress in the model.

Observations of root depth are rare in tropical forests. Canadell et al. (1996) report an average root depth of 7.3 +/- 2.8 m in tropical evergreen forests, and of 3.7 +/- 0.5 m in tropical deciduous forests. Roots have been found quite deep in some locations (ie: 18 m in northeastern Para state, Nepstad et al., 1994; Jipp et al., 1998). Roots as shallow as 2-3 m have been documented in China, Ghana, and the Ivory Coast (Canadell et al., 1996). Previous work using SiB3 has shown good agreement with observed carbon and moisture fluxes throughout the Amazon using a 10 m soil (Baker et al., 2008; Baker et al., 2011a).

In this study, we experimentally adjust the maximum soil depth at the two sites to obtain results that best match the available observations (for more details see Chapter 3). At Tapajós, we judge the best match based on: lowest root mean square error (RMSE) between modeled and observed (K67) latent heat flux, lowest RMSE between modeled and observed ANPP in the control and treatment plots, and closest match between modeled and observed decreases in ANPP during the exclusion experiment. We find the best agreement with these metrics using a 14 m soil. Given the depth of the soil and water table observed in the Tapajós region, 14 m-deep roots does not seem unreasonable. Roots were found up to 12 m deep during the exclusion experiment (Nepstad et al., 2002).

At Caxiuanã, the metrics for calibration of the root depth parameter are the closest match between the modeled and observed NPP in the control and treatment plots in 2005, between the drought-induced decreases in NPP in 2005, and decreases in ET in 2002 and 2003. The best agreement occurs with a 2 m soil, which is much shallower than observed at Caxiuanã. Root biomass was measured to 5 m depth in the exclusion plot, and roots were observed to 10 m depth in the control plot (Fisher et al, 2007). Root fraction is similar at Tapajos and Caxiuana down to 4 m, and below that depth Tapajos has slightly more roots (Figure 2.2). SiB3's root profile is more weighted toward surface roots compared to the two sites. However, since SiB3 weights root water uptake by the amount of water available in each layer, the actual root fraction has less of an impact on results than the available water. The fact that SiB3 requires such a shallow soil to accurately capture the drought response at Caxiuanã represents a bias toward either too much soil moisture, not enough transpiration (since strong ET would dry the soil), or an overly-insensitive stress response to low to moderate soil moisture at this site in the model. Further evaluation of the optimal soil depth is provided in the Results of this chapter.

2.2d Other changes to SiB3

Leaf area index (LAI) in SiB3 is calculated from the GIMMSg normalized difference vegetation index (NDVI) product (Tucker et al., 2005). In the tropical evergreen biome, it is assumed to be a constant value. During the exclusion experiments, LAI varied with time and between the control and treatment plots (Meir et al., 2009). Therefore, we replace SiB3's NDVI-derived LAI with annual values from the

experiments (Table 2.2). This also changes the fraction of photosynthetically active radiation (fPAR), as described in Sellers et al. (1996b). Both canopy photosynthesis and conductance are linearly related to fPAR. Since the observed LAI's are lower than SiB3's default LAI's, using the observed LAI should reduce the GPP and ET, and produce a larger difference between the control and treatment plots.

In an additional sensitivity experiment, we use observed soil textures. At Caxiuanã, we change the soil to match the observations of 15% clay and 79% sand (Fisher et al., 2006), which is a sandier soil than the IGBP soil. We also raise the saturated hydraulic conductivity (k_{sat}) to the observed value of 0.00216 m/s (Fisher et al. 2008), which increases the drainage. These changes have the effect of decreasing the soil moisture at Caxiuanã, which could help capture the observed drought response with the 10 m soil. We adjusted soil texture at Tapajós to 60% clay and 38% sand, but the higher clay content did not significantly alter the results.

In summary, at Tapajós we run a version of SiB3 with observed annual LAI, and at Caxiuanã we run a version of SiB3 with observed LAI and soil hydraulics parameters. We also adjust root depth to 14 m at Tapajós and to 2 m at Caxiuanã.

In addition to changing root depth, soil texture, and LAI, we have tried: 1) modifying root fraction to match observations at Caxiuanã, 2) accounting for the effects of the laterite layer at Caxiuanã by decreasing porosity and water content below 4 m, and 3) replacing the Clapp and Hornberger water retention curves with those of van Genuchten (1980). In general these did not greatly improve the model over what has been discussed, and so results are not included. The use of the van Genuchten curves could

improve soil moisture in SiB3, but a difficulty in this approach is determining the parameters based on limited observations in tropical forests. A more detailed parameter study could lead to more realistic results.

2.3 Water deficit

Cumulative water deficit (CWD) can help identify anomalously dry years or seasons (e.g. Malhi et al., 2009b; Aragão et al. 2007) and is used in this study to diagnose critical points in ecosystem drought response. It is essentially the cumulative difference between precipitation and evaporation and represents soil moisture depletion, and is calculated as:

$$CWD_{t=0} = P_0 - E_0 \quad \text{Equation 2.10}$$

$$CWD_t = CWD_{t-1} + P_t - E_t;$$

if $CWD > 0$, then $CWD = 0$

Most previous studies using CWD use observed precipitation and estimate E as 100 mm/month, meaning that when monthly precipitation is less than 100 mm the forest enters into water deficit ($CWD < 0$). In this study, we use the modeled latent heat, which will account for drought-induced adjustments to ET and allows for seasonal fluctuations in ET.

3. RESULTS

3.1 Tapajós Exclusion

The default version of SiB3 (with 10m soil) overestimates NPP, GPP, and ecosystem respiration in the control plot (17.3, 34.7, 34.6 MgC/ha/yr, respectively) compared to values derived from observations at the K67 tower (14.4, 31.4, 29.8 MgC/ha/yr, respectively) (Table 2.3) (Malhi et al., 2009a). The K67 the forest assimilates slightly more carbon than it respire (Malhi et al., 2009a), while SiB3 assumes annual net carbon balance.

Results from the treatment plot show that the default version of SiB3 is oversensitive to decreased precipitation. The observed ANPP decreased by 30% in the treatment plot compared to the control in 2002, and by 42% in 2003 (years three and four of exclusion, respectively; Brando et al., 2008). SiB3 simulates reductions in ANPP of 54% in 2002 and 48% in 2003 (Figure 2.3). Beginning in the dry season of 2001, SiB3 simulates a strong reduction in PAW, with reductions in latent heat flux and photosynthesis following (Figure 2.4). On average, SiB3's GPP decreases to 25.9 MgC/ha/yr in the treatment plot, while total respiration decreases to 27.7 MgC/ha/yr (Table 2.3). Similar to the GPP results, SiB3 produces a strong reduction in ET in 2002, and continues to overestimate ET reduction throughout the exclusion when compared to values from Markewitz et al. 2010 (Figure 2.3c, d).

In the calibrated version of SiB3, a 14 m soil provides a buffer against reduced rainfall, although after four years of exclusion this effect is reduced (Figure 2.4). In the control plots, annual ANPP, monthly latent heat and photosynthesis all increase slightly with the 14 m soil (Figure 2.3). In the treatment plot, the ANPP is closer to the observed values during 2002, 2003, and 2005 and thus the calibration improves these metrics of the simulation. The greatest improvement occurs during 2002, when the default SiB3 most strongly overestimates the drought effects. During this year, the 14m soil has more PAW and therefore photosynthesis and latent heat flux do not experience the severe decrease seen in the default SiB3 (Figure 2.4). Since the evaporation from the 14m soil is higher than in the default SiB3, the PAW continues to decrease until it is similar to the levels in the default soil by 2004. At this point the extra buffering capacity from the deeper soil profile does not provide any further resistance to drought stress, as the soils are not refilled during the wet season in the treatment plot.

Using site observations of LAI enables SiB3 to more accurately simulate fluxes from the canopy, as well as water uptake by the trees. Relative to the default SiB3, the observed LAI improves the ANPP drought response from 2002-2005 (Figure 2.3a). The lower LAI reduces GPP, LH, and respiration in both plots, and modeled GPP (31.5 MgC/ha/yr) is very close to the values derived from ecosystem flux measurements (Table 2.3; Malhi et al., 2009). LAI is especially low in the treatment plot, and hence ET is lower, leading to more soil moisture and less ecosystem stress (the product of soil moisture stress, humidity stress, and temperature stress). The relative decreases in ANPP and ET are closer to observations (Figure 2.3).

The volumetric water content (VWC) is underestimated during the dry seasons (for the control) and the dry-down (for the treatment) in all three versions of SiB3 applied at Tapajós (Figure 2.5), especially in the layers below 3.5 m. Potentially this error is due to the sandy soil used in the default SiB3. The soil from the LAI experiment has slightly higher water content and is thus the closest to observations. Therefore we found that a more realistic soil texture did not improve simulations of ecosystem fluxes, although changes to canopy LAI did. Experiments using more clay-rich soil in SiB3 still indicated over-sensitivity to reduced rainfall with a 10 m soil (60% clay and 38% sand following Nepstad et al. (2004), parameters shown in Table 2.1).

3.2 Caxiuanã exclusion

At Caxiuanã, GPP was estimated from the nearby eddy covariance tower (Carswell et al., 2002; Malhi et al., 2009) and was modeled using an ecosystem model with site-specific parameters (Fisher et al., 2007). The control GPP according to these values ranges from 30.9 to 38.2 MgC/ha/yr. SiB3's GPP falls within this range (34.7 MgC/ha/yr) (Table 2.4). Because of SiB3's assumption that NPP is 50% of GPP, the simulated NPP is too high compared to previous estimates (Metcalf et al., 2010; Malhi et al., 2009). SiB3's total ecosystem respiration is within the range of observations, although the observations support a higher fraction of respiration from autotrophic components (Table 2.4).

The default SiB3 is only marginally affected by the enforced drought (Figure 2.6). The average measured sap flow at Caxiuanã was 44% lower in the treatment plot in 2002,

and 41% lower in 2003 (Fisher et al., 2007). The effect was greatest in the dry season, when treatment sap flow was reduced by up to 82% compared to the control (Figure 2.7). However, SiB3's ET is barely affected by the drought and there is little seasonality in the ET response. At most the annual ET decreases by 4.8% in 2004. Measured NPP in 2005 at the exclusion plot was 77% of the NPP in the control plot (Metcalf et al., 2010). In the default SiB3 exclusion, NPP is roughly 90% of the control value from 2003-2005. GPP decreased by ~13% in 2002 and 2003 according to the model of Fisher et al. (2007), while the decrease during those years in SiB3 was 3% and 8%. An increase in respiration was observed in the treatment plot, mostly from increases in canopy and stem respiration (Metcalf et al., 2010). These observations are consistent with seasonal leaf respiration measurements made elsewhere in the Amazon (Metcalf et al. 2010b, Miranda et al. 2005). As with Tapajós, the default SiB3 simulates a decrease in all components of respiration when productivity declines (Table 2.4). The increase in respiration with drought at Caxiuanã is not well understood, and the majority of land surface models would likely also predict declines in respiration via direct links from GPP to respiration or functions that relate respiration to moisture stress.

Decreasing total plant available soil moisture in SiB3 enables a better simulation of the exclusion experiment. This can be accomplished either by reducing the soil depth to 2 m, or by changing the soil texture inputs. The 2m soil results in a very strong seasonal cycle in PAW in both the control and TFE plots (Figure 2.8). In response to the strong changes in PAW in the control plot, the model predicts some moisture stress in the dry season, and reduced latent heat and photosynthesis. Modeled GPP is 32.2 ± 3.4 MgC/ha/

yr, which is still within the range of values reported for Caxiuanã (Table 2.4). In the treatment plot, SiB3 with adjusted the soil depth better matches both the NPP and sap flow observations. In 2005, the modeled NPP in the treatment plot was 77% of that in the control plot, the same as the observed decrease (Metcalf et al., 2010). The 2 m soil is the only version that captures the strong decrease in treatment plot sap flow early in the dry seasons of 2002 and 2003 (Fisher et al., 2007) (Figure 2.7). However, the fractional decrease in ET is not as large as the observed fraction (figure 2.6d) because ET is systematically underestimated in the control plot (figure 2.6e, figure 2.7a).

Changing soil texture parameters also decreases the soil moisture (Table 2.1) because the sandier soil has lower porosity, and the higher k_{sat} produces more drainage. The SiB3 with observed soil and LAI parameters produces the lowest values of NPP in both the control and treatment plots and the closest match to observations in 2005 (Figure 2.6). Modeled GPP is 28.4 ± 1.8 MgC/ha/yr, which is on the low end of previous values reported at Caxiuanã (Table 2.4). However, there is no improvement in the modeled seasonal effect of the drought on ET (Figure 2.7).

The default SiB3 has too much soil moisture at Caxiuanã (Figure 2.9). Even with the reduced rainfall, SiB3's soil is able to recuperate much of what is lost through ET during the wet seasons. Also SiB3's ET is ~20% too low, so more water is available for soil recharge. This is consistent with the default SiB3 showing very little drought response. The VWC is similar in the version with 2m soil depth, but the total plant available water content is less, resulting in a more severe (and more realistic) response. Using the sandier soil texture decreases the VWC to levels below what was observed.

3.3 Optimal soil depth at Caxiuanã and Tapajós

We ran a series of experiments to find the optimal rooting depth in SiB3 at the two exclusion sites. At Tapajós, the 10 m soil has the least error in the control plot for annual ANPP and monthly latent heat flux, while the 15 m soil has the least error in the treatment plot. A 14 m soil best captures the timing and intensity of drought effects on ANPP and ET, and therefore we choose 14 m as the optimal depth at Tapajós (Table 2.5).

At Caxiuanã, the 10 m soil captures the relative amount of ET during the dry seasons in the control and treatment plots. However, the deep soil provides too much of a buffer for the forest to drought. A shallow soil better captures the observed NPP and ET. We choose 2 m as the optimal depth (Table 2.6). During the rainfall exclusion experiment at Caxiuanã, roots were observed to 9 m (Fisher et al., 2007). The fact that SiB3 requires such a small soil water reservoir to match observed drought response indicates that the default SiB3 (with 10 m soil) is too resistant to drought at this site.

3.4 Environmental controls on ET and NPP

Observations from the control plots at both sites indicate that under normal conditions, soil moisture does not limit ET (Meir et al., 2009; Carswell et al., 2002). On days when both measurements are available, the correlation between VWC in the Tapajós control plot and latent heat from the K67 tower is negative ($r = -0.57$, $n=73$ days, 95% significant t-test). Although not significant at 95%, the relationship is also negative between VWC and sap flow in the Caxiuanã control plot ($r = -0.29$, $n=26$ days). SiB3 also simulates a significant negative relationship between daytime VWC and ET in the

control plots ($r = -0.39$ at Tapajós and $r = -0.48$ at Caxiuanã). ET in the SiB3 control plots has high positive correlations with VPD, canopy air space temperature, and incoming radiation. These variables are all higher during the dry season, when soil moisture is low. Both observations and SiB3 show increased ET during dry seasons in regions that are not water-limited (e.g.: Carswell et al., 2002; Saleska et al., 2003; Baker et al., 2011). Observations also show high correlations between ET and net radiation in the equatorial Amazon forest, with a weaker relationship in regions where water stress occurs (Hasler and Avissar, 2007).

When water supply is limited, meteorological drivers have less impact and soil moisture exerts a stronger control on ET and NPP. At Caxiuanã, the trees in the treatment plot became water-stressed and a positive correlation between sap flow and VWC emerged ($r = 0.33$, $n=28$ days). A strong positive correlation was also observed between ANPP and VWC at Tapajós ($r=.72$, $p=0.012$) (Brando et al., 2008). In SiB3, VWC and ET have a weak positive correlation ($r = 0.05$) at Tapajós. At Caxiuanã, the relationship is negative in both cases, since the forest was not water stressed in the SiB3 treatment experiment. With the shallow soil at Caxiuanã, there is a weak but significant positive correlation between VWC and ET ($r=0.26$) in the treatment plot. Modeled NPP is highly correlated with incoming radiation at both sites, and with VPD at Caxiuanã. In the default SiB3 treatment case, there is a strong relationship emerges between NPP and VWC ($r=0.67$) at Caxiuanã.

3.5 Thresholds in ecosystem resistance

In terms of monitoring and predicting drought impacts, a useful concept is the idea “thresholds” in ecosystem resistance. These are points after which the response to the drought increases very rapidly and in a perhaps irreversible manner. Some thresholds were observed during the exclusion experiments. At Tapajós in October 2001 (the second year of exclusion), the PAW decreased to less than 30% of the PAW_{max} in the entire soil profile, and stayed there for most of the rest of the experiment. 2002 was anomalously dry, even in the control plot (Nepstad et al., 2007). In November 2002, water stress (as indicated by measurements of pre-dawn leaf water potential) reached a critical point, after which large tree survivorship decreased significantly (Nepstad et al., 2007: see their Figure 5). At Caxiuanã, sap flow reduced rapidly starting in mid-August 2002. During this time, volumetric water content from 0-5 m was less than $0.16 \text{ m}^3/\text{m}^3$ (Figure 2.9). In the observed soil/LAI version of SiB3 this coincides with PAW below 40%. Therefore at both experiments, PAW below 30-40% of PAW_{max} coincides with a strong ecosystem response.

SiB3 appears to reach a drought threshold during 2001-2002 at Tapajós. The average dry season precipitation at Tapajós was 470 mm, but during the six month dry season of 2001, only 215 mm of rain fell. Coincident with this unusually dry dry season, there were large reductions in PAW, photosynthesis, and latent heat, and increases in sensible heat flux (Figure 2.4) in all versions of SiB3. After December 2001, the treatment’s cumulative water deficit diverges from the control plot. The average PAW_{frac} , soil moisture stress factor, and total ecosystem stress factor decreased from 0.56, 0.87,

and 0.65 in 2001 to 0.18, 0.55, and 0.40 in 2002, respectively. The CWD decreased from -223 mm in 2001, to -708 mm in 2002. The timing of this response agrees well with the decline in PAW to below 30% of maximum PAW reported by Nepstad et al. (2007).

Drought stress was not simulated in the default SiB3 Caxiuanã experiment (Figure 2.8). The highest levels of ecosystem stress occurred after two years of exclusion, during December 2003. At this time, PAW_{frac} and ecosystem stress were 0.38 and 0.62, and the water deficit was -457 mm. To further investigate the thresholds at Caxiuanã, we run the default SiB3 with rainfall reduced by 75%, rather than 50%. Soil moisture steadily drops during the first two years of exclusion (2002-2003). The most dramatic decreases in latent heat flux and photosynthesis occur between the dry seasons of 2002 and 2003. By late 2003, average latent heat flux is 40% less in the treatment plot than in the control plot, and photosynthesis is 60% less. Average dry season PAW, soil moisture stress, and total ecosystem stress were 0.41, 0.80, and 0.63 in the dry season of 2002, and were 0.09, 0.36, and 0.27 in the dry season of 2003, respectively. The CWD increased from -440 mm in the dry season of 2002 to -870 mm in the dry season of 2003. Soil moisture levels off in the following two years, at this point the soil is near wilt point and the ability of plants to withdraw water is severely limited.

In summary, SiB3 simulated strong reductions in GPP and ET when PAW_{frac} was between 0.09-0.41 at Caxiuna and between 0.18-0.56 at Tapajós. At these values the soil moisture stress factor was 0.37-0.80 at Caxiuanã and 0.55-0.87 at Tapajós, and CWD was between -440 and -870 mm at Caxiuanã and between -223 and -708 mm at Tapajós. Compared to the observed response at Caxiuanã, SiB3 did not simulate stress at the

observed levels of soil moisture. This suggests that adjustments to SiB3's soil moisture stress calculations could improve results at Caxiuanã. For example, adjusting the wssp parameter (Equation 2.1) could result in slightly higher stress for medium-range PAW, although such tuning would likely intensify the drought response at Tapajós.

4. DISCUSSION

Our preliminary results show that the default SiB3 captures the response and timing of the drought reasonably well at Tapajós, although the intensity of the drought is slightly overestimated compared to observations. On the other hand, the drought and decreasing soil moisture have little effect on the default SiB3 at Caxiuanã, possibly due to overestimation of soil moisture availability or underestimation of stress at moderate moisture levels. We next discuss some areas that might affect SiB3's ability to reproduce the observed drought responses.

4.1 Exploring differential responses at Caxiuanã and Tapajós

The two forest sites responded differently to drought in both the observations and in SiB3. As discussed in the introduction, the forest at Caxiuanã responded faster to the drought in terms of mortality, LAI and soil respiration. Considering the differences in the precipitation climatology and depth to water table between the sites, it is possible that the forest at Tapajós has more highly-developed drought tolerance-mechanisms than at Caxiuanã. We hypothesize that the forest at Tapajós has both the need and the ability to develop deeper roots than at Caxiuanã. These differences are not represented in the default version of SiB3. Our results show better agreement with observations using a 2 m soil at Caxiuanã and a 14 m soil at Tapajós.

The SiB3 photosynthesis and ET are more sensitive to drought at Tapajós. Differences between the sites in the model include initial soil moisture, driving meteorology, and parameters related to canopy geometry and thickness, roughness length, PBL and canopy air space resistances, and fraction C3/C4 vegetation. The Tapajós meteorology has less annual rainfall, a more severe dry season, and lower humidity. Running the Caxiuanã parameters with the Tapajós meteorology results in a stronger drought response than seen with the Caxiuanã meteorology. In particular, lowering the humidity at Caxiuanã evokes a stronger response. The increased VPD in the canopy air space increases the ET and dries the soil faster. Therefore, part of SiB3's difficulty with simulating the Caxiuanã exclusion is that it is simply too wet (in terms of both precipitation and humidity) for the model to respond under its current configuration. This is consistent with the seasonal replenishment of soil moisture simulated by SiB3 in the treatment plot at Caxiuanã (Figure 2.9). Relatively high amounts of water vapor in the canopy air limit evaporation at Caxiuanã compared to observations (Fisher et al., 2007; Figure 2.7). This could keep the SiB3 soil from drying out and delay the occurrence of drought stress in the model.

4.2 Implications for modeling forest drought tolerance

Tropical forests employ several mechanisms to cope with dry conditions, and one should not expect the entire Amazon forest to respond similarly to a drought (e.g. Phillips et al., 2009). Deep roots are important for capturing the seasonal cycles of surface fluxes under normal conditions and for the drought response at Tapajós. However, different

drought response mechanisms at Caxiuanã mean that we get improved results with a shallow soil. Since rooting and soil depth varies throughout the Amazon, it is realistic to have variable soil depth in ecosystem models. Although since these parameters are poorly observed, a method for estimating them must be used. Climatic data and soil texture have been used in previous studies to estimate root depth (Schenk and Jackson, 2005). Defining deep roots as those below 2 m, they found a low likelihood for deep roots in equatorial rain forests. In this study, two very different soil depths were found to have the best results at the two exclusion sites, although observations at both sites demonstrate that the real soils are at least 8 m deep (Fisher et al., 2008; Belk et al., 2007). The climatic conditions at the sites (longer dry seasons, more frequent dry dry seasons, and less annual rainfall at Tapajós according to GPCP) justify a conceptual model of greater need for a large and accessible water supply at Tapajós. Therefore a future direction for modeling tropical forests can include a climatic predictor of forest drought resistance, which could aid in capturing the heterogeneous effects of drought. More observations of root and soil depth, precipitation, and response to drought in tropical forests could help further constrain this parameterization.

Variable LAI and realistic soil parameters can also help improve model predictions of tropical drought stress. Factors not addressed in this study, such as whether it is primary or secondary forest, tree size, species distribution, and wood density, also affect a forest's drought response (Nepstad et al., 2007; Phillips et al., 2010). Gradients in nutrient variability, fire and disturbance history also influence species composition, and the ability of trees to develop deep rooting systems (Quesada et al., 2009).

4.3 Limitations in SiB3

In both exclusion experiments, trees responded differently to the drought based on tree size, species, and position in the canopy (Nepstad et al., 2007, da Costa et al., 2010). SiB3 can only produce one response because the entire grid cell is represented with the same set of plant characteristics. Tiling is an approach used in other ecosystem models (ie: NCAR's Community Land Model, Oleson et al., 2010) that could improve SiB3's drought response.

The default SiB3 does not include dynamic changes to forest structure that were observed during the exclusions, such as decreased leaf area index, decreased litterfall (Meir et al., 2009; Brando et al., 2008), increased tree mortality (da Costa et al., 2010; Nepstad et al., 2007), and changes to surface roots (Metcalf et al., 2008). A version of SiB with prognostic phenology is being developed (based on Stöckli et al., 2008), and a good test of this model will be at the exclusion sites. An important next step for SiB is to incorporate some of the spatially and temporally varying parameters that affect drought tolerance, such as soil depth and LAI.

Table 2.1. Soil parameters in Tapajos and Caxiuana default SiB. The Caxiuana experiment is discussed in Section 2.2.4. b is used in the soil moisture/potential relationship; ψ_{sat} is the matric potential at saturation (m); K_{sat} is the hydraulic conductivity at saturation (m/s); zm is an exponent used in determining soil moisture effect on heterotrophic respiration, $wopt$ is the optimum soil moisture for heterotrophic respiration, and $wsat$ is a parameter for soil respiration at saturation. ¹Average parameters from Fisher et al., 2008; ²Belk et al., 2007; ³Markewitz et al., 2010.

	<i>Default Soil Parameter (IGBP)</i>	<i>Obs soil and LAI Parameters @Caxiuana</i>	<i>van Genuchten parameters @Caxiuana¹</i>	<i>Obs soil and LAI Parameters @Tapajos</i>	<i>van Genuchten parameters @Tapajos²</i>	<i>van Genuchten parameters @Tapajos³</i>
%clay/sand	36/42	15/79		60/38		
porosity	0.436	0.389	Theta-S = 0.434	0.441	0.450	0.397
field capacity	0.347	0.217		0.380		
wilt point	0.204	0.091	Theta-R = 0.070	0.263	0.220	0.290
PAW _{max} (P-WP)	0.232	0.298	0.364	0.178	0.23	0.107
b parameter	8.634	5.295		12.45		
ψ_{sat}	-0.214	-0.070		-0.2411		
K_{sat}	1.74×10^{-6}	0.002161		3.52×10^{-6}		
zm	0.272	0.362		-0.1198		
wopt	75	75		75		
wsat	0.590	0.538				

Table 2.2. Leaf area index used in the LAI sensitivity tests. Tapajos LAI are from Brando et al. (2008) and Caxiuana LAI are from Fisher et al. (2007). The default values are 6.9288 at Caxiuana, and 6.7537 at Tapajos.

	Tapajos Control	Tapajos TFE	Caxiuana Control	Caxiuana TFE
Default	6.7537	6.7537	6.9288	6.9288
1999	6.30	5.79		
2000	6.30	5.79		
2001	5.94	5.39	5.5	5.4
2002	6.15	4.53	4.8	4.5
2003	5.63	4.26	5.5	4.5
2004	5.46	4.33	5.5	4.5
2005	6.07	4.51	5.5	4.5

Table 2.3. Average annual carbon fluxes at Tapajos from observations at the K67 tower (Malhi et al., 2009), from observations at the control and TFE plots (2000-2004, Brando et al., 2008), and from SiB3 (2000-2004). Units are Mg C/ha/yr.

Tapajos (00-04)	GPP	NPP (ANPP)	Total respiration	Rhet	Rauto	Rcan
Obs: K67 tower	31.4 ± 0.4	14.4 ± 1.3 (11.4 ± 1.2)	29.8 ± 4.4	14.9 ± 1.4	14.9 ± 4.2	
Obs: Tap. Control, TFE		(12.9, 9.9)				
SiB Control (Default)	34.7 ± 2.0	17.3 ± 1.8 (13.0)	34.6 ± 3.5	17.2 ± 3.6	10.7 ± 0.4	6.7 ± 0.4
SiB TFE (Default)	25.9 ± 7.0	12.2 ± 4.6 (9.2)	27.7 ± 6.4	14.0 ± 4.0	8.8 ± 2.0	4.9 ± 1.4

Table 2.4. Average annual carbon fluxes at Caxiuana from observations at the flux tower tower (Malhi et al., 2009), from observations at the control and TFE plots (2005, Metcalfe et al., 2010). GPP in the control and treatment plot is from the modeling study of Fisher et al. (2007) for 2002 and 2003 (denoted by the *). Also shown is GPP estimated from eddy covariance (Carswell 2002). The last two rows are average values from default SiB3 during the modeled exclusion (2002-2005). Units are Mg C/ha/yr.

Caxiuana (02-05)	GPP	NPP	Total respiration	Rhet	Rauto	Rcan
Obs: Cax. Tower	38.2 ± 2.0	10.0 ± 1.2	30.1 ± 4.2	9.4 ± 0.8	21.4 ± 4.1	
Obs: Cax. Control	30.9-31.4*	10.6 ± 0.9	32.6 ± 2.9	10.2 ± 1.0	22.4 ± 2.8	
Obs: Cax. TFE	26.9-27.1*	8.2 ± 1.0	36.6 ± 3.7	10.9 ± 1.5	25.8 ± 3.4	
Obs: Carswell '02	36.3					
SiB3 Control	34.7 ± 2.4	17.4 ± 2.3	34.6 ± 2.7	17.3 ± 2.6	9.9 ± 0.3	7.4 ± 0.3
SiB3 TFE	32.2 ± 2.6	16.0 ± 2.2	32.3 ± 4.1	16.1 ± 4.1	9.5 ± 0.3	6.7 ± 0.5

Table 2.5a. Metrics used for determining optimal soil depth at Tapajos based on ANPP as reported by Brando et al., 2008. 1) RMSE between the control plot ANPP in the model and observations (Brando et al., 2008). 2) RMSE between the treatment plot ANPP in the model and observations. 3) Percent control/treatment ANPP: 5 year average. 4) Year of most severe decline in ANPP & percent control/treatment during that year

Tapajos: ANPP	1	2	3	4
Observation			77.4	2003; 58%
SiB3 - 10 m	1	1.98	70	2002; 46%
SiB3 - 11 m	1	1.68	71.2	2003; 51%
SiB3 - 12 m	1.01	1.4	73	2003; 53%
SiB3 - 14 m	1.03	1.1	75.6	2003; 58%
SiB3 - 15 m	1.04	1.04	77.2	2003; 60%

Table 2.5b. Metrics used for determining optimal soil depth at Tapajos based on monthly latent heat flux measured at the KM83 tower, and compared to the modeling study of Markewitz et al. (2010). 1) RMSE between the control plot latent heat in the model and observed latent heat at the km 83 tower (2001-2003). 2) Percent control/treatment ET: 5 year average (2000-2004). 3) Percent of annual latent heat flux occurring during dry season. 4) Year of most severe decline in ET & percent control/treatment during that year.

Tapajos: LH	1	2	3	4
Observation		91	52	2003; 77%
SiB3 - 10 m	17.39	82	54	2003; 68%
SiB3 - 11 m	17.4	83	54	2003; 69%
SiB3 - 12 m	17.43	85	54	2003; 72%
SiB3 - 14 m	17.47	87	54	2003; 76%
SiB3 - 15 m	17.49	88	54	2004; 77%

Table 2.6a. Metrics used for determining optimal soil depth at Caxiuana based on NPP as reported by Metcalfe et al. (2010). 1) Percent control/treatment NPP (2005). 2) Control NPP in 2005. 3) Treatment NPP in 2005

Caxiuana: NPP	1	2	3
Observations	77	10.6	8.2
SiB3 - 10 m	92	17.4	16
SiB3 - 3 m	84	16.7	14
SiB3 - 2 m	77	16.2	12.5

Table 2.6b. Metrics used for determining optimal soil depth at Caxiuana based on sap flow as reported by Fisher et al. (2007). 1) Percent control/treatment ET in 2002 and 2003. 2) Control ET (2002 - 2003), percent occurring during dry season. 3) Treatment ET (2002 - 2003), percent occurring during dry season

Caxiuana: ET	1a	1b	2a	2b	3a	3b
Observations	56	61	2.45	64	1.50	60
SiB3 - 10 m	100	97	2.54	60	2.49	60
SiB3 - 3 m	92	85	2.47	59	2.27	56
SiB3 - 2 m	84	78	2.4	58	2.07	51

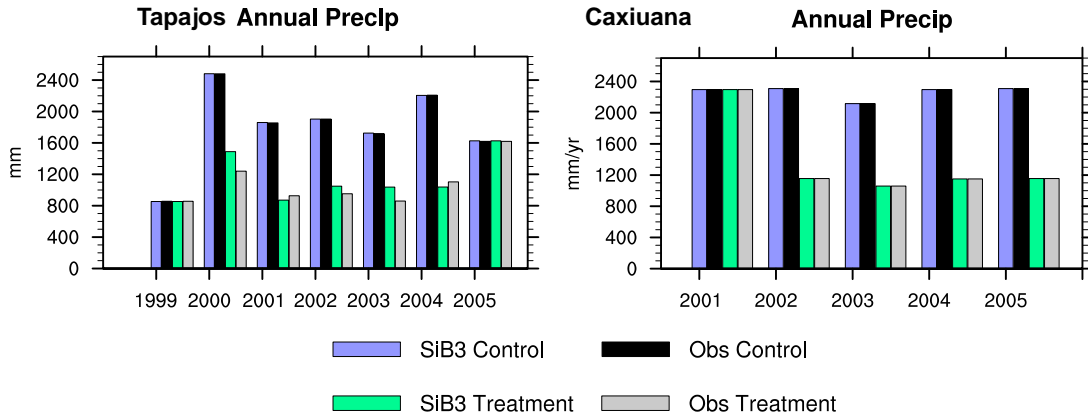


Figure 2.1. Annual precipitation during the Tapajos (left) and Caxiuana (right) experiments. At Tapajos, 1999 precipitation is from July-Dec, and 2005 precipitation is from Jan-Aug.

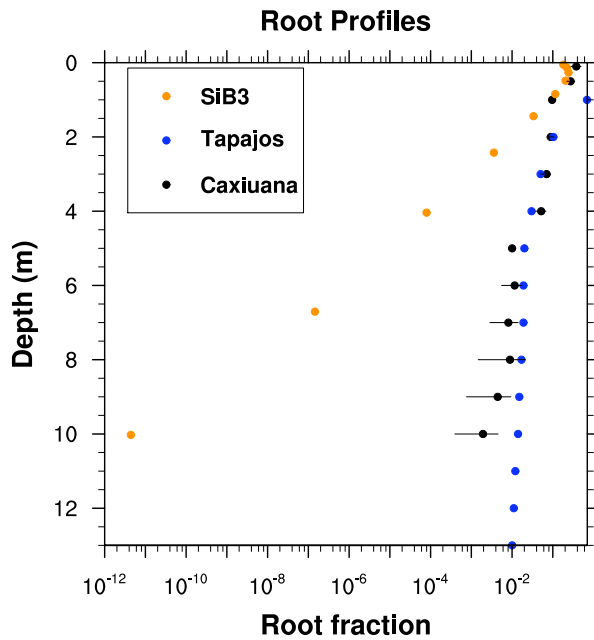


Figure 2.2 Root profiles as observed at Tapajos (Belk et al., 2007) and at Caxiuana (Fisher et al., 2007). Bars indicate standard errors from Caxiuana measurements. Orange circles indicate SiB3 root profile for 10m soil in tropical forest biome.

Tapajos Exclusion

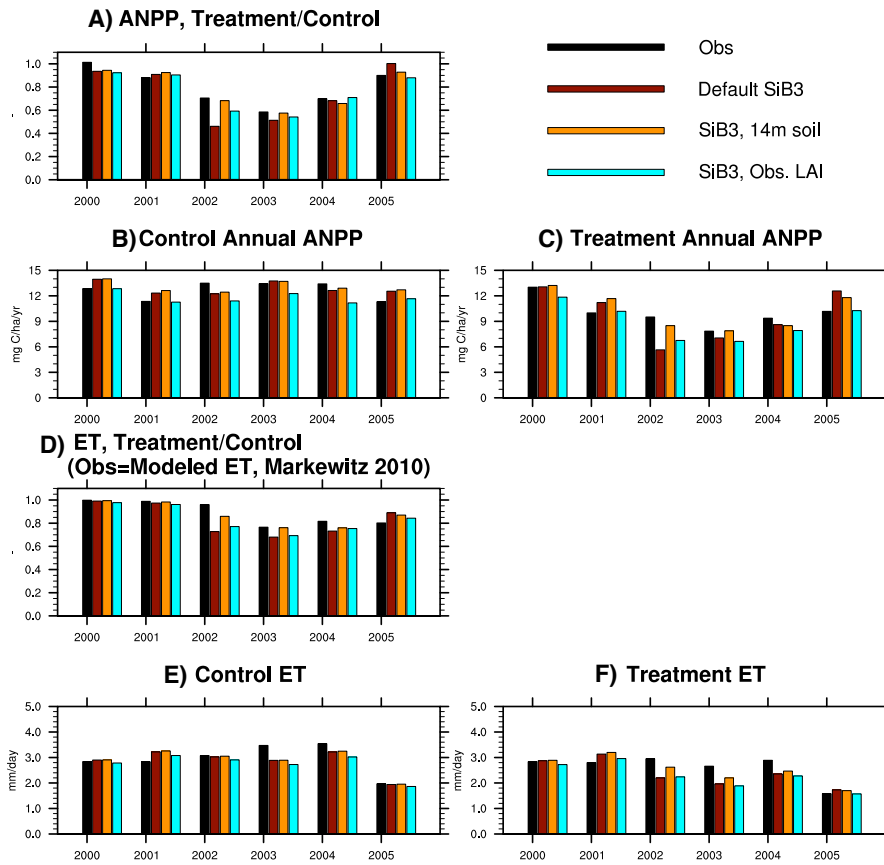


Figure 2.3a Above-ground net primary productivity (ANPP) in the treatment plot compared to the control plot at Tapajos. Observations are from Brando et al. 2008. **3b, c.** Actual values of ANPP in the control and treatment for SiB3 and the observations. **3d.** As in 3a but for evapotranspiration. In this case, “observed” values are from the soil model of Markewitz et al. 2010. **3e,f.** As in 3b and c but for evapotranspiration.

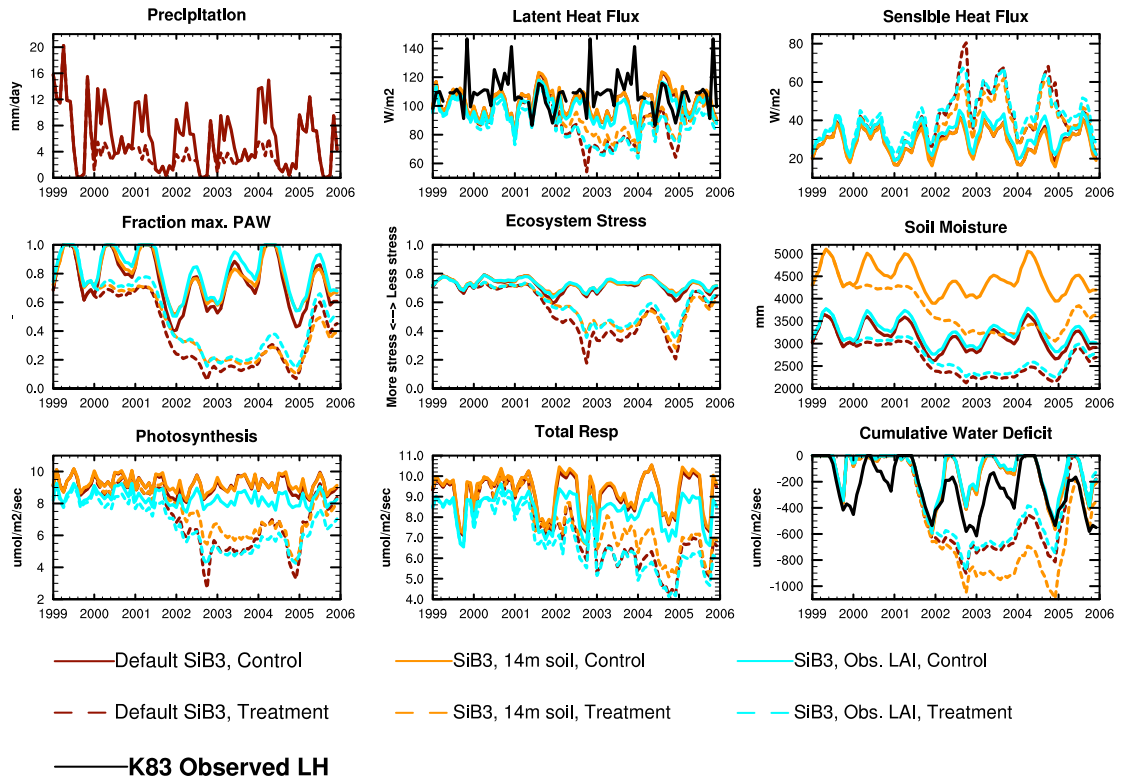


Figure 2.4 Monthly mean results from the SiB3 experiments at Tapajos. Observations are from the K83 flux tower.

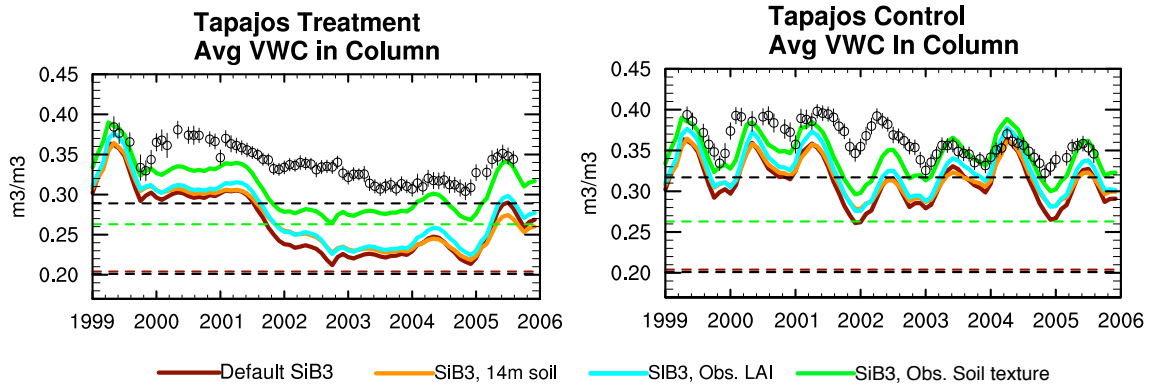


Figure 2.5 Average volumetric water content at Tapajos control (left) and treatment (right). Solid lines are the SiB3 experiments, and open circles are observations, with the line showing standard deviation. Measurements from Markewitz et al. 2010. Dashed lines indicate the wilt point for each soil texture.

Caxiuana Exclusion

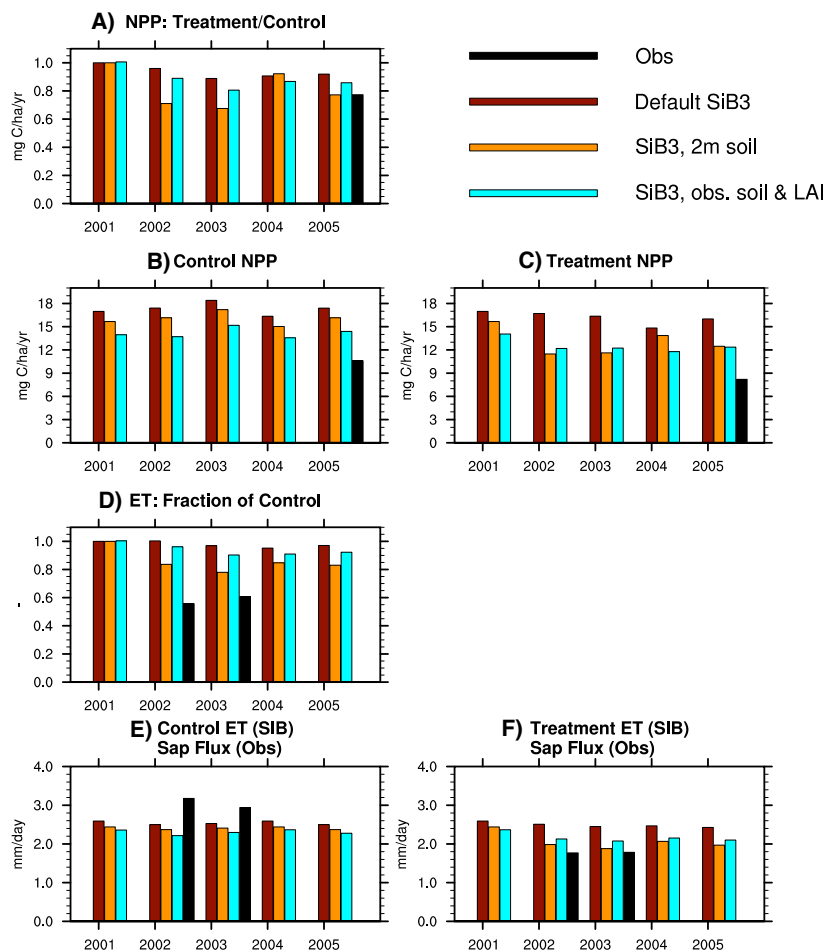


Figure 2.6a Net primary productivity (NPP) in the treatment plot compared to the control plot at Caxiuana. Observations are according to Metcalfe et al. 2010, which were only taken in 2005. **6b, c.** Actual values of NPP in the control and treatment plots for SiB3 and the observations. **6d.** As in 6a but for evapotranspiration. In this case, SiB3 is compared to observations of sap flux from Fisher et al., 2007, which were taken in 2002 and 2003. **6e, f.** As in 6b,c but for evapotranspiration.

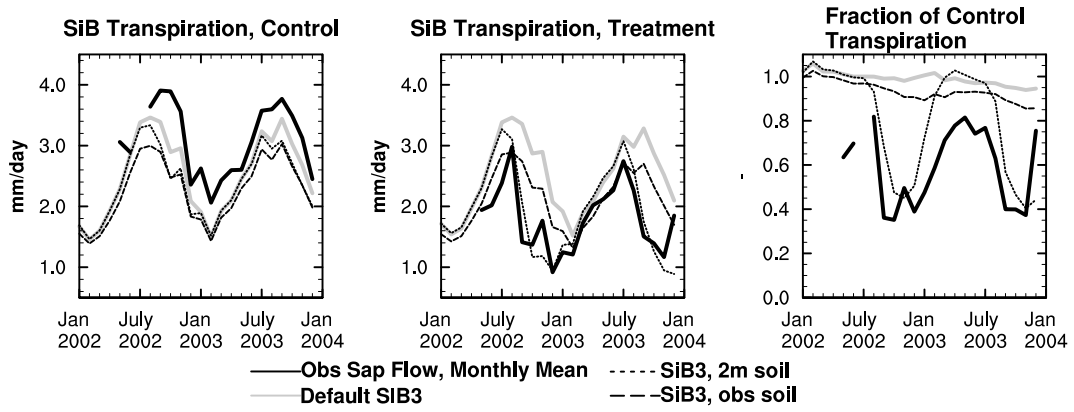


Figure 2.7 Monthly mean observed sap flow and modeled ET at Caxiuana control plot, **b** at the treatment plot, and **c** in the treatment plot compared to the control plot. Sap flow is from daily measurements by Fisher et al., 2007. The blue and orange lines will be discussed later in the text.

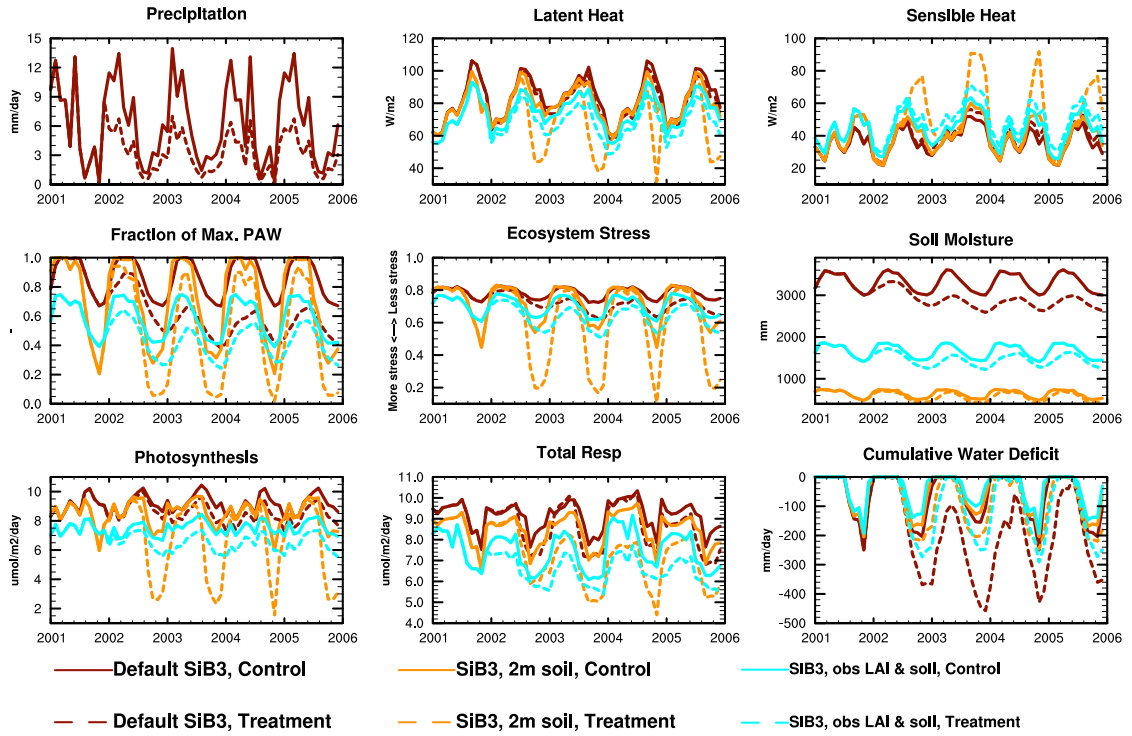


Figure 2.8 Monthly mean results from the SiB3 experiments at Caxiuna.

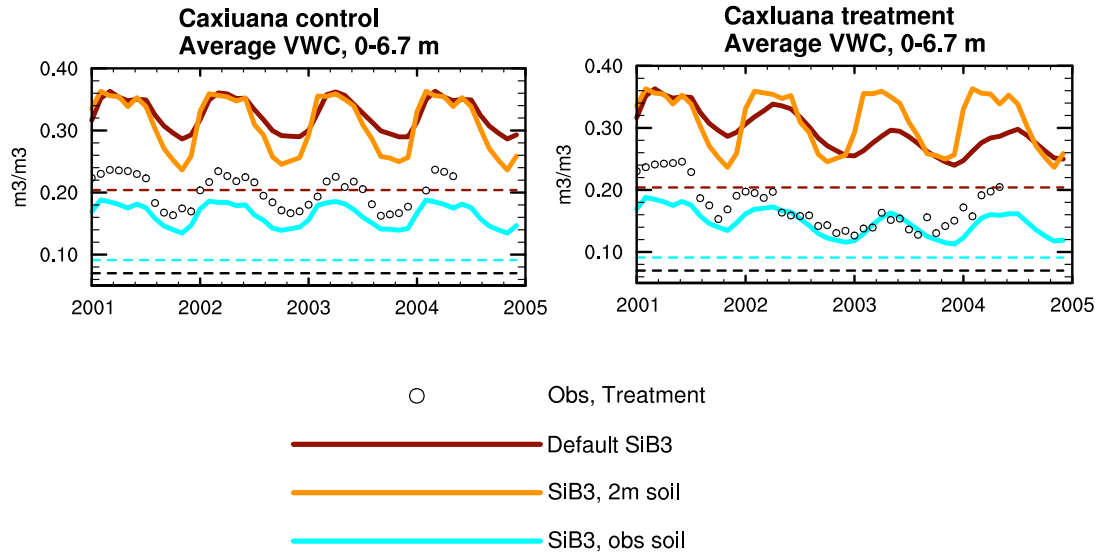


Figure 2.9 Volumetric water content at Caxiuana control and treatment. Solid lines are from the SiB3 experiments, and open circles are observations from Fisher et al., 2007. Dashed lines indicate the wilt point for each soil texture.

CHAPTER THREE:

**REPRESENTING SEASONAL AND INTERANNUAL
DROUGHT RESISTANCE IN AN ECOSYSTEM MODEL**

1. INTRODUCTION

Severe drought in tropical forests dries the soil and can lead to decreased productivity, CO₂ emissions, and increased mortality rates. Ecosystem models assume spatially uniform drought resistance across the Amazon. However, the exclusion experiments at Tapajós and Caxiuanã revealed slightly higher drought tolerance at the Tapajós forest. In this chapter, we use results from the exclusion experiments, precipitation statistics, soil texture, and forest cover to derive an index of stress resistance, which challenges this assumption. High values of the index denote forest that has evolved mechanisms to withstand drought, while low values occur in forests that have little need for drought avoidance techniques. We will test the hypothesis that such an index can accurately represent seasonal and interannual responses to drought.

2. DATA AND METHODS

2.1 Formulation of Stress Resistance Index

We use three data sets for calculating the total stress resistance index: GPCP precipitation, IGBP-DIS soil texture, and forest cover from the SIMAMAZONIA project (<http://www.csr.ufmg.br/simamazonia/>). Monthly mean precipitation from the Global Precipitation Climatology Project (GPCP), version 2.1 (Huffman, 1997; Adler, 2003), is available from 1979-2009 on a 2.5°x2.5° latitude/longitude grid. We chose this product because of the relatively long time period of 31 years. SiB3 is usually run at 1°x1° grid in offline simulations. Therefore, we downscale the GPCP data to a 1°x1° grid. The two other data sets are forest cover from 2001 (Soares-Filho et al., 2006) and soil texture from the International Geosphere-Biosphere Programme (IGBP, 2000).

The total stress resistance index (*TSRI*) is calculated following the chart in Figure 3.1. Ultimately, the *TSRI* is a function of climate, soil texture, and forest cover. We assume that climate will affect root depth, such that forests with occasional dryness have greater need to develop deep roots.

$$TSRI = [root\ depth(CSRI(annual\ P, \# \ of \ dry \ seasons \ that \ are \ unusually \ dry, \ MCWD) + f(texture) + f(forest\ cover)] \quad \text{Equation 3.1}$$

The climatological stress resistance index (*CSRI*) is a function of the annual precipitation, the frequency of drier than usual dry seasons, and the maximum climatological water deficit (*MCWD*) (Figure 3.2). The annual precipitation is calculated beginning the year in September, to line up with the beginning of the hydrologic year in much of the Amazon basin. Dry dry seasons are determined as follows. We first define the dry season as months with less than 100 mm precipitation based on the average seasonal cycle at each point. The mean and standard deviation of dry season precipitation is calculated. Dry dry seasons occur when the dry season precipitation is less than one standard deviation below the mean dry season precipitation.

MCWD is calculated following Malhi et al. (2009a). First, the mean annual precipitation cycle is calculated. Then, the wettest month is found, and we assume that the soil is saturated at this time (soil water deficit, *SWD*=0). Over the next 11 months, we calculate *SWD* as the accumulation of precipitation minus evaporation (assumed to be 100 mm/month):

$$SWD(n) = SWD(n-1) + P(n) - E(n) \quad \text{Equation 3.2}$$

$$MCWD = \min(SWD(1:12))$$

The deficit is constrained to be negative at all times (a negative deficit denotes more water is drawn from the soil column via evaporation than is added through precipitation).

The dry season lasts anywhere from zero to five months in the Amazon forest. The western equatorial Amazon receives the most rainfall (more than 3 m per year - Figure 3.2) and even during the driest three months of the year the average rainfall is greater than 7 mm/day. Annual rainfall decreases and dry season severity and *MCWD* increase to

the south and east of the maximum rainfall.

The three precipitation statistics are collected for three regions: tropical forests in Asia, Africa, and Central/South America. In each region, the spatial mean and standard deviation are calculated, and the data set is standardized. Negative values are assumed to denote drier conditions and therefore stronger resistance (for example, less annual rainfall, more frequent very dry seasons, or higher MCWD) (for this reason, the number of dry dry seasons is multiplied by -1). Positive values denote wetter conditions and therefore we assume that these forests have less need for adaptive mechanisms. Finally, we average the three data sets to create the climatological stress resistance index (CSRI - Figure 3.2d) (note that the final index only exists where SiB3 has tropical evergreen forest).

For a large portion of the Amazon basin, average monthly precipitation is always greater than 100 mm and there is no climatological dry season. We analyzed occurrence of low precipitation months over the 31-year GPCP record and the maximum water deficit at these points (the maximum water deficit is calculated similar to the MCWD except deficit is calculated each year, rather than based on the mean annual cycle). Although some points have years with a ~3 month dry season, the soils remain fairly moist at all times. We conclude that these parts of the forest do not encounter water stress very often and so a high value of the CSRI is appropriate (= low stress resistance).

The next step was to create a data set useable by SiB3 based off the map in Figure 3.2. The most straightforward way to parameterize drought tolerance is by adjusting the amount of water available to the forest. Practically speaking, this means adjusting the

root depth. Previous work comparing SiB3 to observations during two rainfall exclusion experiments yielded an optimal rooting depth of 14 m and 2 m at the Tapajós and Caxiuanã National Forests, respectively. Based on these values, we calculate the *TSRI* at the two sites as:

$$TSRI = (rootd*(\% forest)) + (8*(\% nonforest - \% deforested)) + (0*(\% deforested))$$

Equation 3.3

Here, the assumption is that on the grid-cell level, forest cover mediates resistance. Where nonforest vegetation exists, we assume a root depth of 8 m (e.g. non-forested land near Paragominas, Nepstad et al., 1994). High levels of deforestation significantly decrease the stress resistance of the remaining forests.

We assume that the mean root depth in the Amazon is 10 m, since several ecosystem models have demonstrated improved results using this depth in the tropical forest biome or plant functional type (Baker et al., 2008; Lawrence and Chase, 2009; Verbeeck et al., 2011). Because the CSRI is standardized, we assume 10 m depth corresponds with a CSRI of 0. Also, we assume a maximum depth of 18 m, corresponding with a CSRI of 1.0. We linearly extrapolate between these four points (Tapajós, Caxiuanã, mean and maximum values) to arrive at an equation relating root depth to the CSRI:

$$TSRI = 7.82999*(CSRI) + 10.111$$

Equation 3.4

Next, we account for soil texture. Deep roots are more likely in seasonal forests with coarse or fine soil texture (Schenk and Jackson, 2004), therefore in these regions we increase root depth by 10%. Finally, the index is adjusted for forest cover. This step is the same as described above with Equation 3.3, but now it is applied to the all tropical forest biomes in south/central America. The result is the final *TSRI* shown in Figure 3.3. Stress resistance is highest along the forest edges, where occasional droughts or strong rainfall seasonality have forced forest adaptations. Resistance is low in the forest interior, where rainfall is almost always high, and near the mouth of the Amazon River, where a local maximum in precipitation is located. Resistance is decreased in grid cells with significant deforestation.

As stated above, the values in the index are most closely related to root depths. We compare some values to observations in Table 3.1. The observations are weighted according to Equation 3.3. Manaus is located in a region with high annual precipitation and little interannual variability (annual rainfall is >2500 mm and there is no climatological dry season). Therefore, our index predicts very low drought resistance at this site, although roots are observed to 8 m. Near Paragominas, 54% of the land is deforested, and this strongly reduces resistance. Annual rainfall is ~1900 mm, and six years have unusually dry dry seasons. At this site there is good match between the observations and our index.

It is important to note that while root depth is the simplest way to incorporate evolved stress resistance into SiB3, it would be inaccurate to say the *TSRI* is a map of

root depths. Site to site root depth depends on several factors, such as soil type, local long-term climate, and geology – all of which are poorly observed in tropical forests. However, using the SRI in SiB3 results in realistic responses to seasonal and interannual droughts, and therefore we propose that the index is an appropriate indicator of stress resistance.

2.2 Model simulations

In the results, SiB3-SRI uses the new index. SiB3-Unstressed is the default version of SiB3, with moderate levels of stress resistance in all tropical forests. Despite the nomenclature, SiB3 SRI has higher stress resistance in some regions where the SRI is very high (dark blue in Figure 3.3). Both models are run from 1983-2006 and driven by NCEP Reanalysis meteorology, with precipitation scaled to GPCP to account for known biases in the reanalysis in South America. The models run through the first 23 years once for spin-up, and the results presented here are from the second set of runs. The horizontal resolution is $1^{\circ} \times 1^{\circ}$, and the model time step is 10 minutes.

3. RESULTS

3.1 New Parameterization: Effects on seasonal fluxes

Seasonal cycles of latent, sensible, and carbon fluxes in SiB3 are consistent with observations from multiple tower sites throughout Amazonia (Baker et al., 2011a). The new parameterization has little effect on these seasonal cycles. Here we briefly review the model response at two sites: Manaus (K34; 2.60°S, 60.20°W) and Reserva Jaru (JRU; 10.08°S, 61.93°W).

Manaus has a very wet climate on average, with >2500 mm/year of rainfall. During the driest two months of the year, there is 107-109 mm rainfall (August and September, respectively) (Figure 3.5a). Incoming and net radiation peak during the dry season (July through October). In the observations, both sensible and latent heat fluxes peak in the dry season at Manaus, coinciding with peak incoming radiation. Carbon flux shows slight uptake during most of the year, and slight efflux during the late wet season. SiB3 also produces peak LH and SH during the dry season, although the peak is a few months early in SH. However, the magnitude of wet season LH is underestimated, and SH is overestimated. This is likely related to a dry bias in the reanalysis that drives SiB3, especially during the wet season (Baker et al., 2011a). The sign of SiB3's carbon flux matches observations most of the year. The two exceptions are the early and late wet season. SiB3 simulates the lowest GPP of the year during the early wet season, and therefore the forest is a carbon source. The soils in SiB3 are saturated, and the canopy

assimilation is controlled by light availability. At the end of the wet season, SiB3 switches from a source to a sink a few months before observed, as GPP responds rapidly to increasing radiation and respiration decreases slightly.

The grid cell containing Manaus in SiB3 has much lower resistance in the SRI run, but there is very little effect on the seasonal cycles of latent and sensible heat flux, photosynthesis, and respiration (Figure 3.4a). Due to the reduced drought resistance in SiB3-SRI, dry season ET and GPP are reduced by up to 2% and 4%. The respiration is lower every month, and so the amplitude of the seasonal cycle in carbon flux is damped in SiB3-SRI.

The respiration response is interesting. The largest differences occur during the dry season. During the day, the soils dry slightly as plants transpire water. The drying effect is greater in SiB3-SRI because of the shallower soil, and heterotrophic respiration is higher during the day in this model. At night, heterotrophic respiration is higher in SiB3 Unstressed. Meanwhile, canopy autotrophic respiration is always higher in SiB3 Unstressed because there is less soil moisture stress, and autotrophic respiration is also always higher because there is more assimilation in SiB3 Unstressed. The overall effect is for similar respiration during the day but higher respiration at night in SiB3 Unstressed. Over the course of a month, the total respiration is higher in SiB3-Unstressed.

At JRU, the dry season is very pronounced, and precipitation is less than 100 mm/month from May through September (Figure 3.4b). Very dry dry seasons occurred five times during the GPCP 31 year record, and 63% of the grid cell is deforested. The occurrence of seasonal and interannual drought increases this site's drought resistance,

but the low forest cover decreases it. Overall, the SiB3-SRI has higher drought resistance at this point.

Observed LH and SH show very limited seasonality at JRU (Figure 3.4b). The carbon flux shows uptake during the wet season and efflux during the dry season. The site has a very thin soil, which likely influences this seasonal cycle.

As with Manaus, the changes to the seasonal cycle are small and mostly occur during the dry season, when water limitations might occur. Dry season ET and GPP increase in SiB3-SRI by 1-2% and 3.5%, respectively. Respiration is marginally higher in SiB3-SRI. As a result, the late wet season efflux is increased. Higher GPP during the latter part of the year results in stronger uptake in the dry season and weaker efflux in the early wet season. Since our stress resistance index does not consider variations in geology, it is not surprising that we do not match the observed seasonal cycle of carbon flux at JRU.

The basin-wide seasonal cycles are similar to previous versions of SiB3 (e.g. Baker et al., 2008; Baker et al., 2011b) (Figure 3.5). In the northern hemisphere, precipitation is relatively high all year, with a dry season from September through March. Net radiation is lowest during the wet season, and peaks at the beginning and end of the dry season. SiB3's seasonal cycle of photosynthesis is similar to that of radiation. The high rainfall prevents water limitation and photosynthesis is mostly light-limited. Respiration is slightly higher during the rainy season. As a result, the forest acts as a carbon sink during the beginning and end of the dry season (when GPP and radiation are highest), and as a carbon source during the mid-dry and mid-wet seasons. The simulated seasonal cycles of

GPP and respiration are similar in both versions of the model.

In the southern hemisphere, the dry season is more pronounced and occurs from June through September, coinciding with the austral winter. Incoming radiation peaks late in the dry season. On average, water limitation on photosynthesis is limited, and photosynthesis shows very little simulated seasonal variation. It has a slight minimum at the end of the wet season. Respiration is highest during the wet season. The forest is a carbon source during the wet season, and a carbon sink during the dry season. In SiB3-SRI, forest drought resistance is lower than in SiB3 Unstressed. GPP is less during the dry season and respiration is slightly less year-round. As a result, the wet season source is smaller (Jan. - May) and the late dry season sink is smaller.

3.2 Effect on ecosystem response to interannual climate variations

In SiB3 SRI, the forest is generally more sensitive to interannual variability. Figure 3.6 shows the difference between SiB3 SRI and SiB3 Unstressed in the northern hemisphere tropical forests, southern hemisphere tropical forests, and for the domain-wide tropical forests. The domain-wide differences are mostly due to differences in the southern hemisphere. GPP tends to be lower in SiB3-SRI during or following years with anomalously low precipitation (e.g. 1991, 1997), and vice versa following anomalously wet years (e.g. 1988, 2000). Because of SiB3's assumption of carbon balance, the respiration differences lag the GPP differences. For example, SiB3-SRI assimilates less CO₂ during 1992 than the default SiB3, and so the following year, less carbon is available for respiration. However, there is year-to-year variability in the NEE, with

differences between the models ranging from -0.07 to 0.09 Pg C/yr. The basin-wide NEE is on the order of +/- 0.20 Pg C/yr, and so variations in net ecosystem exchange between the models can be substantial. The models also differ in sensible and latent heat fluxes. Changes to these fluxes have implications for the weather and climate (Harper et al., 2010), and will be the subject of a follow-up paper to this study. Because differences in the model appear to be related to the El Niño Southern Oscillation (ENSO) (Figure 3.6f), we next examine correlations between the Multivariate ENSO Index (MEI) and modeled fluxes.

The MEI is based on six variables observed over the tropical Pacific: sea-level pressure, the zonal and meridional components of the surface wind, sea surface temperature, surface air temperature, and total cloud fraction. A positive MEI indicates El Niño, while negative MEI indicates La Nina. We compute the monthly lag correlation between the MEI and several SiB3 variables. Figure 3.7 shows the correlations that are significant at 99%. A positive MEI (El Niño) is correlation with negative precipitation anomalies, and positive temperature and radiation anomalies in tropical South America (Figure 3.7). The negative correlation with precipitation is greatest in the southern hemisphere at a lag of 0 months, while in the northern hemisphere it is greatest at a lag of 3 months.

The effects of interannual variability on annual fluxes in SiB3 Unstressed are discussed by Baker et al. (2011b), so here we focus on monthly fluxes and explore some differences between the two versions of SiB3. During El Niño there is reduced precipitation throughout much of the Amazon basin (particularly in the east), and warmer

temperatures (Figure 3.8a,b). Negative precipitation anomalies persist for the 6 months preceding and following an MEI event (Figure 3.7a). Basin-wide GPP is negatively correlated with the MEI at positive lags (following an El Niño). A significant correlation emerges in SiB3-SRI at lag 0 ($r = -0.20$) and peaks at 6-7 months ($r = -0.44$) (Figure 3.7d). The forest does not respond as quickly or as strongly in SiB3 Unstressed: GPP becomes significantly correlated with the MEI at a lag of 3 months ($r = -0.21$) and peaks at 7-9 months ($r = -0.37$). Spatially, the strongest response in GPP occurs in the eastern Amazon where GPP is reduced due to soil moisture limitations (Figure 3.9c, d). However, in the west GPP increases since precipitation is not as strongly affected but net radiation increases. The eastern Amazon response to the MEI is stronger in SiB3-SRI. Precipitation remains low for 6 to 9 months, during which time soil moisture is gradually depleted in both runs. After about nine months, the two versions of SiB3 converge.

While GPP is more sensitive to interannual variability in SiB3-SRI, respiration is more sensitive in SiB3 Unstressed. The spatial patterns of correlations between respiration and the MEI are very similar between the models (Figure 3.8e, f). Respiration decreases due to the drier conditions in Guyana, Suriname, and northern Brazil. Elsewhere, respiration increases as a response to warmer temperatures. Domain-wide in SiB3 Unstressed, the respiration has a significant positive correlation with MEI at lag 1-6 months, but it is only significant at 2 months lag for SiB3-SRI (Figure 3.7e). The correlations are stronger in the southern region in both models.

El Niño's are associated with efflux of carbon from the domain. The tendency for reduced GPP and enhanced respiration during El Niño results in positive NEE

correlations with the MEI. The response from NEE is stronger in SiB3-SRI than in SiB3 Unstressed. In SiB3-SRI, the positive correlations with the MEI emerge one month prior to the peak MEI. Domain-wide, the highest correlations occur at a lag of 5 months in SiB3-SRI ($r = 0.55$) and at a lag of 6-7 months in SiB3 Unstressed ($r = 0.48$) (Figure 3.7f). Spatially, the high correlations occur in a zonal pattern south of the Equator and are clearly stronger in SiB3-SRI (Figure 3.8g, h). However, the mechanisms behind the enhanced carbon source during El Niño's are not spatially uniform. In the east, they result from decreased GPP, while in the west they are linked with increased respiration. In the northern hemisphere forests (around Columbia and Ecuador), increased respiration and photosynthesis result in very small net flux, especially in SiB3 Unstressed. Negative correlations between NEE and the MEI exist in the northeast, associated with decreased respiration during El Niño. These results show that El Niño has a spatially varying response on the Amazon forests, and that representing forest resistance in the model results in generally stronger interannual carbon fluxes.

3.3 Case study of two interannual droughts

Here we analyze the effect of two strong droughts on the Amazon forest, as simulated in SiB3-SRI. A strong El Niño occurred during 1997-1998. Most of tropical South America had less than average rainfall in 1997, with precipitation anomalies up to 650 mm/year centered along the equator (Fig. 9a). In 1998, the negative anomalies were strongest to the northwest and southeast. Most of the southern hemisphere forest had reduced precipitation, but increased precipitation occurred in the north central forest (Fig.

10a).

Compared to SiB3 Unstressed, the SRI generally increases stress resistance in the eastern basin and along the edge of the forest, and decreases resistance in the western basin (Figure 3.3). Strong reductions in GPP were simulated in SiB3-SRI in the western and central Amazon during 1997. The strongest decreases occurred in the western Amazon (up to 0.62 kg C/m²/yr, or 6.2 Mg C/ha/yr). Respiration increased in the central-western Amazon basin, linked to increased temperatures, but decreased elsewhere. The net effect on NEE is anomalous carbon uptake in much of the eastern forests, where respiration decreased. In the western forests, the combination of decreased GPP and increased respiration led to an anomalous carbon source. Overall the SRI decreased the forest carbon uptake in 1997, compared to the Unstressed SiB3, mostly due to the stronger GPP reductions in SiB3-SRI.

The drought intensified through early 1998, and GPP was anomalously low almost everywhere in the domain (Figure 3.10). The highest decreases occurred in the western forests. Respiration also was anomalously high in most regions, with the exception of the southwestern basin. The high respiration and low GPP combined for strong carbon fluxes to the atmosphere in 1998 (up to .75 kgC/m²). On average the basin emitted 0.1 kgC/m². The area of evergreen forest in SiB3 is 3.01x10¹² meters, so this represents a flux of .3 Pg C to the atmosphere. In this case, the SRI decreased the flux of carbon from the forest compared to the Unstressed model, mostly because respiration increased more in SiB3 Unstressed.

During the drought of 2005, soil water was reduced by 18-20% its normal levels for

the month of August (Figure 3.11). The drought was most severe during the dry season (JJA). SiB3-SRI simulated reductions of canopy photosynthesis of $\sim 0.10 \text{ kgC/m}^2/\text{month}$ in the western Amazon, where precipitation reductions were the strongest. The model also shows reduced GPP (up to $0.18 \text{ kg C/m}^2/\text{month}$) in the southeastern Amazon, where deforestation has impacted forest stress resistance (38-88% deforestation in this region). As mentioned before, the changes to forest resistance in the model can have important implications for surface heat and moisture fluxes. For example, the difference in latent heat flux between the two models is up to 2.0 mm/day . SiB3-SRI's average August latent heat flux in this region is $3\text{-}4 \text{ mm/day}$, and so this is on the order of a 50% reduction in moisture flux to the atmosphere. Therefore, reductions in forest resistance can reduce the precipitation recycling, potentially reinforcing drought conditions.

4. DISCUSSION

The SRI improves modeled response to severe droughts associated with El Niño and Atlantic SSTs. The changes to seasonal drought response are very small. The index is useful for representing a spatially variable response to drought stress that is consistent with observations. During El Niño events, the SRI results in strong GPP decreases in northeast Brazil, and increases in the western Amazon near Columbia and along the southern edges of the forest (near the border of Brazil with Peru and Bolivia). Respiration increases throughout most of the region, although it decreases to the northeast (near Guyana, Suriname, and northern Brazil). GPP is more tightly correlated to the MEI in SiB3 SRI, while respiration has higher correlations with the MEI in the Unstressed SiB3. Overall, El Niño is associated with efflux of carbon from the region – especially in the northeast, near the mouth of the Amazon River, and in the southern boundary forests. The SRI increases the carbon flux compared to the Unstressed SiB3.

Observations of impacts of the 2005 drought are often conflicting. Ground-based measurements suggest increased forest mortality and decreased growth, while satellite measurements suggest increased productivity due to higher radiation. Our analysis of response to the 2005 drought shows decreases in photosynthesis of 0.10 to 0.18 kg C/m²/month. Over the three months of most severe water deficits and over the area affected by the 2005 drought, this is equivalent to a decrease in photosynthesis of 0.57-1.03 PgC.

This is only slightly less than the biomass loss estimated by Phillips et al. (2009), which included changes to productivity and mortality. In addition, the evaporation is reduced by up to half of its usual value, strongly reducing atmospheric moisture content and feeding back to the canopy.

Ideally we should test the validity of the SRI. The method used in this paper is to test the seasonal and interannual fluxes it produces in SiB3 against observations from flux towers. A second way would be strategically placed rainfall exclusion experiments. An experiment in the everwet western basin would enable testing of the hypothesis that stress resistance is low there. One in the southeast would be enlightening since this is where climate change is projected to have the greatest impacts on precipitation. A third, newly evolving way to test the SRI is through satellite observations. Satellite-derived vegetation indices have high level of uncertainty in the Amazon due to cloud and aerosol contamination. Nevertheless, these metrics of forest health are improving. New products include canopy fluorescence (from the GOSAT satellite) and canopy water content from QuickSCAT (Lee et al., 2012).

Table 3.1 Root depths in parentheses are the optimal values found in SiB3 simulations of the Tapajos and Caxiuana rainfall exclusion experiments.

	Climatologic al Stress Resistance Index	observed or optimal root depth (meters)	%nonforest (% deforested)	adjusted for forest coverage	final Total Stress Resistance Index
Hypothetical minimum	-1.9359				2
Caxiuana	-1.0217	5-10 m (2 m)	8% (7%)	2	
Manaus	-1.1126	8 m	16.8% (7.3%)	7.416	
Hypothetical average	0.0				10
Tapajos	0.6415	10+ m (15.13)	12.5% (11.2%)	14	
Paragominas	0.9628	18 m	53.9% (53.8%)	8.306	
Hypothetical maximum	1.0				18

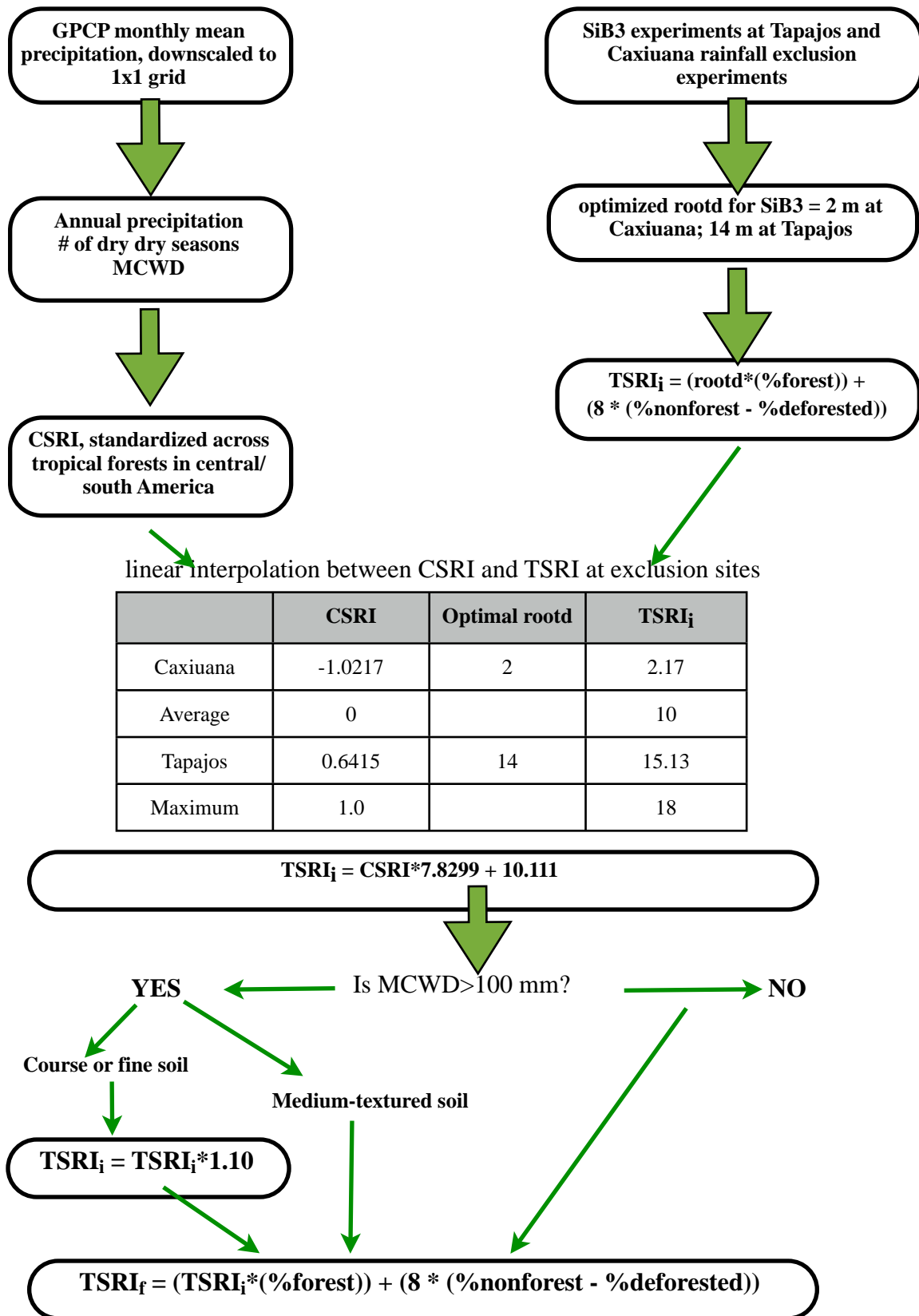


Figure 3.1. Method for calculating the final Total Stress Resistance Index

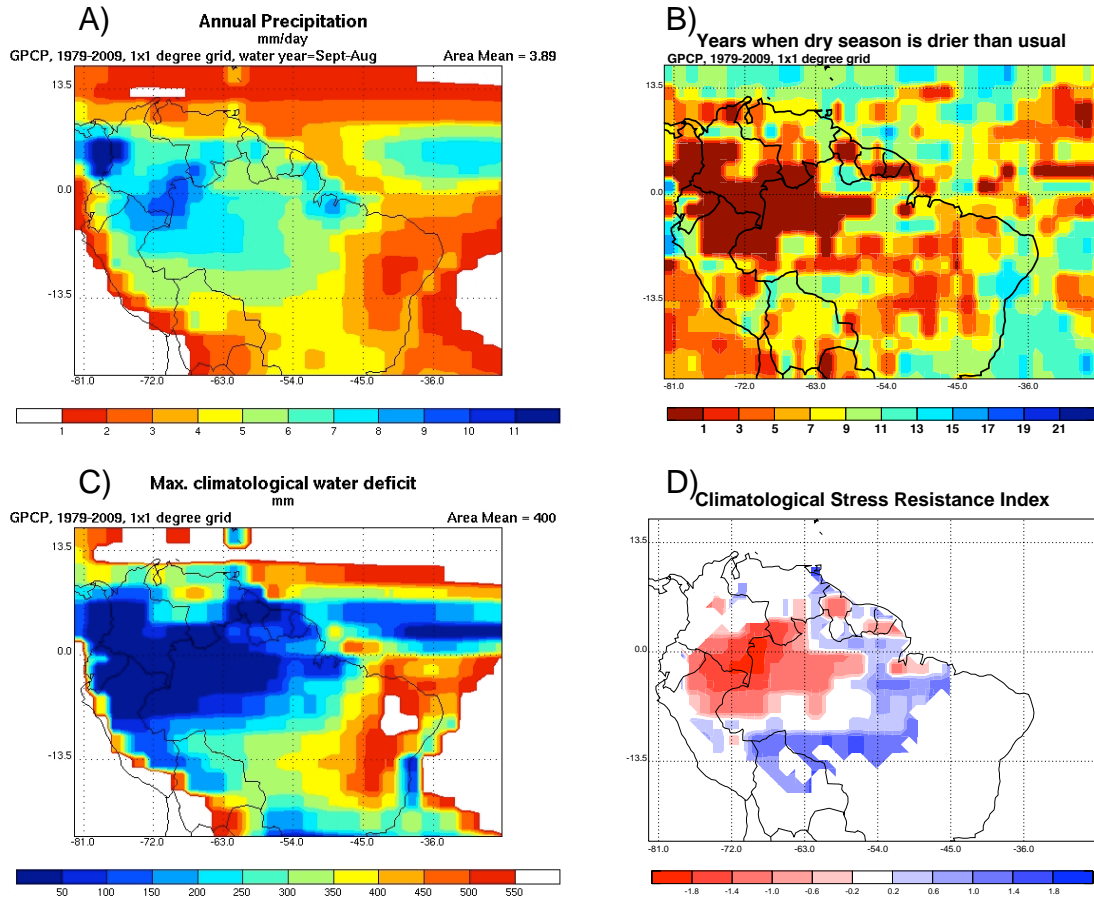


Figure 3.2. A-C Precipitation statistics used in calculating the Climatological Stress Resistance Index (CSRI). D. The CSRI

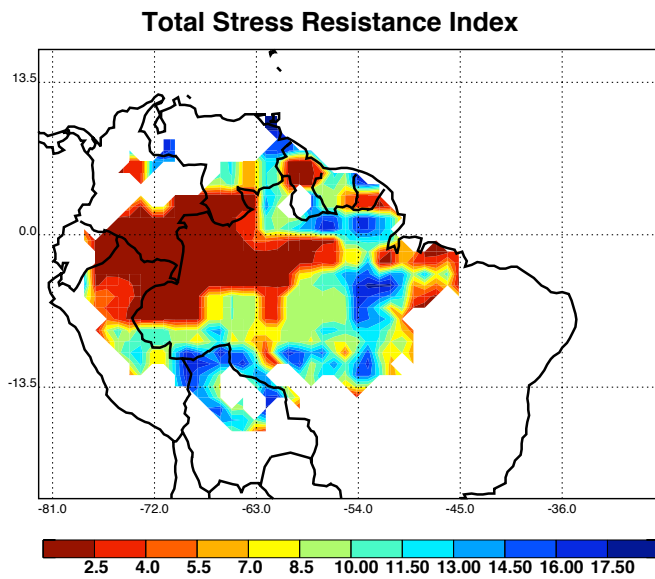


Figure 3.3. The final TSRI

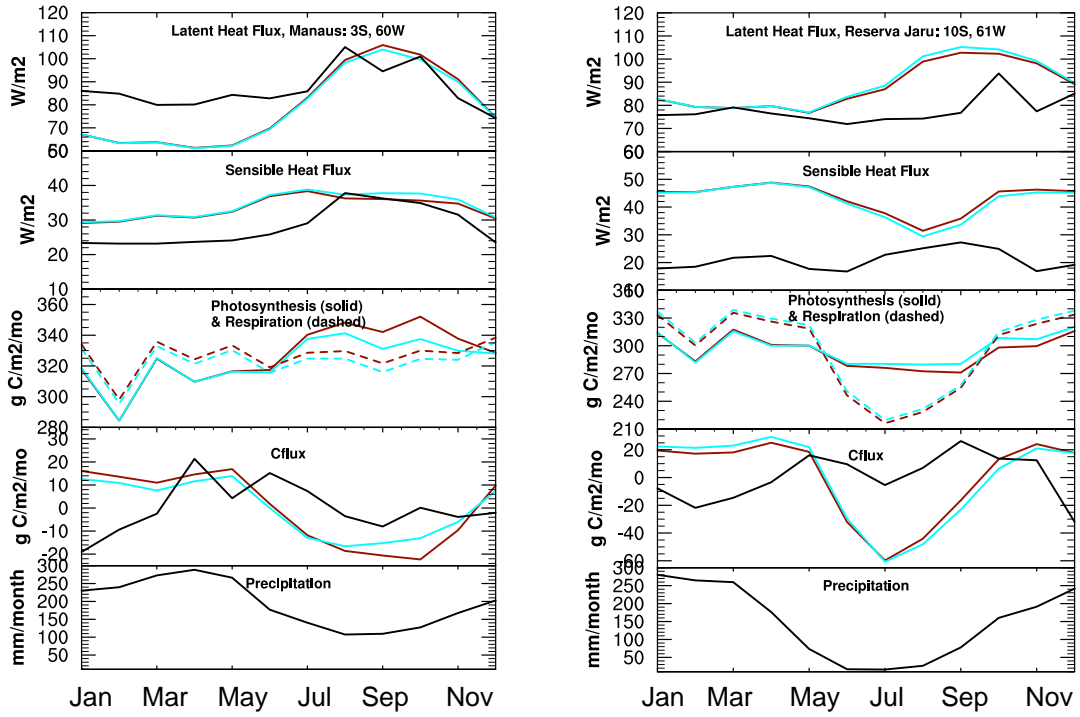


Figure 3.4. Average seasonal cycles at A) Manaus (left) and B) Reserva Jaru (right).
 — Obs
 — SiB3-SRI
 — SiB3-Con

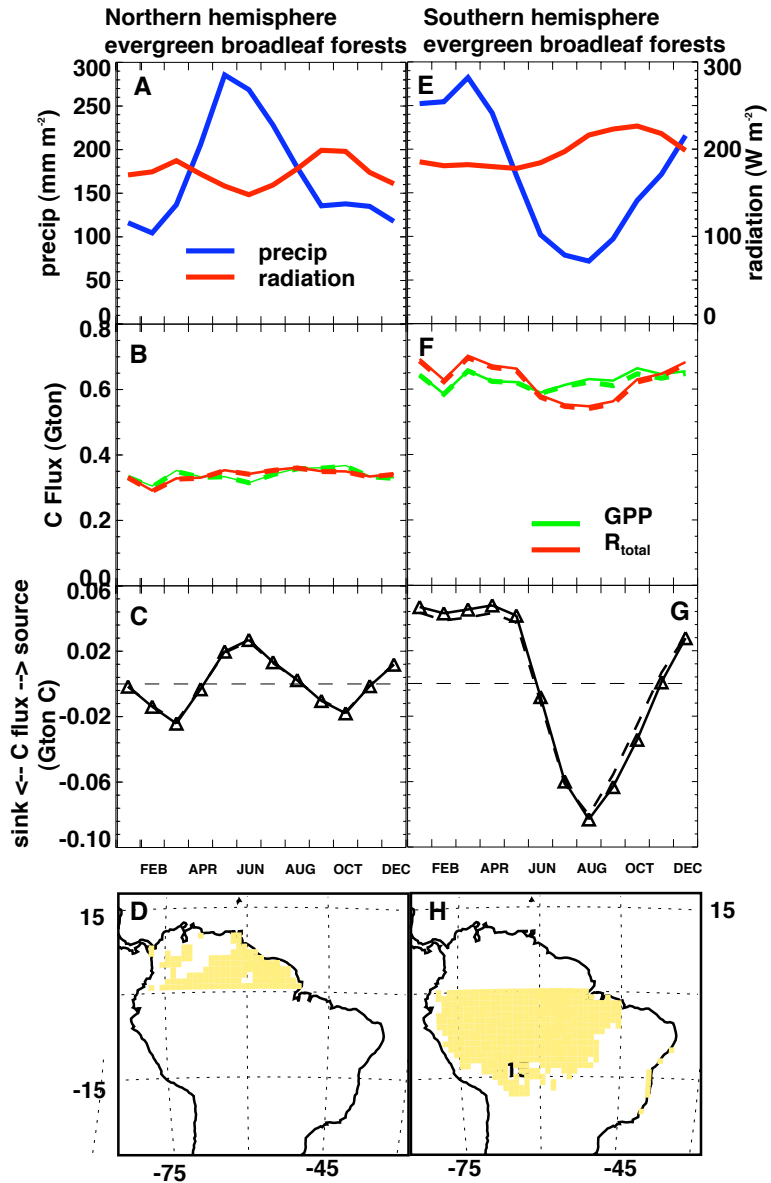


Figure 3.5. Area-averages for northern (A-C) and southern (E-G) hemisphere forests. Points included in the average are in D and H. In B,C and F,G the solid lines are from SiB3-Con, and dashed lines are from SiB3-SRI. Figure reproduced from Baker et al., 2011b.

SiB3 SRI - SiB3 Control: Differences in detrended 3-month running mean anomalies

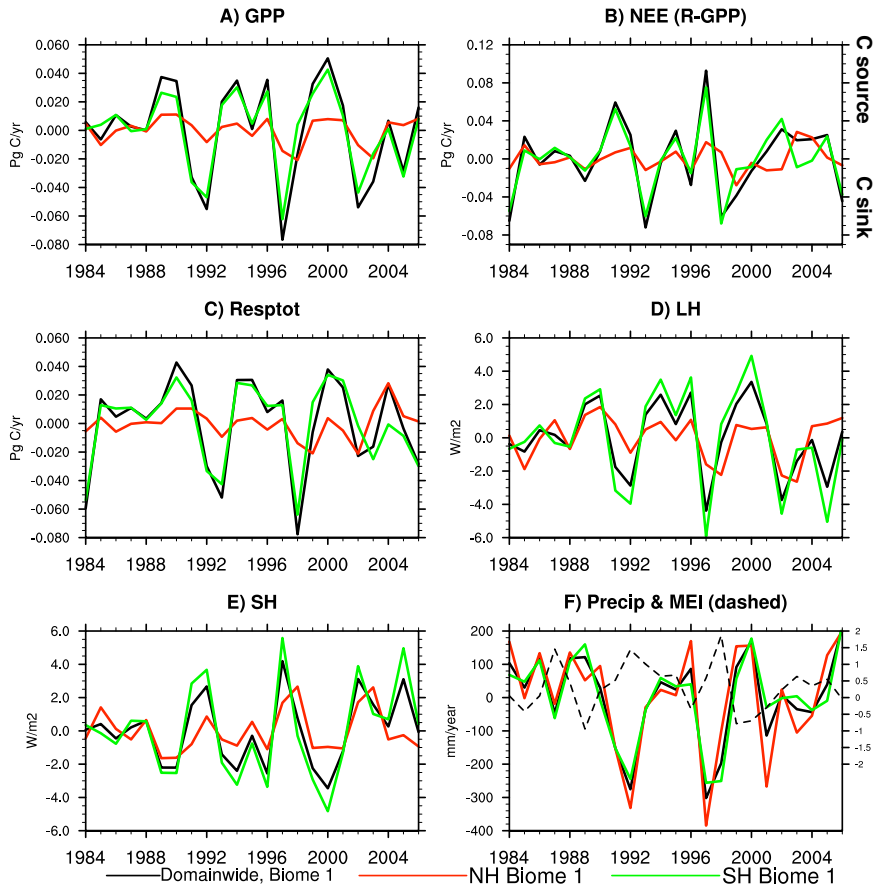


Figure 3.6. Difference between the models' annual average fluxes (A-E). F) Precipitation in each region, and the Multivariate ENSO Index (MEI).

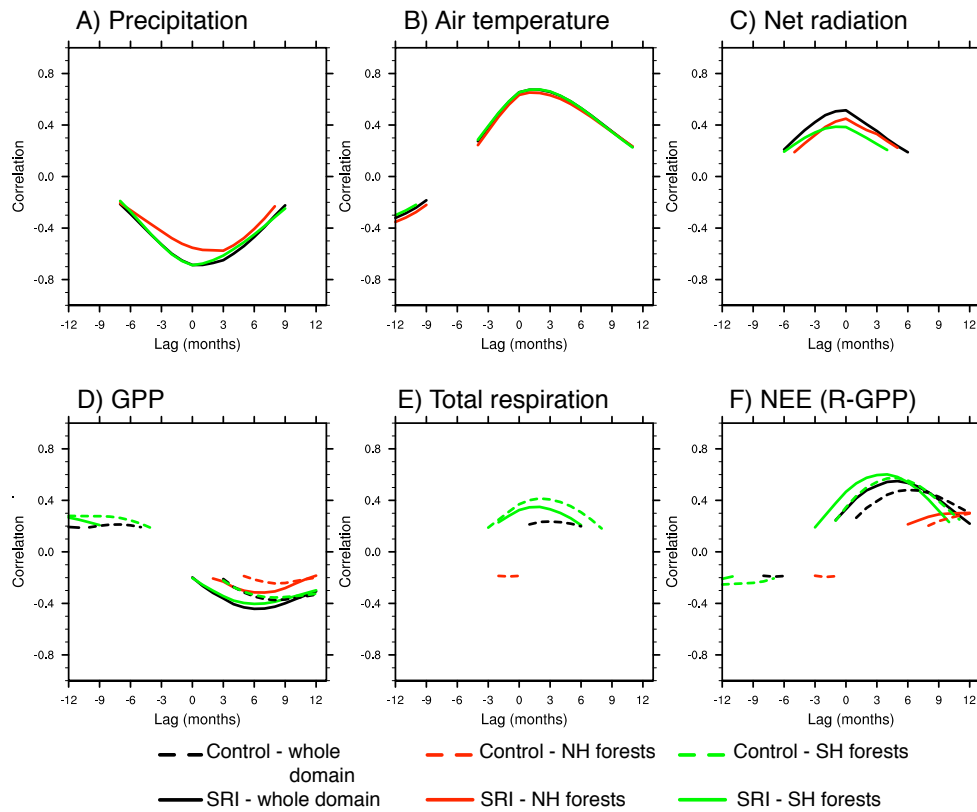


Figure 3.7. Correlations between monthly variables and the Multivariate ENSO Index (MEI). Negative lags indicate the variable leads the MEI, and positive lags indicate the variable lags the MEI. Only correlation coefficients significant at 99% are shown.

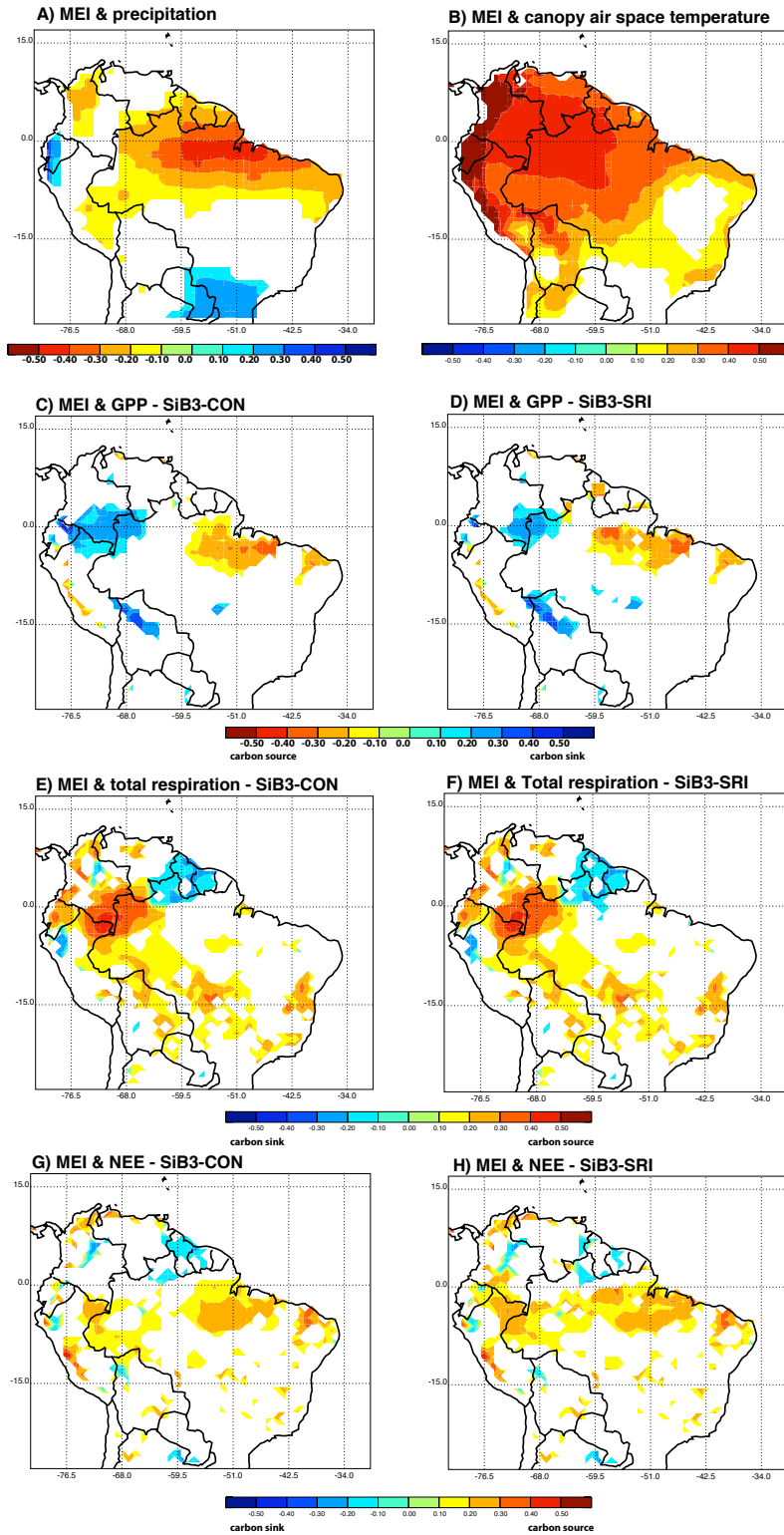


Figure 3.8. Monthly correlations at lag 0 between the MEI and precipitation, air temperature, GPP, respiration, and NEE (R-GPP). For C-H, warm (red) colors indicate a carbon source associated with positive MEI (El Nino); cool (blue) colors indicate a carbon sink during El Nino. Only correlation coefficients significant at 90% are shown.

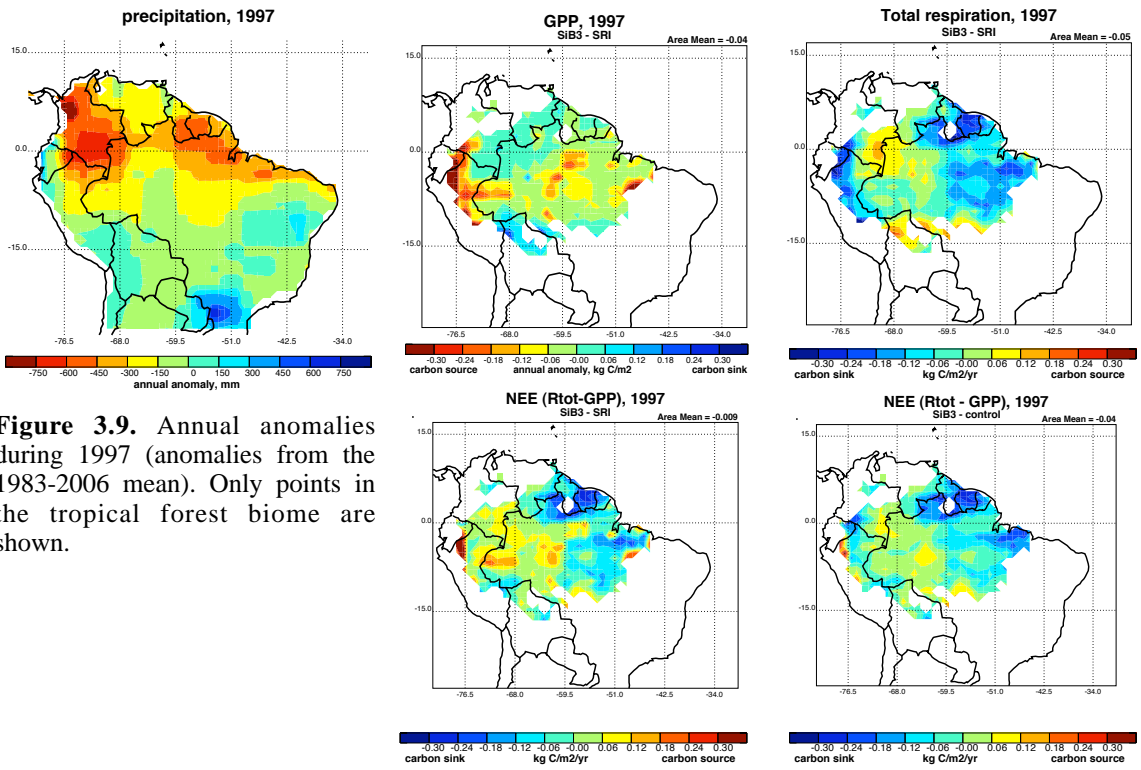


Figure 3.9. Annual anomalies during 1997 (anomalies from the 1983-2006 mean). Only points in the tropical forest biome are shown.

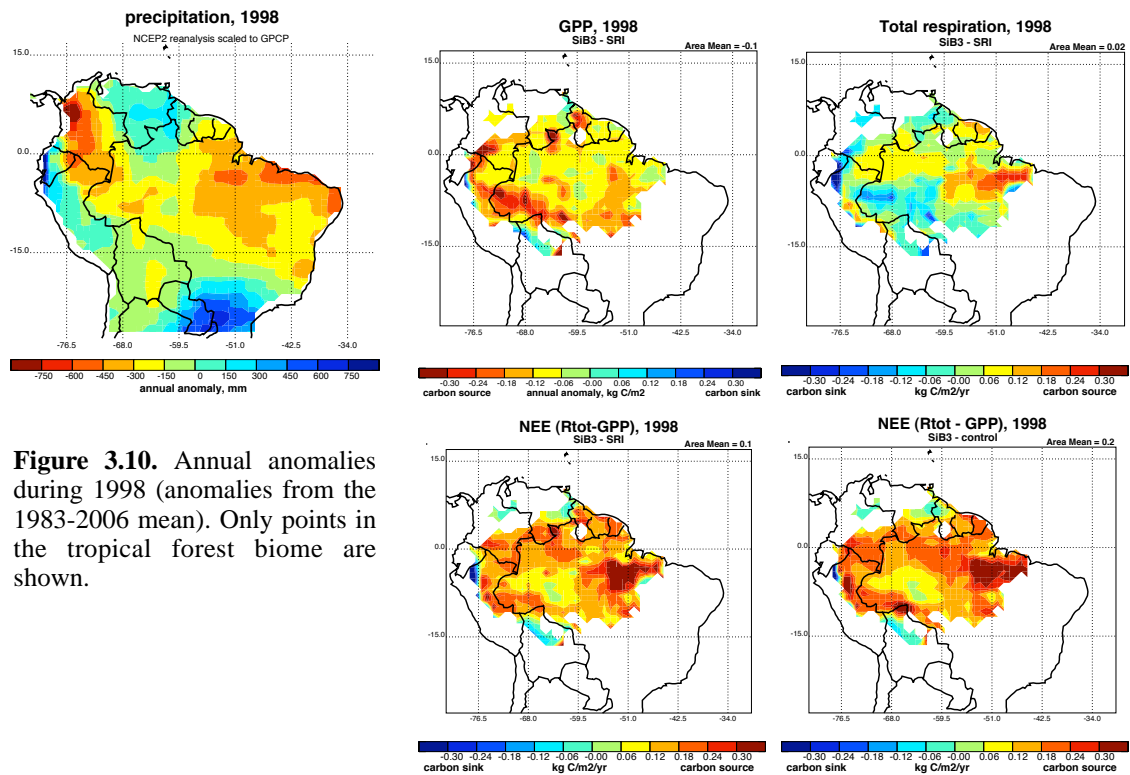


Figure 3.10. Annual anomalies during 1998 (anomalies from the 1983-2006 mean). Only points in the tropical forest biome are shown.

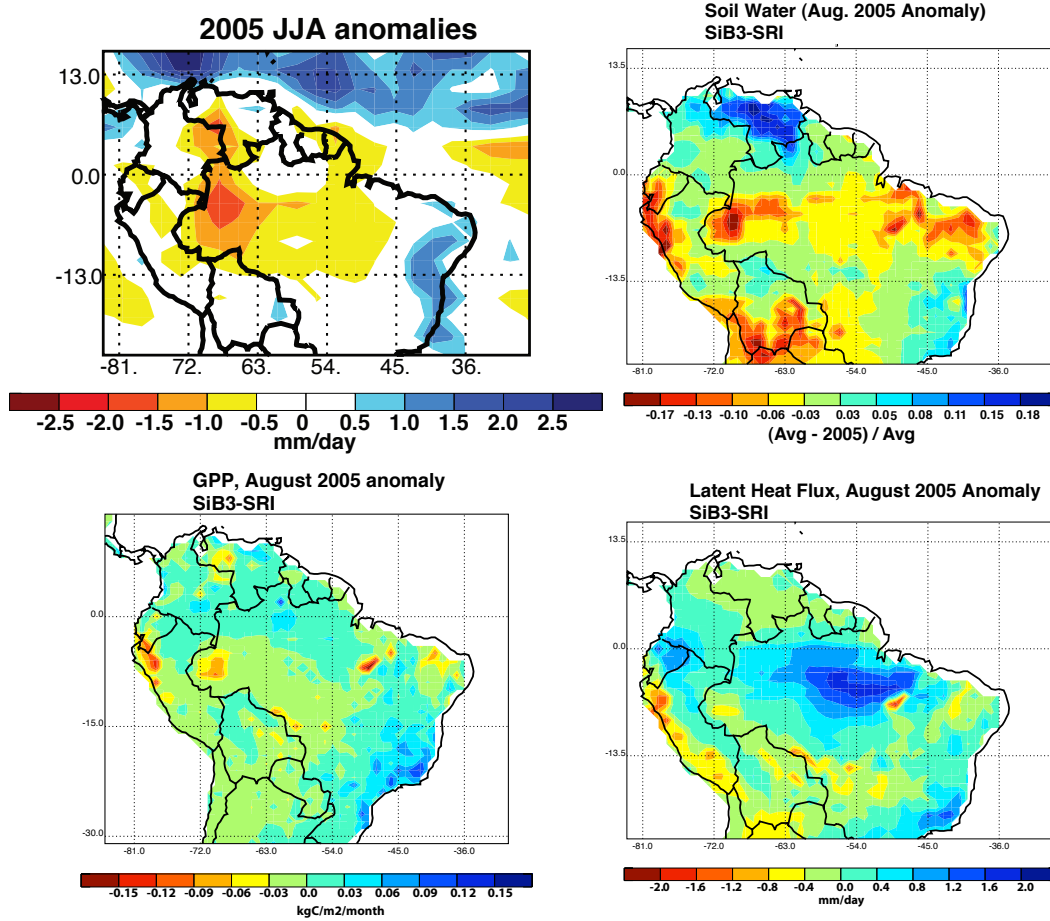


Figure 3.11. Anomalies during the 2005 drought. A) Precipitation anomalies in GPCP during JJA. B) SiB3-SRI anomalous soil water during August (anomaly is from the average August, 1983-2006). C, D) Anomalous GPP and latent heat flux from SiB3-SRI.

CHAPTER 4:

**ROLE OF DEEP SOIL MOISTURE IN MODULATING
CLIMATE IN THE AMAZON RAINFOREST**

A version of this chapter was published by the American Geophysical Union (AGU).
Reproduced by permission of AGU:
Harper AB, AS Denning, IT Baker, MD Branson, L Prihodko, DA Randall (2010): Role
of deep soil moisture in modulating climate in the Amazon rainforest. *Geophysical
Research Letters*, **37**, L05802, doi: 10.1029/2009GL042302. Copyright 2010 AGU.

1. INTRODUCTION

More than one-third of the Amazon's evergreen forests experience dry seasons lasting at least three months (Nepstad et al., 1994), and yet the forest seems to thrive during the dry, sunny months. Understanding the mechanisms that enable the forest to live through extended dry periods is of particular importance considering that changes in both climate and land use are predicted to cause a drier Amazonian climate (Cox et al., 2004).

Adding more realistic root and soil functions in SiB3 resulted in more realistic surface fluxes at certain sites in the Amazon (Baker et al., 2008). This paper aims to examine the effects of these changes on the simulated hydrologic cycle when SiB3 is coupled to a single column version of a GCM. Ultimately, SiB3 will be coupled to a global GCM. This study contributes to our understanding of the interactions between surface properties and climate in Amazonia.

2. METHODS

2.1. SiB

SiB is based on a land-surface parameterization scheme that computes biophysical exchanges (Sellers et al., 1986) and ecosystem metabolism (Sellers et al., 1996; Denning et al., 1996). SiB calculates fluxes of heat, moisture, momentum, and CO² from the gradients of each between the canopy air space (CAS) and the free atmosphere, scaled by a resistance. The monthly maximum value of the normalized difference vegetation index, from the Advanced Very High-Resolution Radiometer data, is used to derive parameters such as leaf area index and photosynthetically available radiation. The potential photosynthetic rate is scaled by these parameters, along with three stress factors that act to maximize carbon assimilation while minimizing water loss. Stress can originate from less than optimal temperature, canopy air space humidity, and soil moisture. This study focuses on the latter.

We compare two versions of SiB3, SiB3 Stressed and SiB3 Unstressed, which have four main differences. The latter version corresponds to the deep soil SiB3 discussed by Baker et al. (2008). The root depths are 3.5 and 10 meters in SiB3 Stressed and SiB3 Unstressed, respectively, allowing the latter to hold more soil moisture. In SiB3 Stressed transpired water is removed from the soil based on root fractions in each layer, which does not account for the importance of hydraulic redistribution and deep roots. Although

root density is low in the deepest layers, most of the water resides in these layers. Observational studies have noted the ability of deep roots to access large amounts of water (e.g., Jipp et al., 1998, Nepstad et al., 1994). In SiB3 Unstressed, transpired water is removed from an “apparent” root fraction, accounting for both actual root fraction and moisture content in each layer.

In SiB3 Stressed, soil moisture stress increases rapidly once soil moisture drops below the wilting point. This response is realistic on a plant-by-plant basis. However, in reality soil moisture and water table depth can vary greatly within a grid cell, and not all plants reach the wilting point at the same time. Therefore, in SiB3 Unstressed, soil moisture stress increases more gradually in response to decreasing soil moisture. Finally, the optimum soil moisture for heterotrophic respiration is increased from 67% to 75% of saturation in SiB3 Unstressed, which is more in line with observations in the Amazon (Baker et al., 2008).

2.2. SCM

We performed numerical simulations using a single-column version (SCM) of BUGS5, an atmospheric GCM that has evolved from the 1980’s UCLA GCM. The model uses a modified sigma coordinate with a prognostic planetary boundary layer (PBL) (Randall et al., 1985). The PBL depth changes due to horizontal mass flux divergence, entrainment of air from above the PBL, and loss of mass due to convection. The entrainment rate is predicted by integrating the turbulent kinetic energy (TKE) conservation equation over the depth of the PBL (Denning et al., 2008). Positive

entrainment occurs due to production of TKE by buoyancy and shear, while consumption by downward buoyancy fluxes and dissipation of TKE reduce entrainment. The PBL depth is constrained to be between 10 and 160 hPa.

BUGS5 uses a modified Arakawa-Schubert cumulus parameterization with prognostic closure (Ding and Randall, 1998), and cloud microphysics as described by Fowler and Randall (2002). The radiative transfer scheme is based on work by Gabriel et al. (2001) and Stephens et al. (2001). Aerosol loading is assumed to be light during the wet season, and heavier during the late dry season when fires are common. Values for aerosol optical thickness, single scattering albedo, and asymmetry factor are assigned as in Table 4.1 based on observations from Franchito et al. (2002), Andreae et al. (2002), Schafer et al. (2002), and Tarasova et al. (1999).

Horizontal advective tendencies of temperature and water vapor are prescribed using relaxation forcing (Randall and Cripe, 1999). Profiles of temperature and water vapor are relaxed toward their observed upstream values, scaled by a relaxation timescale. Relaxation forcing guarantees that the modeled soundings of the state variables will be realistic and enables comparisons of SiB's results to surface observations of fluxes of heat, moisture, and carbon dioxide.

The SCM is forced by six-hourly NCEP Reanalysis II (Kalnay et al., 1996). Since the footprint of the column ($2.5^{\circ} \times 2.5^{\circ}$) is larger than the footprint of the tower, we do not expect the model to exactly mimic the tower observations, but we do expect the same seasonal cycles. We run the model from 2001–2003 five times to allow for soil moisture spin-up. The results shown are from the fifth iteration.

2.3. Site Description

The flux tower in the Tapajós National Forest was operated from 2001 to 2004 as part of the Large-scale Biosphere-Atmosphere Experiment in Amazonia (LBA), an international research initiative led by Brazil. The tower is near the kilometer 83 marker on the Santarem-Cuiaba highway (BR 163), approximately 70 km south of Santarem, in Para, Brazil (3.01°S, 54.58°W). Data from the tower includes half-hourly measurements of air temperature, precipitation, radiation, and fluxes of heat and water vapor. The experimental design and instrumentation are fully described by Goulden et al. (2004), da Rocha et al. (2004), and Miller et al. (2004).

3. RESULTS

3.1. Seasonal Hydrologic Cycle

In SiB3 Stressed, evaporation has a strong seasonal cycle due to increased ecosystem stress. In the dry season this version of the model, the forest transports moisture away from areas of sustained ET. The dry season precipitable water content is 0.6 to 1.6 mm higher, and moisture advection is 1–2 mm day⁻¹ stronger compared to SiB3 Stressed (Figure 4.1b, d). The monthly rainfall totals are not strongly affected by these changes, and modeled and observed rainfall is similar in both versions of the model (Figure 4.1a).

The stronger hydrologic cycle in SiB3 Unstressed is consistent with observations. The plot of P-E (Figure 4.1e) represents our best estimate of the observed hydrologic cycle at the tower. Calculated advection from NCEP Reanalysis variables is also shown in Figure 4.1d. SiB3 Unstressed is within the range of the observations during most months, and particularly during the dry seasons.

3.2. Seasonal Heat and Moisture Fluxes

Simulated fluxes of sensible and latent heat are compared to tower observations in Figure 4.2. The seasonal cycles of latent and sensible heat are too strong in SiB3 Stressed. The errors are largest during the dry season, when latent heat is too low and

sensible heat is too high. The seasonal cycle of latent heat flux is more realistic in SiB3 Unstressed, consistent with results from Baker et al. (2008), who showed that similar changes in an offline version of SiB3 resulted in improved fluxes of CO₂ at the same site.

The differences between SiB3 Stressed and Unstressed have important implications for simulating the regional climate. The canopy air space (CAS) is cooler and more moist in SiB3 Unstressed, although in the observations it is always cooler and drier near the surface. During the dry season, weaker PBL buoyancy and shear result in less TKE production and a generally shallower PBL in SiB3 Unstressed (Figure 4.2f). Because of the decreased PBL depth and temperature and increased PBL moisture, it is unlikely that SiB3 Unstressed will produce a hydrologic shutdown like that in SiB2/BUGS5 (Liu, 2004). The improvements in SiB3 Unstressed could improve simulations of precipitation and moisture fluxes in a global coupled GCM.

3.3. Dynamical Implications

Increased atmospheric moisture can result in increased condensation and latent heating. SiB3 Unstressed consistently has stronger atmospheric heating during the dry season from the surface to 500 hPa. During the wet season, SiB3 Unstressed (SiB3 Stressed) has stronger heating from 400–600 hPa (from 700–925 hPa and from 200–300 hPa). The differences in atmospheric heating between the models primarily by upward motion, which must be compensated for by descending air elsewhere (Hoskins and Karoly, 1981). It is not unreasonable to expect that using SiB3 Unstressed in a global model will result in stronger dry season atmospheric heating throughout the Amazon.

This would result in stronger rising motion above the basin, a low-level vorticity source and an enhanced surface trough to the west (Hoskins and Karoly, 1981). The increased low-level moisture in SiB3 Unstressed results in higher vertically integrated moist static energy and weaker gross moist stability during most months of the simulation, consistent with the results of a stronger hydrologic cycle in this version of the model.

3.4. Wet Season Characteristics

Wet season onset is defined as the first pentad with greater than 3.33 mm day^{-1} of rain, where at least three of the following six pentads are above and four of the previous six pentads are below the threshold (Li and Fu, 2004) (Table 4.2). Figure 4.3 shows the evolution of the PBL, rainfall, and moisture advection during the transition between dry and wet seasons. Prior to wet season onset, SiB3 Unstressed has lower surface sensible heat flux and buoyancy, leading to lower TKE production and entrainment at the PBL top. Both versions of the model relax to the same upstream water vapor profile, but in SiB3 Unstressed the PBL is less diluted by free tropospheric air, surface evaporation is higher, and hence the PBL relative humidity is higher.

In the model, the degree to which these factors influence wet season characteristics is related to the relative importance of local and large-scale processes. In 2002, the wet season begins 15 days earlier in SiB3 Unstressed compared to SiB3 Stressed (Figure 4.3e). Throughout the wet season, the mean entrainment rate and PBL depth are lower, evaporation is higher, and the rainfall rate is higher (Figure 4.3 does not show the full wet season). In late 2002 and early 2003, the upstream profile is drier than the previous year.

During the 2003 wet season, the PBL is deeper in SiB3 Unstressed, and evaporation and precipitation are lower. In both dry seasons, the rainfall intensity is more realistic in SiB3 Unstressed, although cumulative wet season rainfall is more realistic in SiB3 Stressed in 2003 and both models end the wet season too early (Table 4.2).

4. DISCUSSION

This study highlights the importance of root-zone processes in the hydrologic cycle and circulation of the Amazon region. Previous versions of SiB and other ecosystem models parameterize root-zone moisture stress based on shallow soils where roots can only access water in their respective layers. This study and others (Baker et al., 2008; Liu, 2004) show that such parameterizations do not accurately capture the seasonal cycles of heat, moisture, and carbon dioxide fluxes at sites throughout the Amazon. The changes made to SiB3 are motivated by observations in the Amazon and differ from historical land surface treatments in the tropics. In the single column model, all large-scale dynamics are constrained by NCEP II reanalysis and therefore the model's effect on the atmosphere is limited to local processes. Despite this, the changes to the land surface affect the hydrologic cycle, boundary layer, tropospheric dynamics, and wet season characteristics. The improved surface representation will likely affect the large-scale circulation and regional hydrologic cycle if implemented into a fully coupled GCM.

Table 4.1 Aerosol Optical Properties^a

	Wet Season	Transition Season	Dry Season
Optical thickness (SW)	.050	.080	.100
Single scattering albedo (SW)	.989	.989	.989
Asymmetry factor (SW)	.743	.743	.743
Optical thickness (LW)	.030	.040	.100
Single scattering albedo (LW)	.696	.696	.588
Asymmetry factor (LW)	.779	.779	.631

^aBased on preliminary model runs, the wet season is January through June, the transition season is July and August, and the burning season is September through December.

Table 4.2 Comparison of Wet Season Characteristics Between S3_Stressed, Unstressed, and Observations at KM83

	S3_Stressed	S3_Unstressed	KM83
2002 dates	Jan. 15–June 8	Jan. 1–June 18	Jan. 10–June 28
2002 rainrate (mm day ⁻¹)	5.87	6.04	6.25
2002 total rainfall (mm)	821	966	1062
2003 dates	Jan. 15–May 5	Jan. 20–May 5	Jan. 25–June 13
2003 rainrate (mm day ⁻¹)	8.22	7.70	6.47
2003 total rainfall	945	847	938

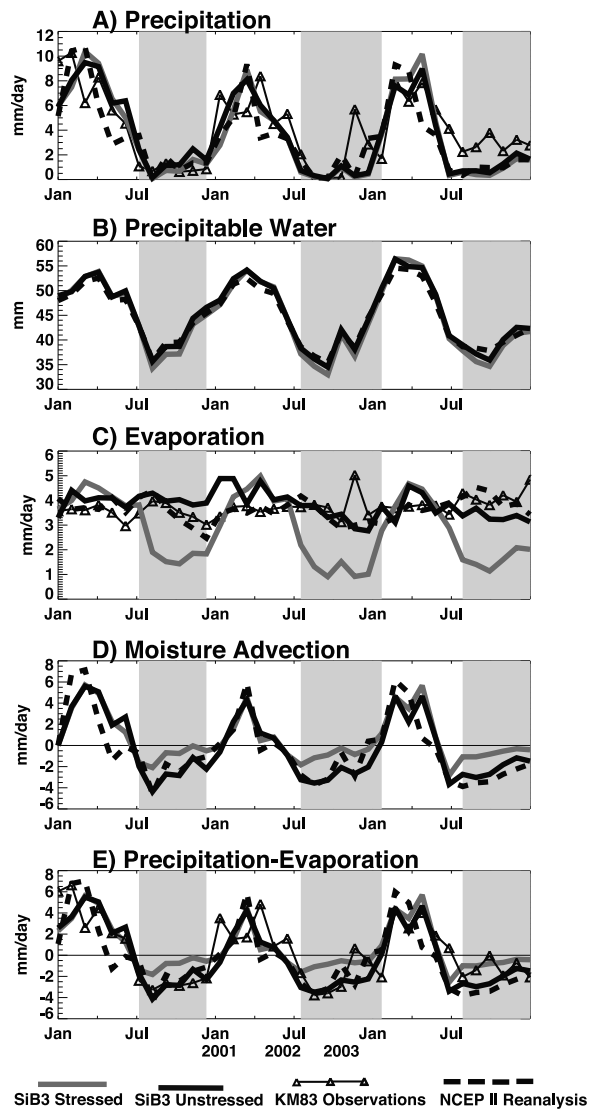


Figure 4.1 (a–e) Monthly mean composites of the hydrologic cycle. In Figure 1d, comparison is made to moisture advection calculated from NCEP Reanalysis precipitation, evaporation, and precipitable water.

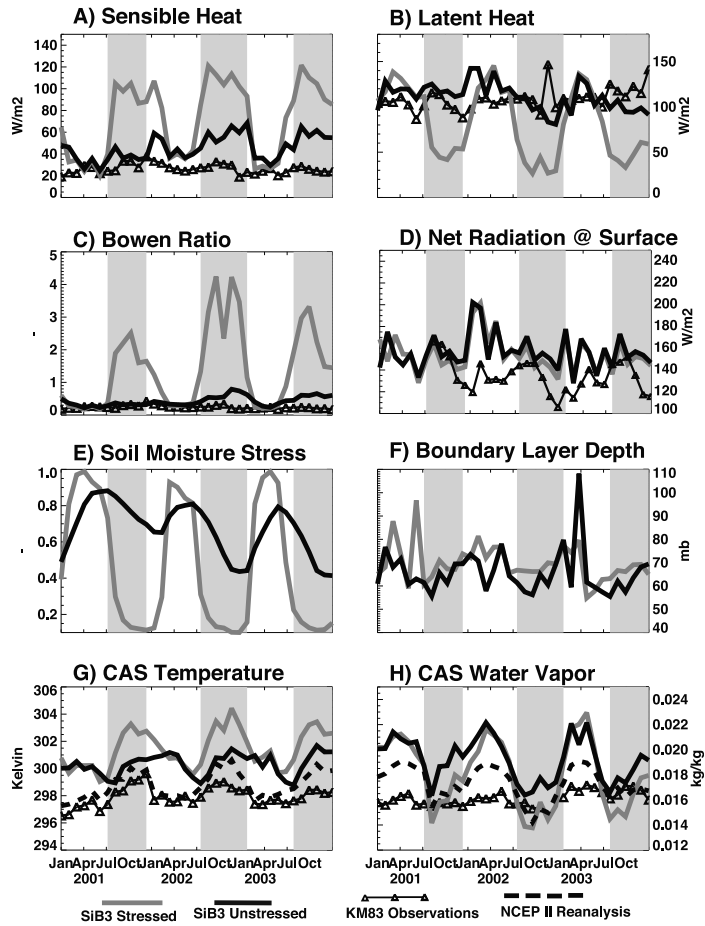


Figure 4.2 a–h) Comparison of modeled and (when available) observed variables. In Figures 2g and 2h, NCEP II Reanalysis values are from 1000 hPa and the tower observations are from a height of 10 meters.

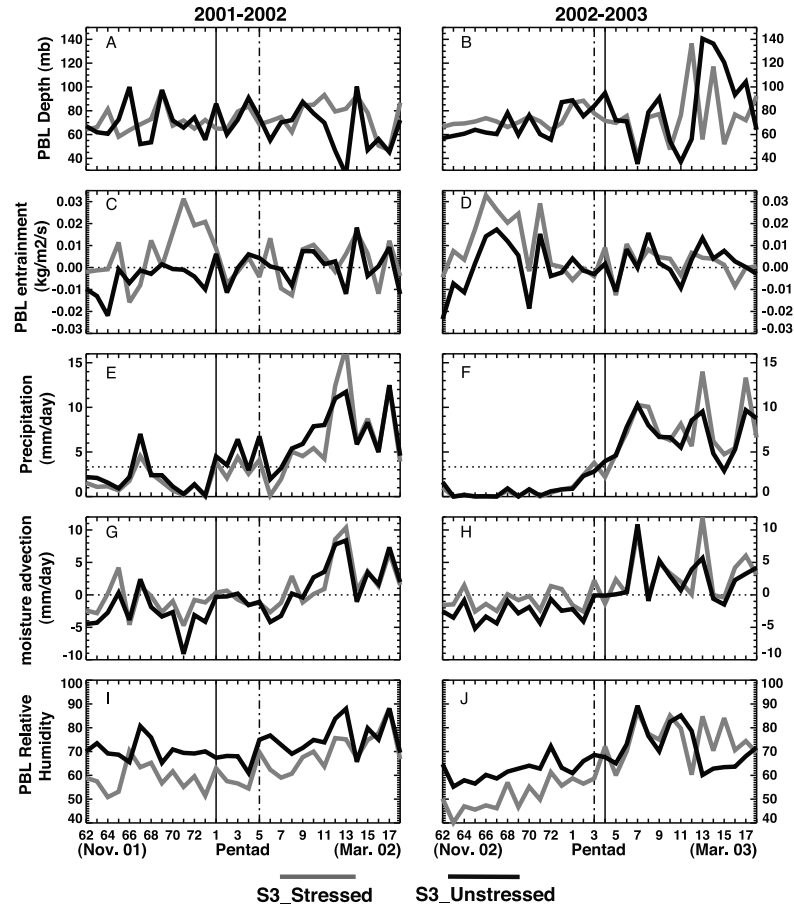


Figure 4.3 Pentad-averaged values for NDJFM of (a, b) PBL depth, (c, d) entrainment at the PBL top, (e, f) precipitation rate, (g, h) vertically averaged moisture advection, and (i, j) PBL relative humidity. The solid (dashed) vertical lines indicate pentad of wet season onset in S3_Unstressed (S3_Stressed). In Figures 3e and 3f, the dotted horizontal line indicates the threshold rain rate for the wet season onset (3 mm/day^{-1}).

CHAPTER 5:
LAND-ATMOSPHERE INTERACTIONS DURING
AMAZONIAN DROUGHTS

1. INTRODUCTION

Severe drought in the Amazon basin has been linked to El Niño and warming in the northern tropical Atlantic. Both conditions are predicted to continue or potentially increase in the future (Li et al., 2006; van Oldenborgh et al., 2005; Cox et al., 2008). Until recently, most ecosystem models did not include the mechanisms that allow the Amazon to thrive during the dry seasons (e.g. Saleska et al., 2003). Adding more realistic root and soil functions in SiB3 resulted in more realistic surface fluxes at sites throughout the Amazon (Baker et al., 2008), and in a more active hydrologic cycle when SiB3 was coupled to a single column GCM (Harper et al., 2010). We have also developed a version of SiB3 with spatially varying stress resistance. Offline simulations using SiB3-SRI showed large impacts to surface heat and moisture fluxes during droughts, which could have important implications for moisture recycling and climate.

As we understand more about the mechanisms of drought adaptation in the Amazon, we are able to improve our land surface models to achieve more realistic seasonal cycles of latent and sensible heat fluxes, and surface fluxes of CO₂. A question that still needs to be answered is how does the forest drought tolerance feed back to affect the climate of Amazonia, and what are the implications for how the forest might respond in the future? The following chapter tests two hypotheses: 1. The ability of the forest to

resist drought stress will decrease drought intensity, and 2. Forest response to drought can influence remote circulation and precipitation patterns.

2. METHODS

2.1 SiB3

This study utilizes the Simple Biosphere model coupled to the BUGS5 GCM. The coupled model is run for 10 years (1997-2006) using three versions of SiB3 - “Stressed”, “Unstressed”, and “SRI”. Monthly sea surface temperatures and sea ice concentrations are prescribed (AMIP, Atmospheric Model Intercomparison Project). The Stressed and Unstressed model were used in a previous study (Harper et al., 2010; Chapter 4) coupled to a single column model of BUGS5. The SRI model is described fully in the two previous papers. Here we briefly review the differences between these models. In all versions, it is assumed that roots exist throughout the soil column. Root density is highest in the upper soil layers, and then decreases exponentially with depth.

In SiB3 Stressed, the soil is 3.5 meters deep and water is removed for transpiration based solely on root fraction in each layer. In addition, soil moisture stress increases rapidly as the soil water potential approaches the wilt point, through the equation:

$$SMstress = \sum_{i=1}^{nsoil} \left(\frac{1 - \frac{\theta_{wp}}{\theta_i}}{1 - \frac{\theta_{wp}}{\theta_{fc}}} \right)$$

Equation 1

where θ_{wp} and θ_{fc} are the water potential at wilt point and field capacity, respectively. θ_i is the water potential in layer i , and SiB3 has ten soil layers.

In SiB3 Unstressed, the soil is 10 meters deep, and roots are weighted by the soil moisture present in each layer:

$$rootr_i = \left(\frac{1 - \frac{\theta_{wp}}{\theta_i}}{1 - \frac{\theta_{wp}}{\theta_{fc}}} \right) (rootf_i) \quad \text{Equation 2}$$

where $rootf$ is the actual root fraction, and $rootr$ is the “apparent” root fraction used for extracting water for transpiration. The apparent root fraction can be higher or lower than the actual root fraction depending on the amount of moisture in each individual layer (Baker et al., 2008). In practice, this enables the deep layers to access soil moisture in amounts disproportionate to their root density and helps avoid unrealistic soil moisture stress in the model. In addition, the soil moisture stress calculation is changed from Equation 1 to Equation 3 - which creates a more gradual stress response to decreasing soil moisture.

$$SM_{stress} = \frac{(1 + wssp) * pawfrac}{(wssp + pawfrac)} \quad \text{Equation 3}$$

A gradual response is more fitting for modeling purposes, since grid cells encompass many plants which reach wilt point at a different time.

SiB3 SRI utilizes the same soil moisture stress equation and apparent root fractions as SiB3 Unstressed. In addition, this version relies on a Stress Resistance Index

(SRI), which is based on the following assumptions. First, we assume that plants in regions with periodic severe drought have higher drought tolerance than the ever-wet regions of the tropical forests. Second, we assume that very fine and very coarse soil textures increase drought tolerance. Third, we assume that deforestation reduces the overall drought tolerance of forests in a grid cell, primarily through the removal of deep rooting systems. Further justification and explanation of the SRI can be found in Chapter 3.

Overall, the forests in SiB3 Stressed are least able to tolerate dry conditions (hence the name “Stressed”). Low soil moisture in SiB3 induces stomatal closure, which reduces evapotranspiration and photosynthesis. This response is based on isohydric plants, which attempt to maintain a minimum leaf water potential in order to prevent xylem cavitation and hydraulic failure under drought conditions. Both SiB3 Unstressed and SiB3 SRI have higher drought tolerance than SiB3 Stressed. Forest drought resistance is highest in SiB3 Unstressed in the interior of the Amazon forest (in the western basin), and in the eastern-most and southern-most forests (Figure 5.1). The SRI is low in these two general areas due to consistently wet conditions and deforestation, respectively.

2.2 BUGS5

BUGS5 uses a dynamical core based on a spherical geodesic grid (Ringler et al., 2000). The geodesic grid solves the vorticity and divergence equations with second-order accuracy. We use a resolution of 10242 grid cells, which is approximately equal to 2-2.5

degrees. The radiation scheme is adopted from NCAR's Community Atmosphere Model (CAM). This utilizes a 2-stream method for calculating broadband and heating rates in the shortwave and longwave (Gabriel et al., 2001; Stephens et al., 2001). The method also accounts for infrared scattering (Stephens et al., 2001).

3. RESULTS

3.1 Overall model performance

The mean January precipitation shows the observed patterns of high precipitation in BUGS5 in the Intertropical Convergence Zone (ITCZ), in the South Pacific Convergence Zone (SPCZ), and over tropical land (Figure 5.2). It also captures the high precipitation in the storm tracks over the northern Pacific and Atlantic oceans. However, magnitudes of precipitation are overestimated throughout much of the tropics, and global precipitation is 25-30% higher than GPCP. There is also too much water vapor in the atmosphere - precipitable water is about 3 mm higher than observed. Most of the overestimation is in the regions of the over-vigorous precipitation: along the ITCZ, in the SPCZ and over tropical South America. Compared to observations from the (1985-1989), the modeled outgoing longwave radiation (OLR) is too high. According to the Earth Radiation Budget Experiment (ERBE), observed low values of OLR are present over tropical land masses (Africa, Indonesia, and South America). In BUGS5, OLR is too high and albedo is too low over all of these regions. This indicates an underestimation of cloud cover, especially high clouds. The albedo is also too low in some of the ocean subtropical dry areas: for example in the Indian Ocean and west of Australia. The model has a warm bias in the northern latitudes and tropical Africa and South America. In some parts of Russia there is no snow on the ground in January, and the albedo is too low.

The tendency for the model to overpredict tropical rainfall in some places while underpredicting cloud cover in others is also seen during July. The model captures observed precipitation maxima in the western Pacific, and in the ITCZ in the eastern Pacific. However, in general precipitation in the tropical Pacific is too high, as is precipitation in the tropical Indian Ocean. Precipitable water is also too high in most of the tropics. Modeled OLR is higher than the global observed average, and surface temperatures are warmer over Northern Hemisphere land.

Two tunable parameters in BUGS5 could improve some of these results. The climate in BUGS5 is very sensitive to the ice-phase parameterization (Fowler and Randall, 2002). “Detsnow” is a parameter representing the fraction of snow that is detrained at the top of convective updrafts, with larger values of *detsnowfac* denoting less detrainment. Snow detrains into anvil clouds and often evaporates before reaching the surface. Detrainment of snow results in a wetter and colder climate (Fowler and Randall, 2002), and so an appropriate adjustment might be to reduce detrainment in order to reduce the precipitable water content. A second parameter is *alpham*, which is used in the prognostic equation of cumulus kinetic energy. CKE is inversely proportional to the square root of alpha. Increasing *alpham* reduces cumulus mass flux, weakens CKE and decreases precipitation. Future sensitivity tests with BUGS5 should involve both increasing *alpham* and increasing *detsnowfac*, but are beyond the scope of the current investigation.

We zoom in on tropical South America and compare annual precipitation between the three models and GPCP. Observed precipitation has a maximum in the northwestern

Amazon. The rainfall decreases to the south and east, with minimum values occurring over eastern Brazil. The models capture the mean pattern of high rainfall in the northwest and lower rainfall in the southeast. However, all models produce too much rainfall in the ITCZ, resulting in a zonal band of high precipitation near the Equator. There is also too much rainfall over high topography and in the SACZ. Precipitation is especially high over the Andes, which the model has difficulty representing due to their sharp relief (Figure 5.4e, f).

The northern Andes mountain range is problematic for GCMs due to its narrowness. Near Quito, Ecuador, the range is less than 2° across, which is smaller than the model resolution (Figure 5.5, Bartholomew, 1962). Elevation changes from roughly 200 m to 3,800 m in the highlands, to a maximum of 5,897 m atop the volcano Cotopaxi, and back to 200 m. In BUGS5 the maximum elevation along the “A” line is only 1,098 m. The mountains are better resolved to the south but maximum elevation of the mountains is not represented. The mountain Sillajhuay (5,982 m) sits near the Chilean/Bolivian border on the “B” Line. In BUGS5 the maximum elevation at 20°S is 3,805 m.

3.2 Modeled seasonal climate in tropical South America

Observed rainfall is high in tropical South America during the austral summer (DJF) (Figure 5.6, right column). A rainfall maximum extends from the northwest Amazon to the southeast through the SACZ. Circulation at 200 hPa is characterized by the Bolivian high and Nordeste low (Figure 5.7). At 850 hPa, air flows westward from the tropical Atlantic Ocean and Caribbean Sea, across the continent toward the Andes.

During the austral fall (MAM), precipitation remains high in the southern Amazon forests. The dry season for most of the Amazon forest occurs during the austral winter (JJA), although precipitation is high in the northern hemisphere forests during this season. Precipitation is relatively low everywhere during SON, with the exception of the northwestern Amazon basin.

Seasonal precipitation patterns are similar in the three versions of the model. These are controlled by large-scale forcings - such as the ITCZ's migration following peak solar radiation and moisture advection from the trade winds. The models produce too much rainfall over the highlands of southeast Brazil during DJF and along the coast near the mouth of the Amazon River from December-May (Figure 5.6). PBL winds in the model slow down soon after passing over land, resulting in premature moisture convergence and exaggerated rainfall near coasts (Figure 5.8). In reality, the trade winds carry moisture westward across the Amazon, and the highest rainfall occurs in the western Amazon basin, when the Andes force the wind to turn toward the south (Figure 5.7). At 200 hPa, the Bolivian high is too weak and located too far to the east in SiB3 Stressed. The anticyclone is stronger in SiB3 SRI and SiB3 Unstressed. This supports previous results which suggested the importance of surface biophysiology on atmospheric circulation (Harper et al., 2010 - Chapter 4). Atmospheric heating related to the highly exaggerated precipitation along the Andes in the model likely influences the incorrect placement of this circulation feature.

During the austral winter, the model produces an unrealistic low-level anticyclone in southern Brazil, and upper-level cyclone above the Venezuelan coast (Figure 5.7). In

this case, the low-level circulation is most unrealistic in SiB3 Unstressed and SRI. In general, precipitation is slightly higher than observed in the models from June-November (Figure 5.6).

We define two regions for further analysis. The southern Amazon region (SAR) is defined as all tropical forest points from 5°-14°S, and 285°-310°W (shown in Figure 5.4a). (Note the naming of this region is for convenience only, since the region includes forest points not technically part of the Amazon River basin.) In the SAR, the observed mean rainfall is 5.8 mm/day (Figure 5.9). The dry season occurs from June through September. Mean precipitation is close to observed in the three versions of the model (Table 5.1), although the standard deviation of monthly precipitation is almost twice as strong in the observations. The wet season precipitation is lower than observed, due to the model placing maximum precipitation to the southeast of the observed maximum (ie: DJF, Figure 5.6).

The second region is the northwestern region (NWR), which includes all tropical forest points from 0°-5°S, and 286°-291°W (Figure 5.4c). In the NWR, mean observed rainfall is 9.12 mm/day. This region is wet year-round, and the month with the least rainfall (August) receives 6.65 mm/day. The driest months are July through September. The models underestimate rainfall in the NWR (Table 5.2, Figure 5.9), mostly during the wettest months of MAM (Figure 5.6).

Recall that drought resistance is lowest in SiB3 Stressed. In the SAR, SiB3 SRI is slightly more resistant than SiB3 Unstressed (Figure 5.1). In the NWR, SiB3 Unstressed is much more resistant. All versions of the model experience large-scale dry periods, but

how the forest responds and the feedbacks between the land and the atmosphere will be different. We create composites of “dry” periods based on the rainfall anomalies in the regions defined above. The anomalies are computed from 5-month running means with the seasonal cycle removed, and represent lower frequency dry and wet periods than month-to-month variations in precipitation. Only grid cells with tropical evergreen biome are used to create the anomaly time series. Dry periods are defined any two (or more) consecutive months with less than 1 standard deviation below the mean precipitation (Figure 5.9). We differentiate effects of the forest resistance on the atmosphere during dry season and wet season droughts. By comparing model differences during dry periods, we can examine effects of forest drought resistance on atmospheric conditions during these times.

3.3 Impacts of stress resistance on seasonal fluxes

To gain an understanding of the primary differences between the models, we first analyze seasonal surface fluxes. Surface fluxes are sensitive to forest drought resistance during the dry season (e.g. Chapter 2). Increased drought tolerance enables plants to open their stomata more during the dry season, and increase photosynthesis and evapotranspiration. In the southern tropical forests, seasonal drought has increased forest resistance. In SiB3-SRI, this increased resistance leads to stronger latent heat flux and weaker sensible heat flux during JJA along the southern edges of the Amazon forest (Figure 5.10). The largest differences occur from 9°-13°S, 50°-54°W (up to 35 and 45 W m⁻² difference in sensible and latent heat fluxes, respectively). As a result, the PBL is

cooler and more moist in SiB3 SRI. The northern tropical forests experience less frequent drought and have decreased drought resistance in SiB3 SRI compared to SiB3 Unstressed. In Venezuela, the latent heat flux is lower and sensible heat flux is higher during the dry season (DJF) in SiB3-SRI (Figure 5.10), resulting in a slightly warmer and drier PBL.

According to NCEP Reanalysis, the air is drier and warmer at 850 hPa during dry seasons compared to wet seasons (Figure 5.12). Modeled dry seasons are drier and cooler than wet seasons. Flux towers in forests from 10°-20°S show minimum temperatures during the dry season, although dry seasons are warmer in equatorial forests (da Rocha et al., 2009). The decreased Bowen ratio in SiB3 Unstressed and SiB3 SRI result in cooler temperatures in the southeastern forests than SiB3 Stressed. In southeastern Brazil, SiB3 Unstressed is slightly drier than the other two models, which makes it closer to the reanalysis in this region (Figure 5.12). In general, the differences in precipitation, 850 hPa specific humidity and precipitable water between the models are not significant at 90%, although the atmosphere in SiB3 Unstressed tends to be slightly more moist.

The differences between the model are also apparent in diurnal composites. We focus on July 2003 in SiB3 SRI and SiB3 Stressed. In the SAR, the soil moisture constraints in SiB3 Stressed result in overall higher stress levels in this model, and so GPP is lower all day (Figure 5.13). The increased sensible heat flux and decreased latent heat flux result in a warmer and drier canopy air space in SiB3 Stressed. Stomatal resistance is also high, and mid-day temperature stress restricts stomatal opening further. The stomatal resistance increases to prevent excessive water loss, and both ET and GPP

decrease after noon. Total precipitation during July 2003 precipitation is closer to the observed value in SiB3 SRI (62 mm compared to 102 mm in SiB3 Stressed and 40 mm in GPCP). Similar to previous results (Harper et al., 2010), higher stress resistance results in the forest acting as a moisture source to other regions, as indicated by the difference between precipitation and evaporation. In SiB3 SRI, P-E is negative during the day since evaporation increases and precipitation only has a slight late-afternoon maximum. Some of the excess moisture also remains in the local atmosphere and results in higher precipitable water content.

In the northwest region, SiB3 SRI has less soil moisture stress but more temperature stress, while the Stressed model has strong late afternoon humidity stress (Figure 5.14). However in general, neither model experiences strong ecosystem stress during July 2003, and daytime stomatal resistance and GPP are similar between the models. However, the dry canopy air space in the Stressed model causes increased ET due to higher VPD. In this region, the monthly precipitation is closer to observations in SiB3 Stressed (174 mm compared to 217 mm in GPCP and 115 in SiB3 SRI).

3.4 Dry periods in the Southern Amazon Region

Observed dry periods in the Southern Amazon region (SAR) occurred during the 1997 El Niño and 2005 drought (Table 5.1). During these times, average precipitation in the region was 4.70 ± 3.38 mm/day. All versions of the model capture the anomalous dry conditions during the 97/98 El Niño, but none reproduce the 2005 drought. Stress resistance in the SAR is highest in SiB3-SRI, with resistance increasing from west to east

(Figure 5.1). In SiB3 Stressed, there are 22 months that fit the criteria for dry months, compared to 13 months in GPCP. SiB3 Unstressed and SRI had 14 and 12 dry months, respectively. Average precipitation is very similar during the dry months, ranging from 5.77 mm/day in SiB3 Stressed to 5.80 mm/day in SiB3 Unstressed.

Since anomalously dry months occur at different times in the models and the observations (Table 5.1), we focus on wet season of 1997-1998 and the dry season of 1999. During the wet season drought of 97-98, the high level of stress resistance in SiB3 Unstressed results in slightly higher precipitation in the SAR compared to SiB3 Stressed (7.2 vs 6.6 mm/day) (Table 5.1 and Figure 5.15d). Since the forest experiences less soil moisture stress, the plants are able to transpire throughout the drought. The latent heat flux is higher and sensible heat flux is lower. There is slightly stronger rising motion at 500 hPa in SiB3 Unstressed (not shown), indicating stronger convection through the droughts.

Recall that the differences between the models are restricted to the tropical forest biome. Despite this, the ability of the forest to tolerate dry periods can enhance precipitation downwind of the Amazon. During the wet season droughts, rainfall in southeastern Brazil is up to 5 mm/day stronger in SiB3 Unstressed than SiB3 Stressed. This region also experiences much higher latent heat flux, higher precipitable water content, lower surface pressure, and stronger CAPE in the Unstressed model. There is slightly more convergence in the SACZ in SiB3 Unstressed at 850 hPa. At 200 hPa, there is an anomalous high above the Pacific Ocean off the Chilean coast, and an anomalous low in southern South America in all the models. This is a reversal of climatological wet

season circulation (Figure 5.7). The low is strongest in SiB3 Unstressed. These circulation patterns result in relatively more rainfall in the SACZ in SiB3 Unstressed.

During dry season droughts in the SAR, there is on average more rainfall in the Stressed model, although for the dry months in 1999 the rainfall is stronger in SiB3 SRI (Table 5.1, Figure 5.16d). During 1999, the latent heat flux is much stronger in SiB3 SRI than in SiB3 Stressed (113 vs 82 W/m²). This flux is equivalent to 1.2 mm/day stronger evaporation in SiB3 SRI. The sensible heat flux is on average 20 W/m² lower in SiB3 SRI. During the dry season droughts, and anomalously southeasterly flow advects anomalously dry air from southern Brazil into the Amazon (Figure 5.16 j,l). Therefore, the additional evaporation simulated by SiB3 SRI represents an important mechanisms for the forest to cope with dry conditions, and weakens the drought intensity in the region.

3.5 Dry periods in the northwestern region

In the northwestern region, the forest drought resistance is much lower in SiB3 SRI than in SiB3 Unstressed (Figure 5.1), while SiB3 Stressed has the lowest resistance overall. During observed dry periods, mean precipitation was 7.74 +/- 2.32 mm/day. The models are drier, with the closest being SiB3 Unstressed (6.10 +/- 0.86 mm/day). There were 12 dry months in the observations and in SiB3 Unstressed, but droughts were longer in SiB3 SRI and Stressed. This results is similar to that in the SAR - increased stress resistance resulted in shorter and less severe droughts compared to SiB3 Stressed.

We focus on droughts during the peak of the wet and dry seasons (Feb.-May and July-Sept., respectively). During the peak wet season droughts, the Unstressed model has the most precipitation (6.5 mm/day) and SiB3 SRI has the least (5.9 mm/day) (Figure 5.17). As seen in the SAR, differences in the forest drought response affect moisture recycling and convection. The former is stronger in SiB3 Unstressed, as evidenced by higher latent heat flux, a more moist PBL, and more precipitable water content. However, convective activity is stronger in the Stressed model as indicated by stronger rising motion at 500 hPa, and higher CAPE. The higher moisture content has more influence and precipitation in the region is stronger in SiB3 Unstressed. Because of limited drought resistance in SiB3 SRI, the latent heat flux is similar to that in the Stressed model, and omega and CAPE are even lower than in the Unstressed model. Therefore in this case, the reduced convection results in reduced precipitation.

The impact of forest drought resistance is felt throughout the troposphere. In SiB3 Stressed the 200 hPa geopotential heights are anomalously low, while in SiB3 Unstressed they are anomalously high and winds are strong. Similar to the wet season droughts in the SAR, there is a tendency for rainfall in the SACZ to be sensitive to forest drought response. In SiB3 Stressed, the 850 hPa winds show an enhancement of normal wet season patterns. Along the equator, winds move westward, and then curve to the southeast as they encounter the Andes. In SiB3 Unstressed, winds are southeasterly across most of the basin. As a result the precipitation in the SACZ is reduced. The conditions in SiB3 Unstressed are similar to the “easterlies” regime discussed by Jones and Carvalho (2002), although there is no corresponding increase in precipitation in the

equatorial Amazon. A reversal of the low-level jet along the eastern flank of the Andes is associated with a reduction in South American monsoonal precipitation. The anticyclonic rotation in southern Brazil at 850 hPa could be linked to the strong 97/98 El Niño, since the Unstressed model is the only version that includes this time period in the composites in Figure 5.16. The anticyclonic rotation has been linked to subsidence over the Amazon during El Niño's (Grimm 2003).

4. DISCUSSION

This study was based on investigating two hypotheses. First, that stress resistance decreases drought intensity. Second, that forest drought response affects precipitation and circulation in remote regions.

4.1 Does stress resistance decrease drought intensity?

Any mechanism that increases evapotranspiration can increase rainfall through enhanced precipitation recycling. However, competing mechanisms such as moisture divergence and large-scale subsidence can reduce precipitation. In the southern Amazon region, we found evidence for enhanced precipitation due to higher stress resistance in most cases (wet season droughts in the SAR and NWR, and the 1999 dry season drought in the SAR). In addition, precipitation was lower in the NWR wet season droughts in SiB3 SRI due to decreased stress resistance. Average precipitation during all dry months was higher in both SiB3 Unstressed and SiB3 SRI compared to SiB3 Stressed in both regions. However, in the SAR the Stressed model's precipitation during dry periods is closer to observations (Tables 5.1, 5.2). The duration of droughts was also shorter in the Unstressed and SRI model. There is not a direct, linear relationship between stress resistance and drought intensity. For example, SiB3 SRI has higher stress resistance on average in the SAR but SiB3 Unstressed had stronger precipitation during droughts.

4.2 Does forest drought response affect remote precipitation and circulation?

As discussed in Harper et al. (2010), changes to atmospheric moisture content and convection result in changes to atmospheric heating profiles due to condensation. In the previous study, using a single column version of BUGS5, we found increased low-level moisture in SiB3 Unstressed, accompanied by higher vertically integrated moist static energy and weaker gross moist stability. All of these factors point toward a more active hydrologic cycle in the unstressed version of the model. In this study, the daytime moisture divergence and precipitation were greater in SiB3 SRI during the dry season of 2003. This can affect circulation patterns such as the Bolivian high. Circulation patterns are different between the models both in the mean (Figure 5.6) and during anomalously dry periods (Figures 5.15-17). The changes in circulation resulted in more intense precipitation in southern Brazil during wet season droughts in the SAR in SiB3 Unstressed and during wet season droughts in the NWR in SiB3 Stressed.

Table 5.1. Top: Months that are anomalously dry in the models and observations. Dry season months are in bold. Bottom: Precipitation statistics for the Southern Region.

	SiB3 Stressed	SiB3 Unstressed	SiB3 SRI	GPCP
Average regional precipitation	5.77+/-1.91	5.80+/-1.96	5.79+/-2.0	5.80+/-3.52
Dry Months	Nov. 97 - June 98	Nov. 97 - Jan. 98	Apr. - May 97	Sept. 97 - June 98
	June - Aug. 99	June - July 00	Nov. 97 - Apr. 98	June - Aug. 05
	June - Sept. 00	Dec. 02 - Feb. 03	May - Sept. 99	
	Apr. - May 02	Nov. 04 - Apr. 05	Oct. - Nov. 04	
	Oct. 03 - Feb. 04			
	Oct. - Nov. 04			
Total dry months	22	14	12	13
Average precipitation during dry months	5.23+/- 1.66	6.24+/-2.05	5.30+/-1.67	4.70+/-3.38
Average during dry season dry months	2.80	2.47	2.59	1.40
Average during wet season dry months	6.54	6.87	6.28	6.77

Table 5.2 Top: Months that are anomalously dry in the models and observations. Bottom: Precipitation statistics for the northwestern region.

	SiB3 Stressed	SiB3 Unstressed	SiB3 SRI	GPCP
Average regional precipitation	6.52+/-1.04	6.66+/-1.17	6.44+/-1.25	9.12+/-2.53
Dry Months	Mar. - Aug. 97	May - June 97	Oct. 97 - Feb. 98	Aug - Sept. 97
	July - Sept. 99	Dec. 97 - Mar. 98	May - Aug. 00	Oct. 99 - Feb. 01
	Feb. - Mar. 00	May - June 99	Nov. - Dec. 01	Dec. 03 - Mar. 04
	Nov. - Dec. 00	June - July 05	Mar. - Apr. 03	June - July 05
	Dec. 02 - Feb. 03	Aug. - Sept. 06	July - Oct. 06	
Total dry months	16	12	17	12
Average precipitation during dry months	5.65+/-0.77	6.10+/-0.86	5.73+/-0.86	7.74+/-2.32
Average during dry season dry months	4.86	6.45	5.04	6.33
Average during wet season wet months	6.01	5.98	6.01	8.45

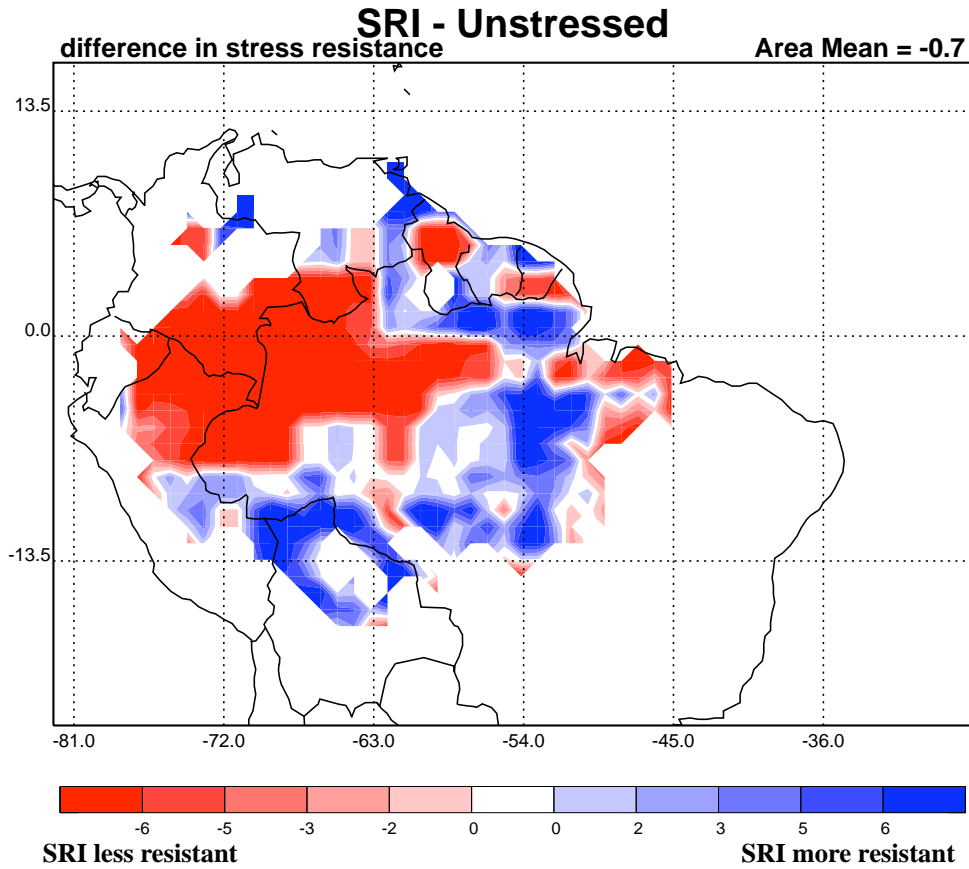


Figure 5.1. Difference in stress resistance between SiB3 SRI and SiB3 Unstressed. Note that both models have higher stress resistance than SiB3 Stressed. The average difference in the southern Amazon region is 1.05 (SRI is slightly more resistant), and the average in the northwestern region is -7.52 (Unstressed is more resistant).

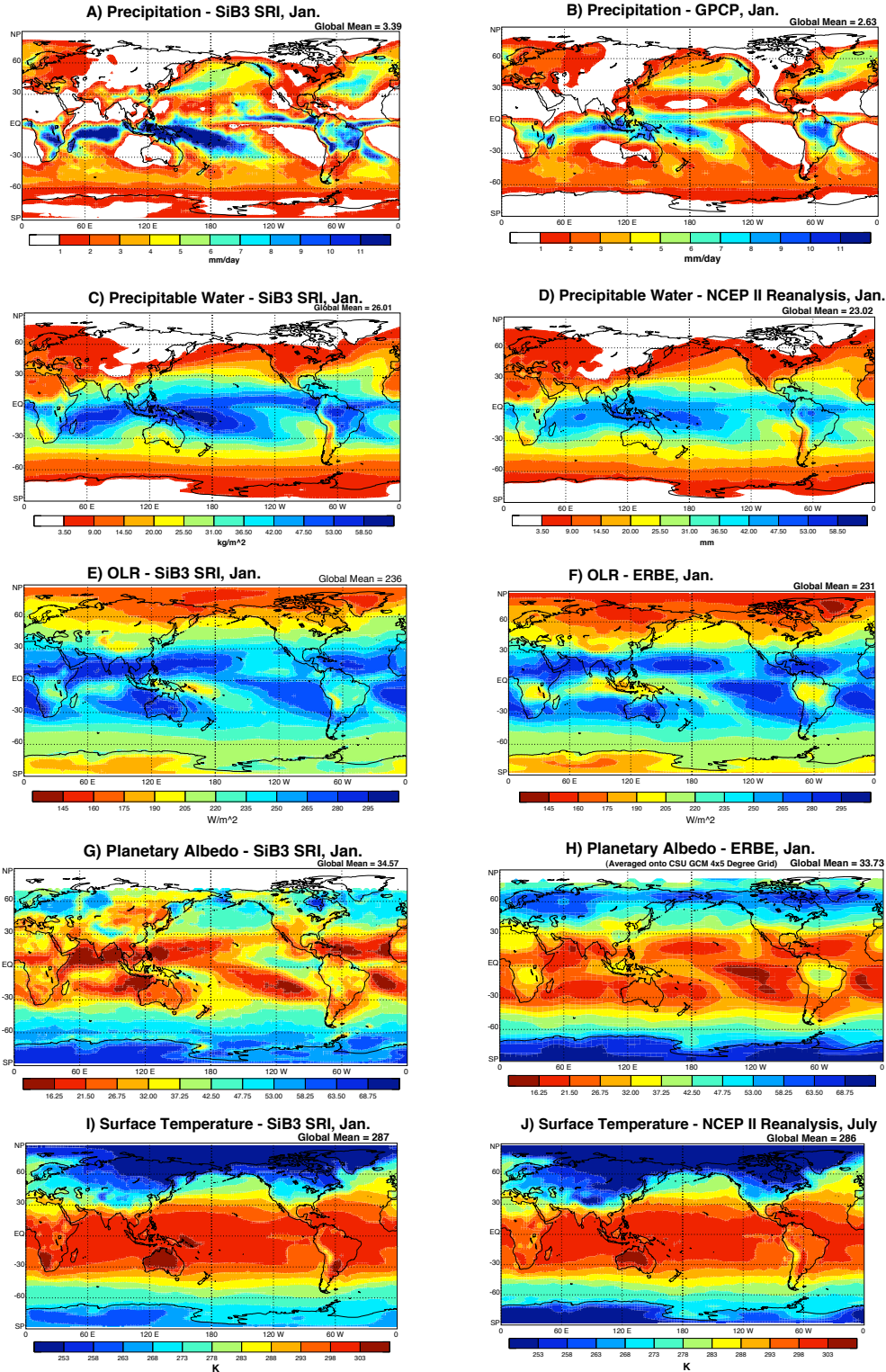


Figure 5.2. Average January precipitation (A, B), precipitable water (C,D), OLR (E,F), albedo (G,H), and surface temperature (I,J) in SIB3 SRI and observations. Model average is from 197-2006, GPCP data is from 1997-2006, ERBE is from 1985-1989, and NCEP II Reanalysis is from 1979-1998.

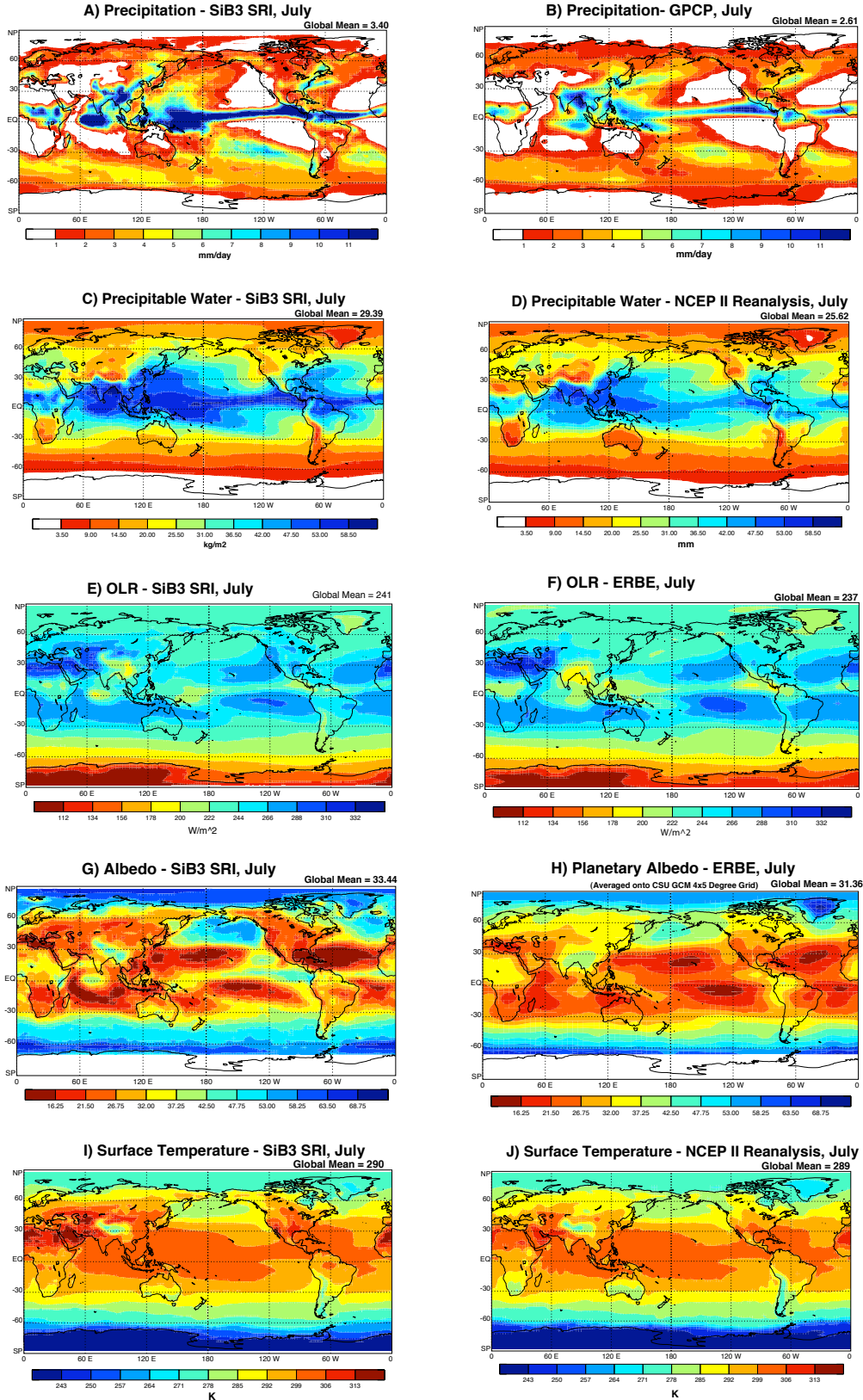


Figure 5.3. As in Figure 2 but for July.

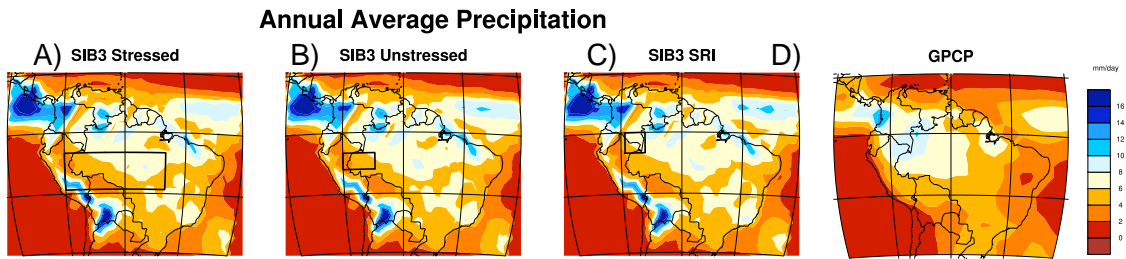


Figure 5.4. Annually averaged precipitation rates for the models and observations (Global Precipitation Climatology Project), 1997-2006. Also shown are the regions discussed throughout the text: A) “Southern Region:” 5-14S, 50-75W; C) “NW Box:” 0-5S, 69-74W. Averages from these regions only include points considered evergreen forest in SiB3.

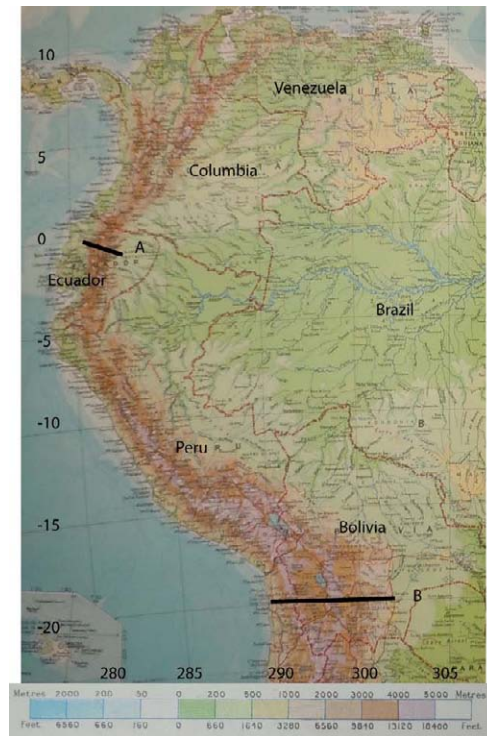
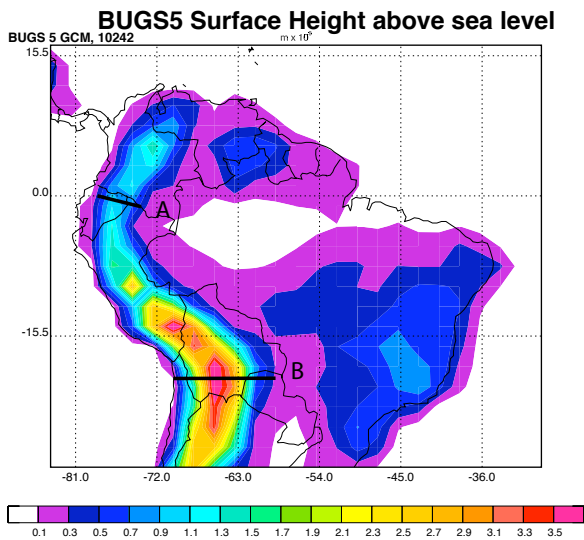


Figure 5.5. Topography in BUGS5 at 10242 resolution (units of km) (left), and actual topography in South America (right). (from *The Advanced Atlas of Modern Geography*, Bartholomew, J., 1962). Bottom: the Cotopaxi volcano, photo from Gerard Prins. The line labeled “A” crosses Cotopaxi, south of Quito, Ecuador. The “B” line follows 20S latitude line and crosses Sillajuay on the Bolivian/Chilean border.

Seasonal Precipitation, mean

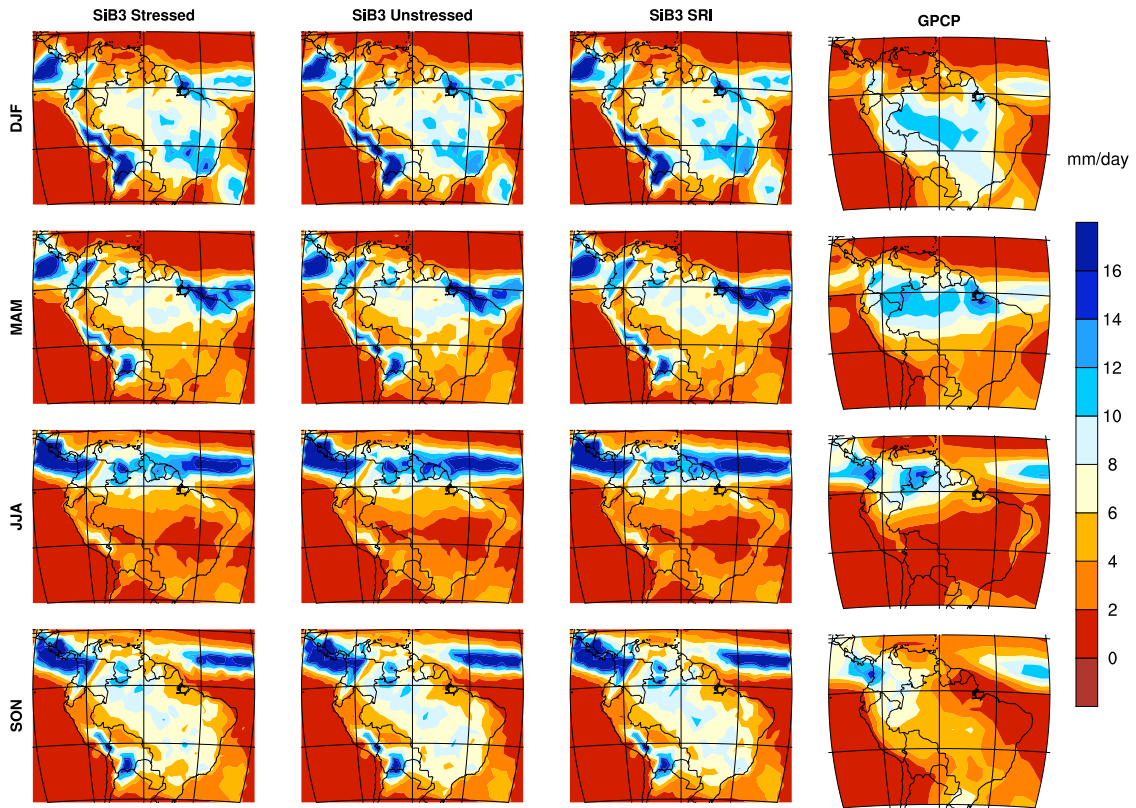


Figure 5.6 Seasonal precipitation in SiB3 Stressed (left column), SiB3 Unstressed (second column), SiB3 SRI (third column), and observations (right column). Seasonal means are for DJF (first row), MAM (second row), JJA (third row), and SON (bottom row).

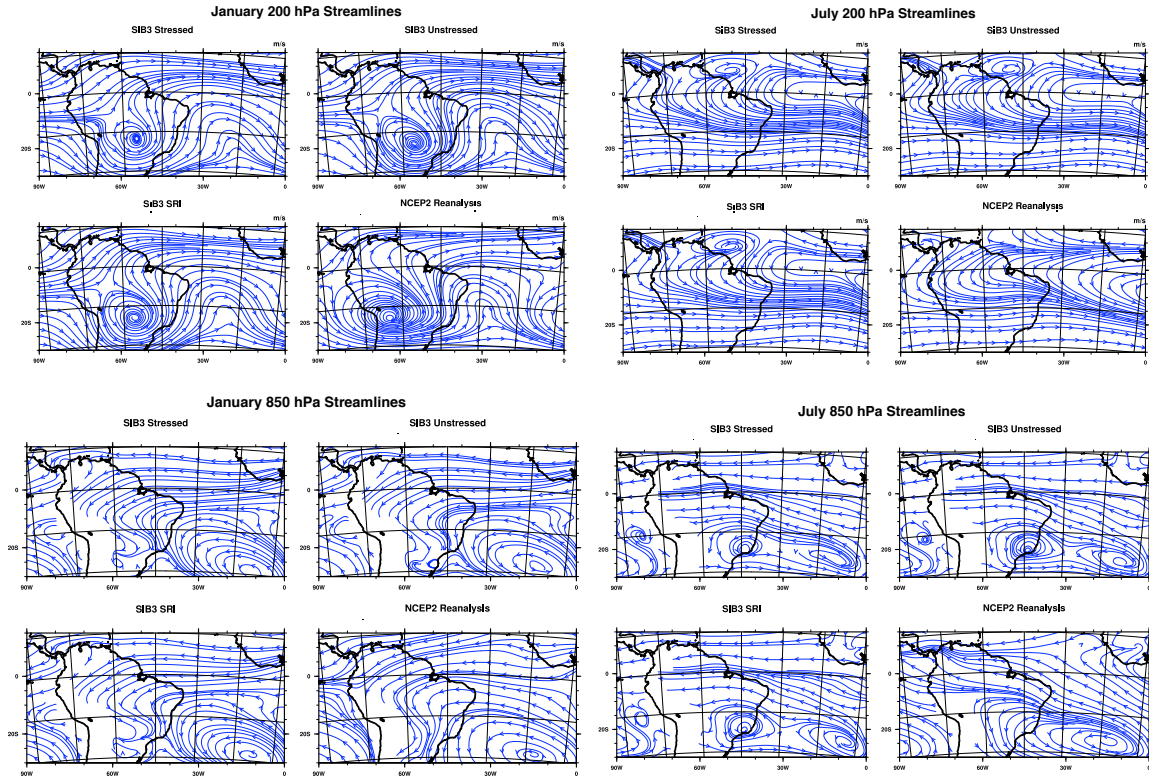


Figure 5.7 Streamlines of circulation at 200 hPa (top) and 850 hPa (bottom) in the models and NCEP II Reanalysis (1997-2006). The models and the reanalysis have been conservatively remapped to a T42 resolution.

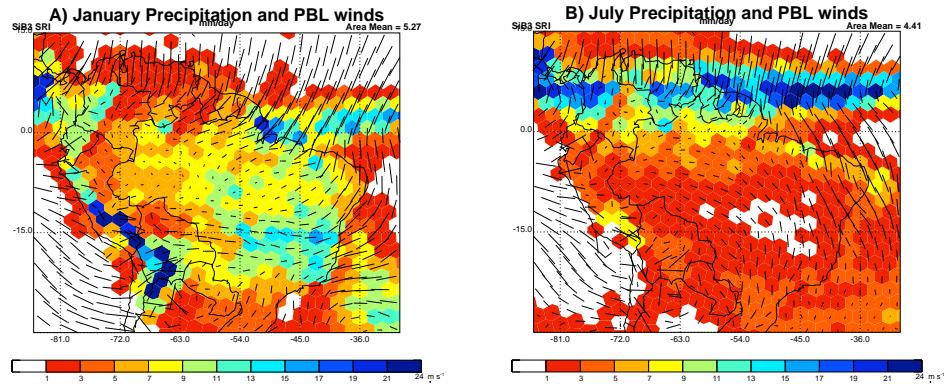


Figure 5.8 Average precipitation and PBL winds during January (A) and July (B) in SiB3 - SRI. Note the native resolution using geodesic grid cells.

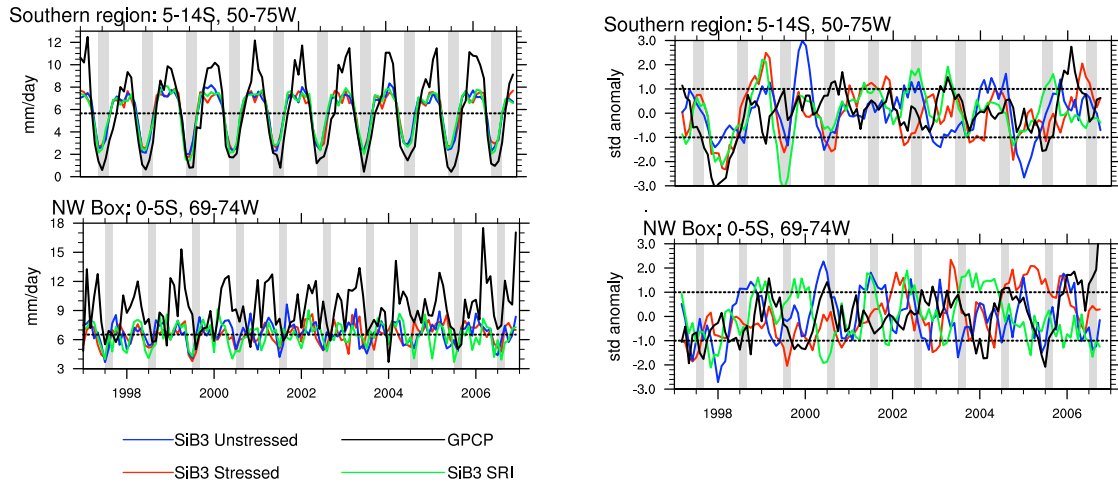


Figure 5.9. Precipitation in the three regions shown in Figure 5.4, averaged over evergreen forest biomes only. Right: Standardized monthly anomalies from deseasonalized 5-month running mean precipitation.

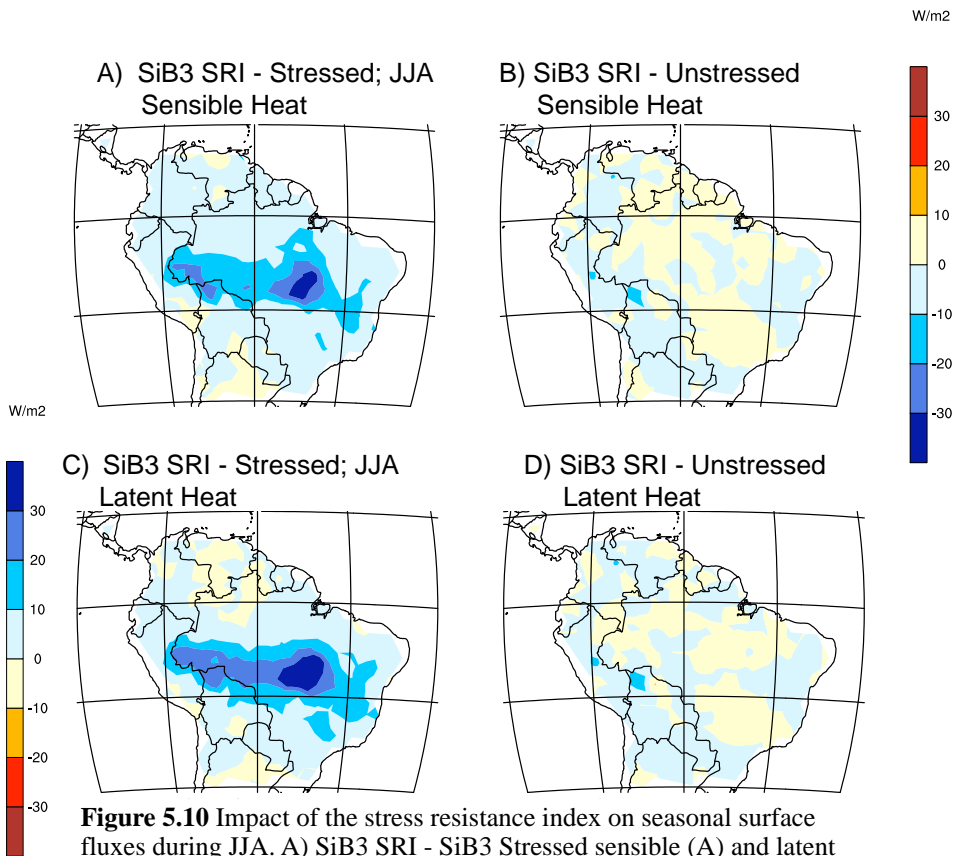


Figure 5.10 Impact of the stress resistance index on seasonal surface fluxes during JJA. A) SiB3 SRI - SiB3 Stressed sensible (A) and latent (C) heat; B) SiB3 SRI - SiB3 Unstressed sensible (B) and latent (D) heat.

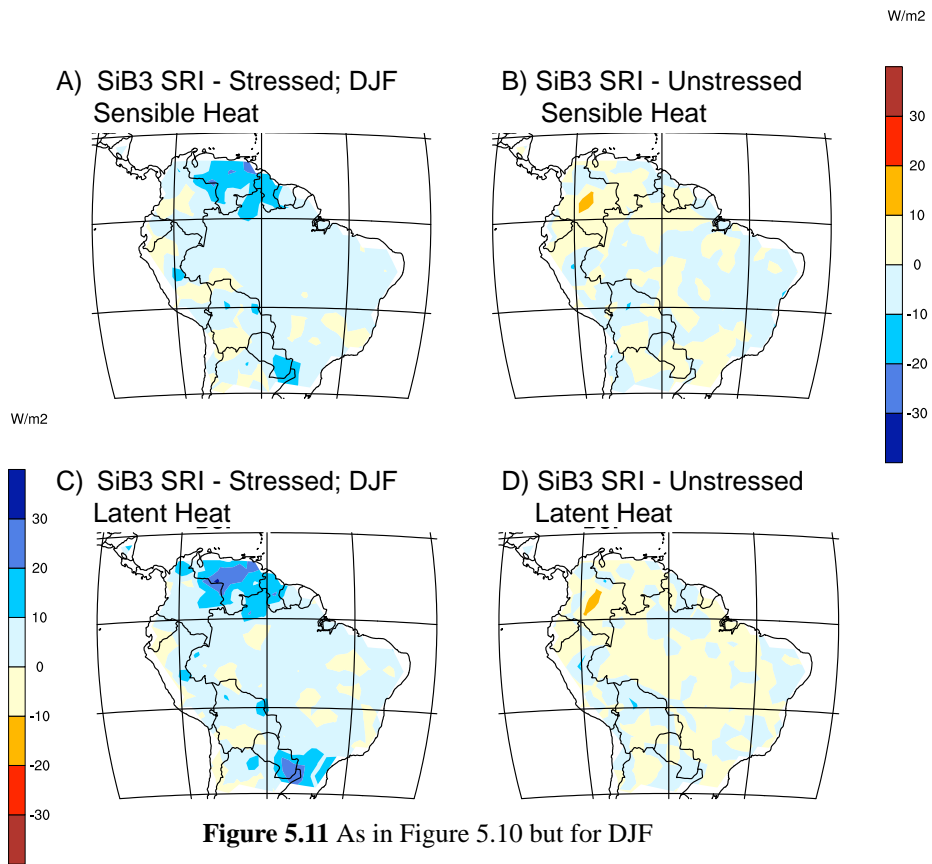
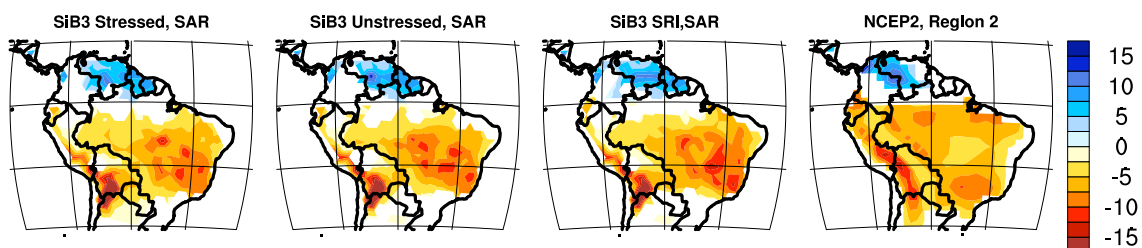
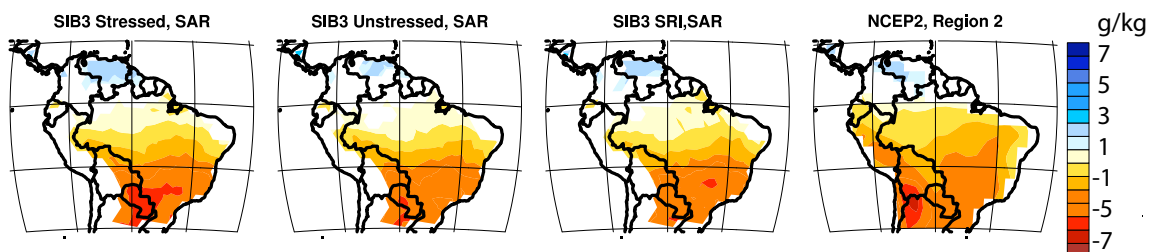


Figure 5.11 As in Figure 5.10 but for DJF

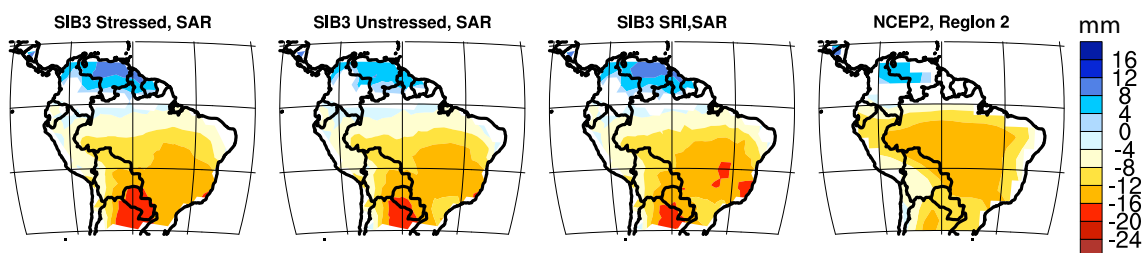
Precipitation Dry-Wet seasons, Differences significant at 95%



Specific Humidity, 850 mb Dry-Wet seasons, Differences significant at 95%



Precipitable Water Dry-Wet seasons, Differences significant at 95%



Air Temperature, 850 mb Dry-Wet seasons, Differences significant at 95%

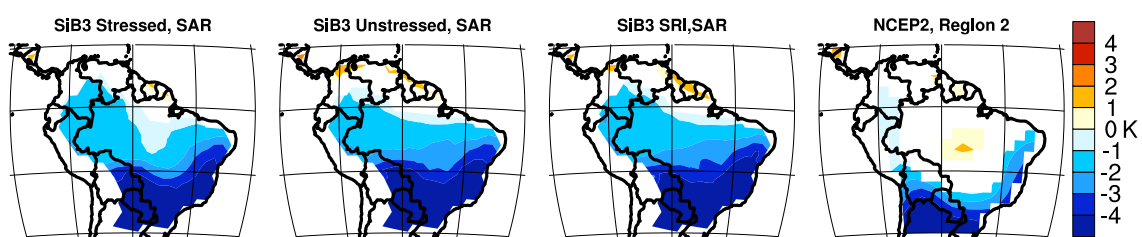


Figure 5.12 Differences between dry and wet season precipitation, 850 hPa specific humidity, precipitable water, and 850 hPa temperature in the three versions of the model and in NCEP2 Reanalysis.

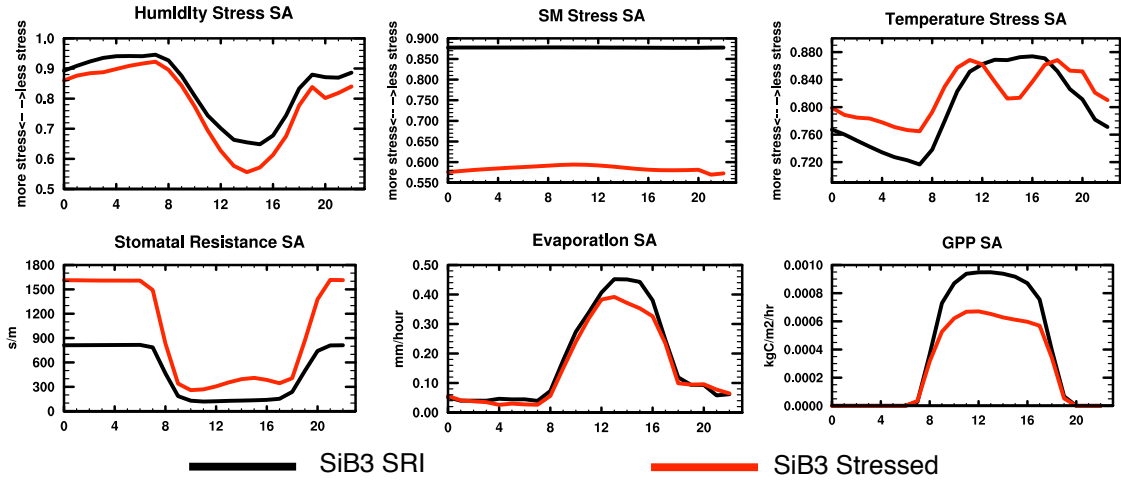


Figure 5.13 Diurnal composites in the Southern Amazon region during July, 2003.

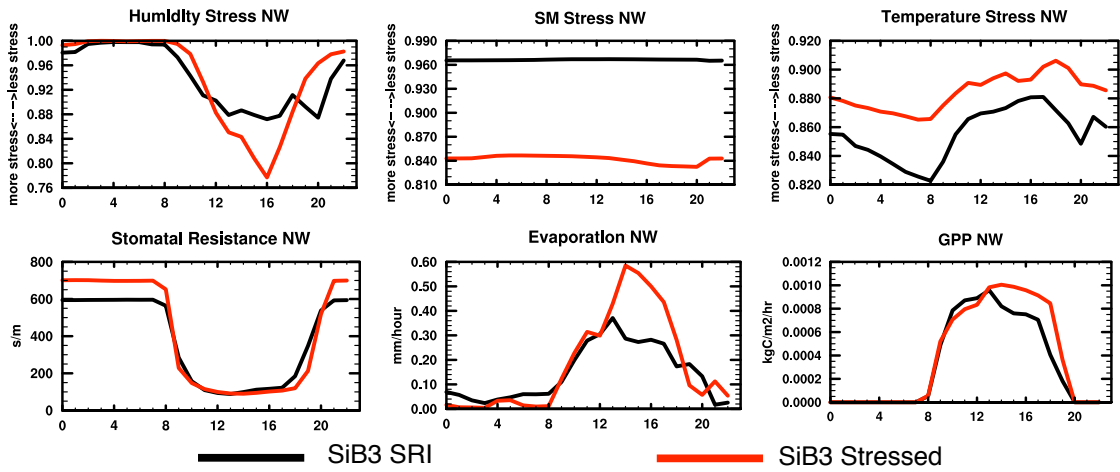


Figure 5.14 Diurnal composites in the northwestern region during July, 2003.

Wet season droughts in the southern Amazon region

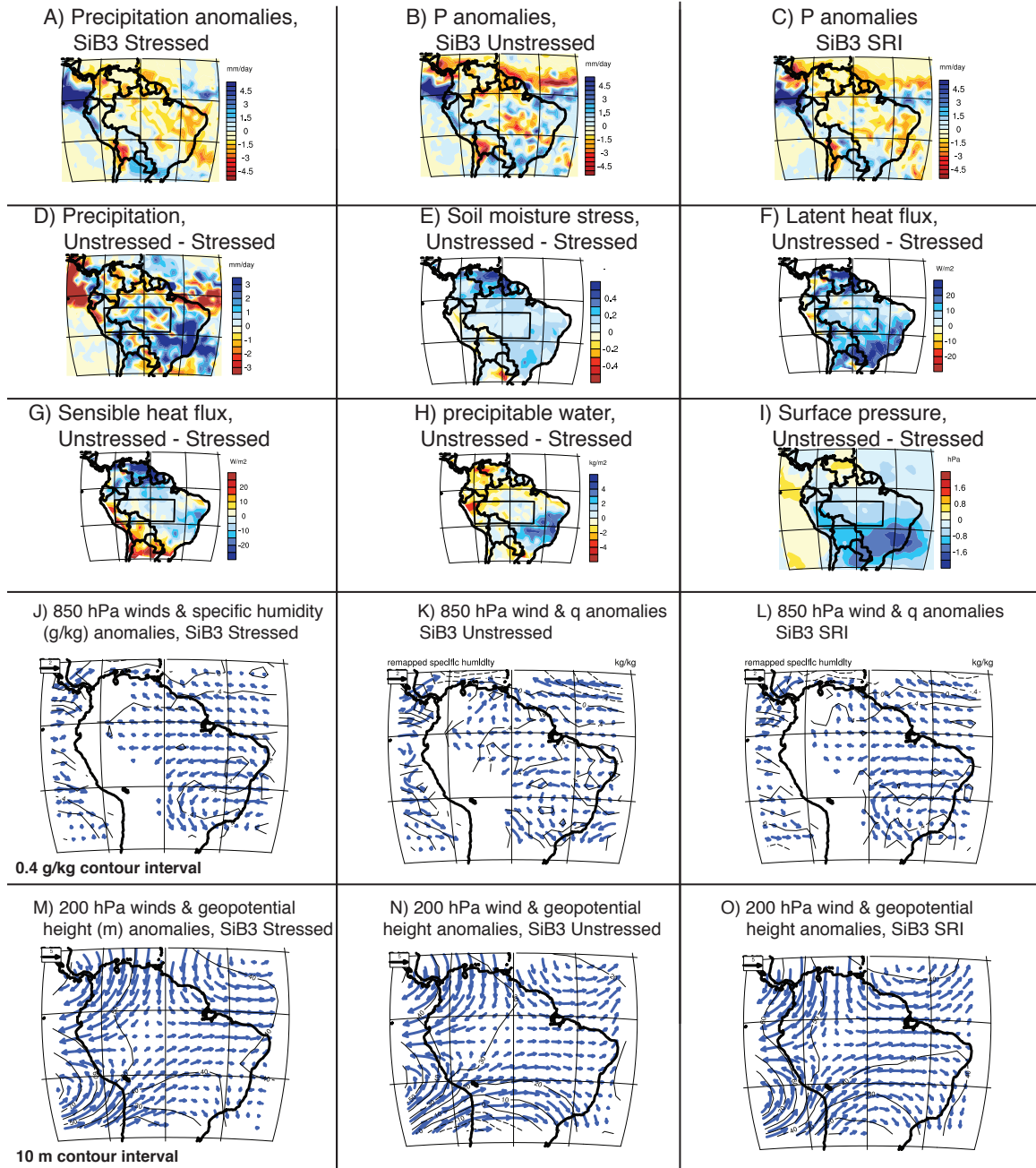


Figure 5.15 Model differences during wet season droughts in the southern Amazon region (box shown in D-I). Precipitation anomalies (seasonal cycle removed) in each of the models (A-C). Differences between SiB3 Unstressed and SiB3 SRI (D-I). Anomalous winds and specific humidity at 850 hPa in each of the models (J-L) and anomalous winds and geopotential height at 200 hPa in each of the models (M-O).

Dry season droughts in the southern Amazon region

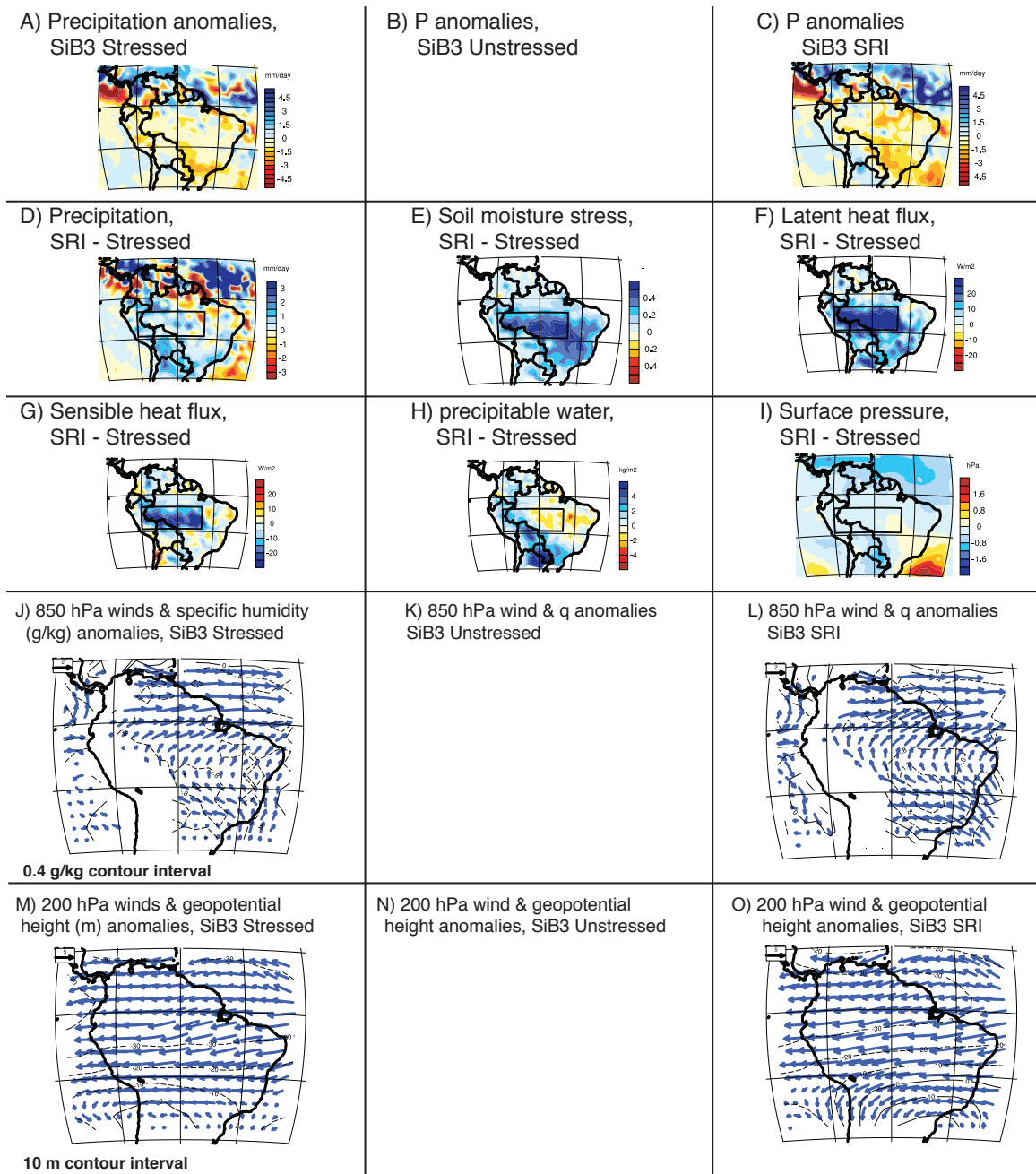


Figure 16. As in Figure 5.15 but for dry season droughts. Note that conditions were not anomalously dry during the winter of 1999 the SAR in SiB3 Unstressed.

Wet season droughts in the northwestern region

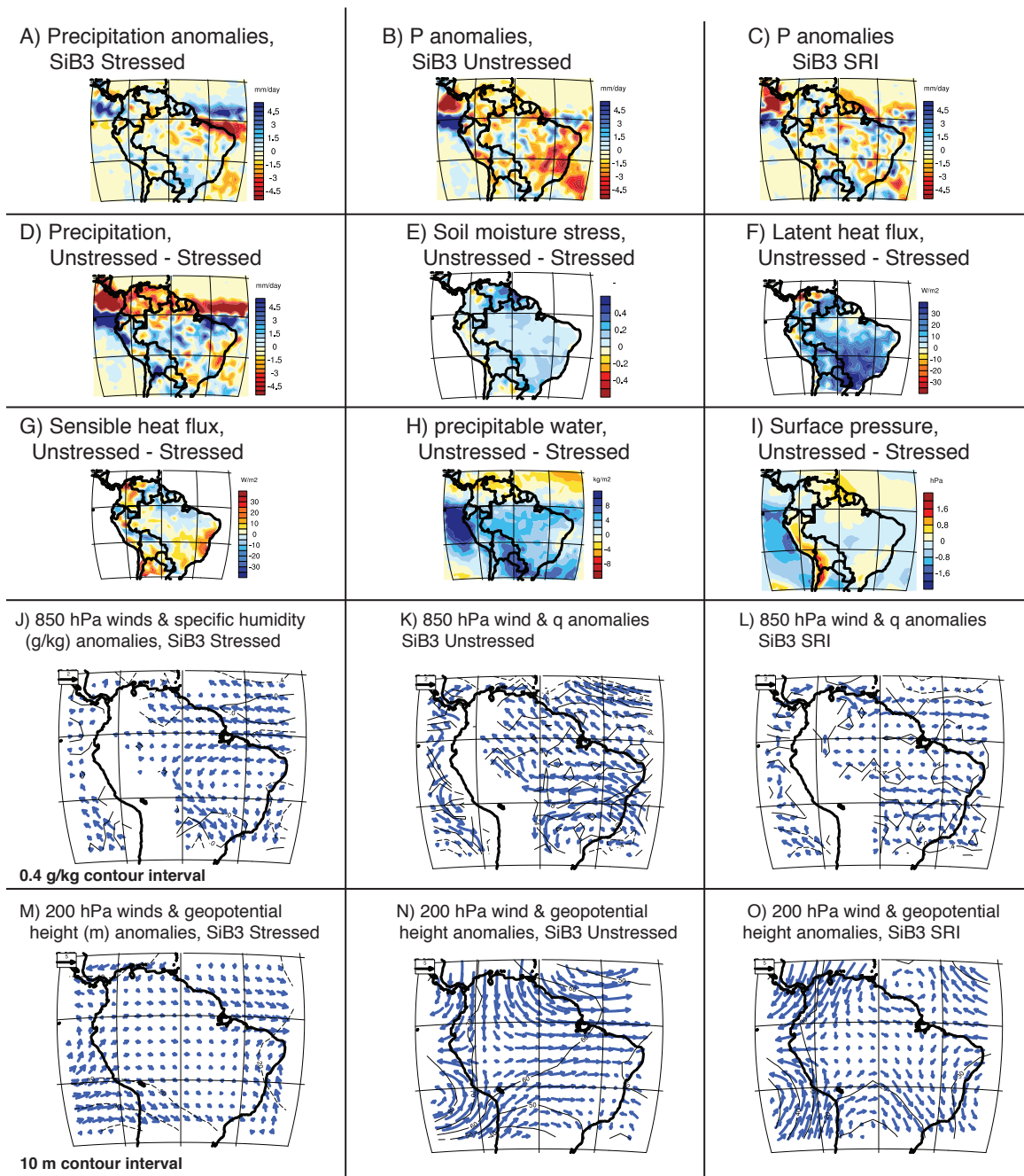


Figure 5.17. As in Figure 5.15 but for the northwestern region.

CHAPTER 6:

CONCLUSIONS

This body of work represents a progression in our understanding of Amazon forest response to drought and potential viability in a drier climate. Previous work with SiB3 focused on including drought tolerance mechanisms and matching observed seasonal cycles of carbon, heat, and moisture fluxes throughout Amazonia (Baker et al., 2008; Baker et al., 2011a). One concern was that of “over-fixing” the problem of seasonal drought stress, such that the model never experiences stress. This motivated our study of SiB3 at the two rainfall exclusion sites. We then incorporated what we learned from the exclusions to develop an index of stress resistance for SiB3. Now instead of the model always being “stressed” or “unstressed”, the forest is able to have a spatially varying response to drought. The final steps of the work were to examine the effects of forest drought response on feedbacks between the forest and atmosphere. Whether the forest continues to transpire and photosynthesize during droughts will have important impacts on the future of the Amazon region. At the beginning of this dissertation, we set out to address the following five questions.

6.1 How well do we understand Amazon forest stress response during extremely dry conditions?

Unfortunately, very little is known on this topic, but recent experiments and drought studies have added insight into the forest response. Drought impacts on the Amazon forest vary spatially based on background climate, soil texture, water table dynamics, and

rooting strategies of plants. The first part of this work (Ch. 2) encompasses the response of two plots of old-growth forest in the equatorial Amazon. The two sites - Caxiuanã and Tapajós - have important differences in root and water table depth, meteorology, soil texture, species distribution, and disturbance history, all of which influence how the forest responds to dry conditions. We evaluated SiB3's response to drought and investigated ways to make the model more realistic in terms of drought impacts on ET and NPP. We also looked into metrics such as fraction of maximum PAW and water deficit for determining possible ecosystem thresholds in drought tolerance.

The default version of SiB3 matches observed seasonal cycles of latent heat flux and NEE throughout the region (Baker et al. 2008), and it replicates the effects of the exclusion at Tapajós in a manner consistent with observations. However, at Caxiuanã SiB3 does a poor job of simulating the effects of the exclusion, and in terms of drought effects on NPP and ET we get the best results using a version of SiB3 with an artificially shallow soil. Our simulation also improves when we use observed values of LAI, as the variation in canopy structure throughout the experiment represents important reactions of the forest to drought. Another improvement we note in the model is the use of soil texture and hydraulic conductivity that match site observations. For example, changing the saturated soil hydraulic conductivity increases drainage and produces a more realistic drought response.

6.2 Can modeled plant available water and ecosystem stress indicate thresholds in ecosystem drought tolerance?

In addition to informing future model development, this study points us to some important thresholds in tropical forest drought response. These have been discussed from an observational point of view (e.g. Meir and Woodward 2010; Malhi et al., 2009b; Nepstad et al., 2008), and can lend guidance for monitoring the forest under a changing climate. In general, the forest's functioning (as indicated with modeled GPP and ET) is most affected when PAW drops below 30-35% of its maximum value and CWD is greater than -500 mm. At Tapajós, it took SiB3 three years to reach these levels, and the superposition of a dry dry season on the exclusion experiment likely aided in depleting soil moisture to these levels. At Caxiuanã, the model required very strong (75%) reductions in rainfall for two years to reach this threshold. The timing of the changes in photosynthesis and latent heat flux in SiB3 at Tapajós matches well with observed decreases in PAW and ANPP and increases in tree mortality.

6.3 How do climatology, soil texture and forest cover affect forest stress resistance?

In Chapter 3, the concept of stress resistance is developed, based on the hypothesis that precipitation climatology, forest cover, and soil type impact the ability of a forest to tolerate drought. The assumption is that regions that experience periodic drought have developed mechanisms with which to withstand drier conditions. We also assume that deforestation decreases stress resistance through removal of rooting systems and reduced precipitation recycling, and that deep roots are more likely in seasonal forests with coarse

or fine soil texture. We create an index of stress resistance that can be used in ecosystem models. Compared to the default version of SiB3, using the SRI increases stress resistance in the eastern basin and decreases resistance in the western basin.

The SRI has little effect on mean seasonal cycles of carbon fluxes and latent and sensible heat flux. Differences arise during dry periods – such as during the dry season or during anomalously dry years. During these times, photosynthesis decreases, especially in the southern hemisphere forests, and NEE increases. Both of these are more strongly correlated with the MEI in SiB3-SRI – indicating that the effect of spatially varying stress resistance is to increase carbon efflux from the Amazon forest during El Niños. Photosynthesis is also decreased during the unusually strong drought of 2005.

In addition, during droughts the sensible heat flux increases and latent heat flux decreases. The changes could lead to a warmer, drier PBL and could further inhibit precipitation. This provides justification for the final two parts of this work, which involve coupling SiB3 to a GCM.

6.4 How does forest stress resistance affect the climate?

In Chapter 4, we test the impacts of drought tolerance mechanisms in SiB3 in a single column version of the BUGS5 GCM. One version of SiB3 experiences strong ecosystem stress during the dry season (SiB3 Stressed), while the other has a more realistic ability to sustain evaporation and photosynthesis through the dry season (SiB3 Unstressed). This latter version has a larger soil moisture pool, the ability of roots to access water anywhere in the rooting profile, and a more gradual increase in soil moisture

stress with decreasing soil moisture.

We compare two versions of SiB3 to understand the effects of surface biophysics on the seasonal hydrologic cycle, atmospheric circulation and wet season characteristics in the equatorial Amazon. Results are compared to observations at the Tapajós tower, located in the equatorial forest. The more realistic surface biophysics in SiB3 Unstressed result in a more active and realistic hydrologic cycle, with stronger evapotranspiration and moisture divergence during the dry seasons. The surface changes also affect the latent heating of the lower troposphere and the column moist static energy. Therefore, accurately representing surface processes is vital for understanding and simulating the climate of the region.

6.5 Can forest stress resistance affect drought intensity, and circulation in regions outside of Amazonia?

Lastly, we examine effects of drought tolerance on climate in the full GCM during ten years (1997-2006). In this study, we add the version of SiB3 with the SRI, in addition to SiB3 Stressed and Unstressed. We found that increased stress resistance usually decreased drought intensity, and that changes in surface fluxes in Amazonia impact circulation patterns elsewhere in South America.

Forests can tolerate drought conditions by avoiding plant water deficits, tolerating the deficits, or by employing water use efficiency mechanisms (Jones, 1994). This study suggests a fourth mechanism: drought mitigation. In the Amazon, access to deep soil moisture is important for drought survival. This study highlights the importance of these

mechanisms for precipitation recycling and possible drought mitigation. Dry periods were generally less intense and lasted for fewer months in the models with higher stress resistance.

Although this study does not directly address land use change, an important implication is that forest preservation is extremely important for enabling the Amazon forest to withstand a potentially drier climate. The more primary forest there is, the more we can expect for precipitation recycling to reduce drought intensity as suggested by results in Chapter 5. Simulations with SiB3 SRI offline showed that in the southeastern Amazon, where deforestation decreased the SRI, the 2005 drought reduced forest productivity (Ch. 3). Deforestation can result in enhanced forest mortality during droughts, and forests along edges are more prone to desiccation and fire impacts (Malhi et al., 2008). A positive feedback exists between dryness, forest cover, and fire incidence. The combination of deforestation and climate change in the future could have very severe impacts on the Amazon.

Parts of the Amazon that are subject to occasional drought might be more drought tolerant than previously thought. Results showing extreme ecosystem stress and forest dieback under climate change should be revisited to ensure the proper feedbacks are occurring between the land and atmosphere. On the other hand, interior forests might be less drought tolerant than is currently represented in ecosystem models. This could be especially problematic since recent intense droughts affected parts of the forest that are usually very wet (Phillips et al., 2009; Lewis et al., 2011).

7. BIBLIOGRAPHY

- Adams, H. D. (2010), Climate-induced tree mortality: Earth system consequences, *Eos*, 91.
- Adler, R. F., et al. (2003), The version-2 global precipitation climatology project (GPCP) monthly precipitation analysis (1979-present), *JOURNAL OF HYDROMETEOROLOGY*, 4(6), 1147-1167.
- Allen, C. D., et al. (2010), A global overview of drought and heat-induced tree mortality reveals emerging climate change risks for forests, *FOREST ECOLOGY AND MANAGEMENT*, 259(4), 660-684.
- Anderson, L. O. (2010), Remote sensing detection of droughts in Amazonian forest canopies *New Phytologist*.
- Andreae, M. O., et al. (2002), Biogeochemical cycling of carbon, water, energy, trace gases, and aerosols in Amazonia: The LBA-EUSTACH experiments, *JOURNAL OF GEOPHYSICAL RESEARCH-ATMOSPHERES*, 107(D20).
- Aragao, L. E. O. C., Y. Malhi, R. M. Roman-Cuesta, S. Saatchi, L. O. Anderson, and Y. E. Shimabukuro (2007), Spatial patterns and fire response of recent Amazonian droughts, *Geophys. Res. Lett.*, 34(7), L07701.
- Asner, G. P., A. R. Townsend, and B. H. Braswell (2000), Satellite observation of El Nino effects on Amazon forest phenology and productivity, *GEOPHYSICAL RESEARCH LETTERS*, 27(7), 981-984.
- Baker, I. T., H.R. da Rocha, A.B. Harper, A.S. Denning, A.C. Araujo, L.S. Borma, H.C. Freitas, M.L. Goulden, A.O. Manzi, S.D. Miller, A.D. Nobre, N. Restrepo-Coupe, S.R. Saleska, R. Stockli, C. von Randow, S.C. Wofsy (2011), Surface ecophysiological behavior across vegetation and moisture gradients in Amazonia, *AGRICULTURAL AND FOREST METEOROLOGY*, *submitted*.
- Baker, I. T., A.B. Harper, A.S. Denning, R. Stockli (2011), Regional ecophysiology in Amazonia: Annual cycles and response to climate variability, *GLOBAL BIOGEOCHEMICAL CYCLES*, *in prep*.
- Baker, I. T., L. Prihodko, A. S. Denning, M. Goulden, S. Miller, and H. R. da Rocha (2008), Seasonal drought stress in the Amazon: Reconciling models and observations, *Journal of Geophysical Research-Biogeosciences*, 113.
- Bartholomew, J. (1962), *The advanced atlas of modern geography*, 51 pp., McGraw-Hill, New York.
- Belk, E. L., D. Markewitz, T. C. Rasmussen, E. J. Maklouf Carvalho, D. C. Nepstad, and E. A. Davidson (2007), Modeling the effects of throughfall reduction on soil water content in a Brazilian Oxisol under a moist tropical forest, *Water Resources Research*, 43(8).
- Brando, P., D. Ray, D. Nepstad, G. Cardinot, L. M. Curran, and R. Oliveira (2006), Effects of partial throughfall exclusion on the phenology of *Coussarea racemosa* (Rubiaceae) in an east-central Amazon rainforest, *Oecologia*, 150(2), 181-189.
- Brando, P. M., S. J. Goetz, A. Baccini, D. C. Nepstad, P. S. A. Beck, and M. C. Christman (2010), Seasonal and interannual variability of climate and vegetation indices

- across the Amazon, *Proceedings of the National Academy of Sciences*, 107(33), 14685-14690.
- Brando, P. M., D. C. Nepstad, E. A. Davidson, S. E. Trumbore, D. Ray, and P. Camargo (2008), Drought effects on litterfall, wood production and belowground carbon cycling in an Amazon forest: results of a throughfall reduction experiment, *Philosophical Transactions of the Royal Society B-Biological Sciences*, 363(1498), 1839-1848.
- Carswell, F. E., et al. (2002), Seasonality in CO₂ and H₂O flux at an eastern Amazonian rain forest, *Journal of Geophysical Research-Atmospheres*, 107(D20).
- Carvalho, L. M. V., A. E. Silva, C. Jones, B. Liebmann, P. L. S. Dias, and H. R. Rocha (2011), Moisture transport and intraseasonal variability in the South America monsoon system, *CLIMATE DYNAMICS*, 36(9-10), 1865-1880.
- Chambers, J., E. Tribuzy, L. Toledo, B. Crispim, N. Higuchi, J. dos Santos, A. Araujo, B. Kruijt, A. Nobre, and S. Trumbore (2004), Respiration from a tropical forest ecosystem: Partitioning of sources and low carbon use efficiency, *Ecological Applications*, 14(4, Suppl. S), S72-S88.
- Chapin, F., P.A. Matson, H.A. Mooney (2002), *Principles of Terrestrial Ecosystem Ecology*, 436 pp., Springer-Verlag, New York.
- Clapp, R. B., and G. M. Hornberger (1978), Empirical Equations for some Soil Hydraulic Properties, *Water Resources Research*, 14(4), 601-604.
- Cox, P., R. Betts, M. Collins, P. Harris, C. Huntingford, and C. Jones (2004), Amazonian forest dieback under climate-carbon cycle projections for the 21st century, *Theoretical and Applied Climatology*, 78(1-3), 137-156.
- Cox, P., R. Betts, C. Jones, S. Spall, and I. Totterdell (2000), Acceleration of global warming due to carbon-cycle feedbacks in a coupled climate model, *NATURE*, 408(6809), 184-187.
- Cox, P. M., P. P. Harris, C. Huntingford, R. A. Betts, M. Collins, C. D. Jones, T. E. Jupp, J. A. Marengo, and C. A. Nobre (2008), Increasing risk of Amazonian drought due to decreasing aerosol pollution, *Nature*, 453(7192), 212-U217.
- da Costa, A. C. L. (2010), Effect of 7 yr of experimental drought on vegetation dynamics and biomass storage of an eastern Amazonian rainforest *New Phytologist*.
- da Rocha, H., M. Goulden, S. Miller, M. Menton, L. Pinto, H. de Freitas, and A. Figueira (2004), Seasonality of water and heat fluxes over a tropical forest in eastern Amazonia, *ECOLOGICAL APPLICATIONS*, 14(4, Suppl. S), S22-S32.
- da Rocha, H. R., et al. (2009), Patterns of water and heat flux across a biome gradient from tropical forest to savanna in Brazil, *JOURNAL OF GEOPHYSICAL RESEARCH-BIOGEOSCIENCES*, 114.
- Davidson, E. A., D. C. Nepstad, F. Y. Ishida, and P. M. Brando (2008), Effects of an experimental drought and recovery on soil emissions of carbon dioxide, methane, nitrous oxide, and nitric oxide in a moist tropical forest, *Global Change Biology*, 14(11), 2582-2590.

- DeLucia, E. H., J. E. Drake, R. B. Thomas, and M. Gonzalez-Meler (2007), Forest carbon use efficiency: is respiration a constant fraction of gross primary production?, *Global Change Biology*, 13(6), 1157-1167.
- Denning, A. S., G. J. Collatz, C. G. Zhang, D. A. Randall, J. A. Berry, P. J. Sellers, G. D. Colello, and D. A. Dazlich (1996), Simulations of terrestrial carbon metabolism and atmospheric CO₂ in a general circulation model .1. Surface carbon fluxes, *TELLUS SERIES B-CHEMICAL AND PHYSICAL METEOROLOGY*, 48(4), 521-542.
- Denning, A. S., N. Zhang, C. Yi, M. Branson, K. Davis, J. Kleist, and P. Bakwin (2008), Evaluation of modeled atmospheric boundary layer depth at the WLEF tower, *Agricultural and Forest Meteorology*, 148(2), 206-215.
- Dias, P. L. S., W. H. Schubert, and M. Demaria (1983), LARGE-SCALE RESPONSE OF THE TROPICAL ATMOSPHERE TO TRANSIENT CONVECTION, *Journal of the Atmospheric Sciences*, 40(11), 2689-2707.
- Ding, P., and D. A. Randall (1998), A cumulus parameterization with multiple cloud base levels, *JOURNAL OF GEOPHYSICAL RESEARCH-ATMOSPHERES*, 103(D10), 11341-11353.
- Fearnside, P. M. (2005), Deforestation in Brazilian Amazonia: History, rates, and consequences, *Conserv. Biol.*, 19(3), 680-688.
- Fisher, J. B., et al. (2009), The land-atmosphere water flux in the tropics, *GLOBAL CHANGE BIOLOGY*, 15(11), 2694-2714.
- Fisher, R. A. (2006), Evidence from Amazon forests is consistent with isohydric control of leaf water potential, *Plant and Cell Environment*.
- Fisher, R. A. (2007), The response of an eastern Amazonian rain forest to drought stress: results and modeling analyses from a throughfall exclusion experiment *Global Change Biology*.
- Fisher, R. A. (2008), Evaluating climatic and soil water controls on ET at two Amazonian forest sites *Agricultural and Forest Meteorology*.
- Fowler, L. D., and D. A. Randall (2002), Interactions between cloud microphysics and cumulus convection in a general circulation model, *Journal of the Atmospheric Sciences*, 59(21), 3074-3098.
- Franchito, S. H., E. C. Moraes, and V. B. Rao (2002), Simulations with a radiation model and comparisons with LBA data sets, *JOURNAL OF GEOPHYSICAL RESEARCH-ATMOSPHERES*, 107(D20).
- Friedlingstein, P., et al. (2006), Climate-carbon cycle feedback analysis: Results from the (CMIP)-M-4 model intercomparison, *Journal of Climate*, 19(14), 3337-3353.
- Furley, P. A. (1992), Edaphic Changes at the Forest Savanna Boundary with Particular Reference to the Neotropics, *Nature and Dynamics of Forest-Savanna Boundaries*, 91-117.
- Gabriel, P. M., P. T. Partain, and G. L. Stephens (2001), Parameterization of atmospheric radiative transfer. Part II: Selection rules, *Journal of the Atmospheric Sciences*, 58(22), 3411-3423.

- Galbraith, D., P. E. Levy, S. Sitch, C. Huntingford, P. Cox, M. Williams, and P. Meir (2010), Multiple mechanisms of Amazonian forest biomass losses in three dynamic global vegetation models under climate change, *NEW PHYTOLOGIST*, 187(3), 647-665.
- Gandu, A. W., and P. L. S. Dias (1998), Impact of tropical heat sources on the South American tropospheric upper circulation and subsidence, *JOURNAL OF GEOPHYSICAL RESEARCH-ATMOSPHERES*, 103(D6), 6001-6015.
- Goulden, M., S. Miller, H. da Rocha, M. Menton, H. de Freitas, A. Figueira, and C. de Sousa (2004), Diel and seasonal patterns of tropical forest CO₂ exchange, *ECOLOGICAL APPLICATIONS*, 14(4, Suppl. S), S42-S54.
- Gower, S. T. (1987), RELATIONS BETWEEN MINERAL NUTRIENT AVAILABILITY AND FINE ROOT BIOMASS IN 2 COSTA RICAN TROPICAL WET FORESTS - A HYPOTHESIS, *Biotropica*, 19(2), 171-175.
- Grimm, A. M. (2003), The El Nino impact on the summer monsoon in Brazil: Regional processes versus remote influences, *JOURNAL OF CLIMATE*, 16(2), 263-280.
- Group, G. S. D. T. (2000), Global gridded surfaces of selected soil characteristics, International Geosphere-Biosphere Programme - Data and Information System (IGBP-DIS), edited, Oak Ridge National Laboratory Distributed Active Archive Center, Oak Ridge, Tennessee.
- Harper, A. B., A. S. Denning, I. T. Baker, M. D. Branson, L. Prihodko, and D. A. Randall (2010), Role of deep soil moisture in modulating climate in the Amazon rainforest, *Geophysical Research Letters*, 37.
- Hasler, N. (2007), What controls evapotranspiration in the Amazon basin?
- Hirota, M., C. Nobre, M. D. Oyama, and M. M. C. Bustamante (2010), The climatic sensitivity of the forest, savanna and forest-savanna transition in tropical South America, *NEW PHYTOLOGIST*, 187(3), 707-719.
- Hodnett, M. G., and J. Tomasella (2002), Marked differences between van Genuchten soil water-retention parameters for temperate and tropical soils: a new water-retention pedo-transfer functions developed for tropical soils, *Geoderma*, 108(3-4), 155-180.
- Huete, A., K. Didan, Y. Shimabukuro, P. Ratana, S. Saleska, L. Hutya, W. Yang, R. Nemani, and R. Myneni (2006), Amazon rainforests green-up with sunlight in dry season, *Geophysical Research Letters*, 33(6).
- Huffman, G. J., R. F. Adler, P. Arkin, A. Chang, R. Ferraro, A. Gruber, J. Janowiak, A. McNab, B. Rudolf, and U. Schneider (1997), The Global Precipitation Climatology Project (GPCP) Combined Precipitation Dataset, *BULLETIN OF THE AMERICAN METEOROLOGICAL SOCIETY*, 78(1), 5-20.
- Hutya, L., J. Munger, C. Nobre, S. Saleska, S. Vieira, and S. Wofsy (2005), Climatic variability and vegetation vulnerability in Amazonia, *Geophysical Research Letters*, 32(24).
- Ichii, K., H. Hashimoto, M. A. White, C. Potters, L. R. Hutya, A. R. Huete, R. B. Myneni, and R. R. Nemanis (2007), Constraining rooting depths in tropical rainforests using satellite data and ecosystem modeling for accurate simulation of

- gross primary production seasonality, *GLOBAL CHANGE BIOLOGY*, 13(1), 67-77.
- IGBP, G. S. D. T. (2000), International Geosphere-Biosphere Programme, edited by D. a. I. System, Oak Ridge National Laboratory Distributed Active Archive Center, Oak Ridge, Tennessee, U.S.A. [<http://www.daac.ornl.gov>], Potsdam, Germany.
- IPCC (2007), *The Physical Science Basis: Contribution of Working Group I to the Fourth Assessment Report of the Intergovernmental Panel on Climate Change*, 996 pp., Cambridge University Press, Cambridge, UK and New York, USA.
- Jackson, R., J. Canadell, J. Ehleringer, H. Mooney, O. Sala, and E. Schulze (1996), A global analysis of root distributions for terrestrial biomes, *Oecologia*, 108(3), 389-411.
- Jarvis, P. G. (1986), Coupling of carbon and water interactions in forest stands, *Tree Physiology*, 2(1-3), 347-368.
- Jipp, P., D. Nepstad, D. Cassel, and C. De Carvalho (1998), Deep soil moisture storage and transpiration in forests and pastures of seasonally-dry amazonia, *Climatic change*, 39(2-3), 395-412.
- Jones, C., and L. M. V. Carvalho (2002), Active and break phases in the south American Monsoon system, *JOURNAL OF CLIMATE*, 15(8), 905-914.
- Jones, H. (1992), *Plants and microclimate*, 428 pp., Cambridge University Press, Cambridge.
- Kalnay, E., et al. (1996), The NCEP/NCAR 40-year reanalysis project, *BULLETIN OF THE AMERICAN METEOROLOGICAL SOCIETY*, 77(3), 437-471.
- Kleidon, A., and M. Heimann (1998), A method of determining rooting depth from a terrestrial biosphere model and its impacts on the global water and carbon cycle, *GLOBAL CHANGE BIOLOGY*, 4(3), 275-286.
- Kleidon, A., and M. Heimann (1999), Deep-rooted vegetation, Amazonian deforestation, and climate: results from a modelling study, *GLOBAL ECOLOGY AND BIOGEOGRAPHY*, 8(5), 397-405.
- Kozlowski, T. T., and S. G. Pallardy (2002), Acclimation and adaptive responses of woody plants to environmental stresses, *Botanical Review*, 68(2), 270-334.
- Lawrence, P. J., and T. N. Chase (2009), Climate Impacts of Making Evapotranspiration in the Community Land Model (CLM3) Consistent with the Simple Biosphere Model (SiB), *JOURNAL OF HYDROMETEOROLOGY*, 10(2), 374-394.
- Lee, J.-E., R. S. Oliveira, T. E. Dawson, and I. Fung (2007), Root functioning modifies seasonal climate (vol 102, pg 17576, 2005), *Proceedings of the National Academy of Sciences of the United States of America*, 104(33), 13531.
- Lenters, J., and K. Cook (1997), On the origin of the Bolivian high and related circulation features of the South American climate, *Journal of the Atmospheric Sciences*, 54(5), 656-677.
- Lewis, S. L., P. M. Brando, O. L. Phillips, G. M. F. van der Heijden, and D. Nepstad (2011), The 2010 Amazon Drought, *SCIENCE*, 331(6017), 554-554.

- Li, W., and R. Fu (2004), Transition of the large-scale atmospheric and land surface conditions from the dry to the wet season over Amazonia as diagnosed by the ECMWF re-analysis, *Journal of Climate*, 17(13), 2637-2651.
- Li, W., R. Fu, and R. Dickinson (2006), Rainfall and its seasonality over the Amazon in the 21st century as assessed by the coupled models for the IPCC AR4, *Journal of Geophysical Research-Atmospheres*, 111(D2).
- Liu, J. (2004), Investigation of ecosystem drought stress and its impacts on carbon exchange at tropical forests, Colorado State University, Fort Collins.
- Liu, J. (2004), Investigation of ecosystem drought stress and its impacts on carbon exchange in tropical forests, Colorado State University, Fort Collins.
- Malhi, Y. (2009), Comprehensive assessment of carbon productivity, allocation and storage in three Amazonian forests, *Global Change Biology*.
- Malhi, Y., L. Aragao, D. Galbraith, C. Huntingford, R. Fisher, P. Zelazowski, S. Sitch, C. McSweeney, and P. Meir (2009a), Exploring the likelihood and mechanism of a climate-change-induced dieback of the Amazon rainforest, *Proceedings of the National Academy of Sciences of the United States of America*, 106(49), 20610-20615.
- Malhi, Y., J. T. Roberts, R. A. Betts, T. J. Killeen, W. H. Li, and C. A. Nobre (2008), Climate change, deforestation, and the fate of the Amazon, *Science*, 319(5860), 169-172.
- Malhi, Y., and J. Wright (2004), Spatial patterns and recent trends in the climate of tropical rainforest regions, *PHILOSOPHICAL TRANSACTIONS OF THE ROYAL SOCIETY OF LONDON SERIES B-BIOLOGICAL SCIENCES*, 359(1443), 311-329.
- Marengo, J. A., C. A. Nobre, J. Tomasella, M. D. Oyama, G. S. De Oliveira, R. De Oliveira, H. Camargo, L. M. Alves, and I. F. Brown (2008), The drought of Amazonia in 2005, *Journal of Climate*, 21(3), 495-516.
- Markewitz, D., S. Devine, E. A. Davidson, P. Brando, and D. C. Nepstad (2010), Soil moisture depletion under simulated drought in the Amazon: impacts on deep root uptake, *New Phytologist*, 187(3), 592-607.
- McDowell, N. (2008), Mechanisms of plant survival and mortality during drought: why do some plants survive while others succumb to drought? .
- McNabb, K., L.G. da Silva Costa, M. Menezes, B. Lockaby (2010), LBA-ECO ND-08 Jari Fine Root Biomass, edited, Oak Ridge National Laboratory Distributed Active Archive Center.
- Meinzer, F. C., G. Goldstein, and J. L. Andrade (2001), Regulation of water flux through tropical forest canopy trees: Do universal rules apply?, *TREE PHYSIOLOGY*, 21(1), 19-26.
- Meir, P., P.M. Brando, D. Nepstad, S. Vasconcelos, A.C.L. Costa, E. Davidson, S. Almeida, R.A. Fisher, E.D. Sotta, D. Zarin, and G. Cardinot (2009), *The effects of drought on Amazonian rain forests*, American Geophysical Union Geophysical Monograph Series, Washington, D.C.

- Metcalfe, D. B. (2010), Shifts in plant respiration and carbon use efficiency at a large-scale drought experiment in the eastern Amazon *New Phytologist*.
- Metcalfe, D. B., et al. (2008), The effects of water availability on root growth and morphology in an Amazon rainforest, *Plant and Soil*, 311(1-2), 189-199.
- Miller, S., M. Goulden, M. Menton, H. da Rocha, H. de Freitas, A. Figueira, and C. de Sousa (2004), Biometric and micrometeorological measurements of tropical forest carbon balance, *ECOLOGICAL APPLICATIONS*, 14(4, Suppl. S), S114-S126.
- Nepstad, D. (2004), Amazon drought and its implications for forest flammability and tree growth: a basin-wide analysis
- Nepstad, D., C. Decarvalho, E. Davidson, P. Jipp, P. Lefebvre, G. Negreiros, E. Dasilva, T. Stone, S. Trumbore, and S. Vieira (1994), The Role of Deep Roots in the Hydrological and Carbon Cycles of Amazonian Forests and Pastures, *Nature*, 372(6507), 666-669.
- Nepstad, D., et al. (2002), The effects of partial throughfall exclusion on canopy processes, aboveground production, and biogeochemistry of an Amazon forest, *Journal of Geophysical Research-Atmospheres*, 107(D20).
- Nepstad, D. C., C. M. Stickler, B. Soares-Filho, and F. Merry (2008), Interactions among Amazon land use, forests and climate: prospects for a near-term forest tipping point, *Philosophical Transactions of the Royal Society B-Biological Sciences*, 363(1498), 1737-1746.
- Nepstad, D. C., I. M. Tohver, D. Ray, P. Moutinho, and G. Cardinot (2007), Mortality of large trees and lianas following experimental drought in an amazon forest, *Ecology*, 88(9), 2259-2269.
- Oleson, K. W., D.M. Lawrence, G.B. Bonan, M.G. Flanner, E. Kluzek, P.J. Lawrence, S. Levis, S.C. Swenson, P.E. Thornton, A. Dai, M. Decker, R. Dickinson, J. Feddema, C.L. Heald, F. Hoffman, J.-F. Lamarque, N. Mahowald, G.-Y. Niu, T. Qian, J. Randerson, S. Running, K. Sakaguchi, A. Slater, R. Stockli, A. Wang, Z.-L. Yang, Xi. Zeng, and Xu. Zeng (2010), Technical Description of version 4.0 of the Community Land Model (CLM)*Rep.*, 257 pp, National Center for Atmospheric Research, Boulder, CO.
- Oliveira, R., T. Dawson, S. Burgess, and D. Nepstad (2005), Hydraulic redistribution in three Amazonian trees, *Oecologia*, 145(3), 354-363.
- Ostle, N. J. (2009), Integrating plant-soil interactions into global carbon cycle models *Journal of Ecology*.
- Phillips, O. L., et al. (2009), Drought Sensitivity of the Amazon Rainforest, *Science*, 323(5919), 1344-1347.
- Phillips, O. L., et al. (2010), Drought-mortality relationships for tropical forests, *New Phytologist*, 187(3), 631-646.
- Poorter, L., and L. Markesteijn (2008), Seedling traits determine drought tolerance of tropical tree species, *Biotropica*, 40(3), 321-331.
- Poulter, B. (2009), Modeling the sensitivity of the seasonal cycle of GPP to dynamic LAI and soil depths in tropical rainforests *Ecosystems*.

- Randall, D., D. Dazlich, C. Zhang, A. Denning, P. Sellers, C. Tucker, L. Bounoua, S. Los, C. Justice, and I. Fung (1996), A revised land surface parameterization (SiB2) for GCMs .3. The greening of the Colorado State University general circulation model, *Journal of Climate*, 9(4), 738-763.
- Randall, D. A., J. A. Abeles, and T. G. Corsetti (1985), Seasonal Simulations of the Planetary Boundary-Layer and Boundary-Layer Stratocumulus Clouds with a General-Circulation Model, *Journal of the Atmospheric Sciences*, 42(7), 641-676.
- Randall, D. A., and D. G. Cripe (1999), Alternative methods for specification of observed forcing in single-column models and cloud system models, *JOURNAL OF GEOPHYSICAL RESEARCH-ATMOSPHERES*, 104(D20), 24527-24545.
- Ringler, T. D., R. P. Heikes, and D. A. Randall (2000), Modeling the atmospheric general circulation using a spherical geodesic grid: A new class of dynamical cores, *Mon Weather Rev*, 128(7), 2471-2490.
- Romero-Saltos, H., L. Sternberg, M. Moreira, and D. Nepstad (2005), Rainfall exclusion in an eastern amazonian forest alters soil water movement and depth of water uptake, *American Journal of Botany*, 92(3), 443-455.
- Saleska, S., et al. (2003), Carbon in amazon forests: Unexpected seasonal fluxes and disturbance-induced losses, *Science*, 302(5650), 1554-1557.
- Saleska, S. R., K. Didan, A. R. Huete, and H. R. da Rocha (2007), Amazon forests green-up during 2005 drought, *Science*, 318(5850), 612.
- Schafer, J. S., T. F. Eck, B. N. Holben, P. Artaxo, M. A. Yamasoe, and A. S. Procopio (2002), Observed reductions of total solar irradiance by biomass-burning aerosols in the Brazilian Amazon and Zambian Savanna, *GEOPHYSICAL RESEARCH LETTERS*, 29(17).
- Schenk, H. J., and R. B. Jackson (2004), Mapping the global distribution of deep roots in relation to climate and soil characteristics, *Geoderma*, 126(1-2), 129-140.
- Sellers, P., D. Randall, G. Collatz, J. Berry, C. Field, D. Dazlich, C. Zhang, G. Collelo, and L. Bounoua (1996), A revised land surface parameterization (SiB2) for atmospheric GCMs .1. Model formulation, *Journal of Climate*, 9(4), 676-705.
- Sellers, P. J., Y. Mintz, Y. C. Sud, and A. Dalcher (1986), A Simple Biosphere Model (SiB) for use within General-Circulation Models, *Journal of the Atmospheric Sciences*, 43(6), 505-531.
- Shuttleworth, W. J. (1989), MICROMETEOROLOGY OF TEMPERATE AND TROPICAL FOREST, *Philosophical Transactions of the Royal Society of London Series B-Biological Sciences*, 324(1223), 299-334.
- Silver, W. L., J. Neff, M. McGroddy, E. Veldkamp, M. Keller, and R. Cosme (2000), Effects of soil texture on belowground carbon and nutrient storage in a lowland Amazonian forest ecosystem, *Ecosystems*, 3(2), 193-209.
- Soares, B. S., D. C. Nepstad, L. M. Curran, G. C. Cerqueira, R. A. Garcia, C. A. Ramos, E. Voll, A. McDonald, P. Lefebvre, and P. Schlesinger (2006), Modelling conservation in the Amazon basin, *NATURE*, 440(7083), 520-523.
- Sotta, E. D. (2007), Effects of an induced drought on soil carbon dioxide efflux and soil CO₂ production in an Eastern Amazonian rainforest, Brazil.

- Stephens, G. L., P. M. Gabriel, and P. T. Partain (2001), Parameterization of atmospheric radiative transfer. Part I: Validity of simple models, *Journal of the Atmospheric Sciences*, 58(22), 3391-3409.
- Sternberg, L., M. Moreira, and D. Nepstad (2002), Uptake of water by lateral roots of small trees in an Amazonian Tropical Forest, *Plant and Soil*, 238(1), 151-158.
- Stockli, R., T. Rutishauser, D. Dragoni, J. O'Keefe, P. E. Thornton, M. Jolly, L. Lu, and A. S. Denning (2008), Remote sensing data assimilation for a prognostic phenology model, *Journal of Geophysical Research-Biogeosciences*, 113(G4).
- Tarasova, T. A., C. A. Nobre, B. N. Holben, T. F. Eck, and A. Setzer (1999), Assessment of smoke aerosol impact on surface solar irradiance measured in the Rondonia region of Brazil during Smoke, Clouds, and Radiation - Brazil, *JOURNAL OF GEOPHYSICAL RESEARCH-ATMOSPHERES*, 104(D16), 19161-19170.
- van Genuchten, M. T. (1980), A closed-form equation for predicting the hydraulic conductivity of unsaturated soils, *Soil Science Society of America Journal*, 44, 892-898.
- van Oldenborgh, G. J., S.Y. Philip, M. Collins (2005), El Nino in a changing climate: a multi-model study, *Ocean Science*, 1, 81-95.
- Verbeeck, H., P. Peylin, C. Bacour, D. Bonal, K. Steppe, and P. Ciais (2011), Seasonal patterns of CO₂ fluxes in Amazon forests: Fusion of eddy covariance data and the ORCHIDEE model, *JOURNAL OF GEOPHYSICAL RESEARCH-BIOGEOSCIENCES*, 116.
- von Randow, C., et al. (2004), Comparative measurements and seasonal variations in energy and carbon exchange over forest and pasture in South West Amazonia, *Theoretical and Applied Climatology*, 78(1-3), 5-26.
- Zeng, N., J. H. Yoon, J. A. Marengo, A. Subramaniam, C. A. Nobre, A. Mariotti, and J. D. Neelin (2008), Causes and impacts of the 2005 Amazon drought, *ENVIRONMENTAL RESEARCH LETTERS*, 3(1).